EVALUATION OF IN-SITU STRESSES FROM MODIFIED FLATJACK TESTING METHODOLOGY IN THE NEAR SURFACE ENVIRONMENT

by

Alexander Mckenney

Submitted in partial fulfilment of the requirements
for the degree of Master of Applied Science

at

Dalhousie University
Halifax, Nova Scotia
January 2018

© Copyright by Alexander Mckenney, 2018

TABLE OF CONTENTS

LIST OF TABLES

LIST OF FIGURES

ABSTRACT

In this study, the ASTM flatjack methodology was modified in several ways. The overlapping borehole slot was replaced with a ‘standard’ saw cut slot which produced a smooth semi oval opening for the installation of various shapes and sizes of flatjack without the need for grout. This methodology was tested initially in the field at Pioneer Coal in Stellarton and later in a lab program. Lab tests were conducted on specially prepared concrete blocks to evaluate the ratio between flatjack pressure and applied load. The lab tests results were used along with numerical modeling to develop correction factors to compensate for the difference in shape and size between the different flatjacks and the slot shapes used. Finally, a relationship was established between slot closure and the applied stress for the tested geometries.

LIST OF ABBREVIATIONS AND SYMBOLS USED

σ_1 - Maximum principle stress

σ_2 - Intermediate principle stress

σ_3 - Minimum principle stress

σ_H - Maximum horizontal stress

σ_h - Minimum horizontal stress

σ_v - Vertical stress

ε - Strain

E - Young's Modulus

τ - Shear stress

K - A correction factor accounting for discrepancies between the internal hydraulic pressure and the output pressure of a flatjack

J - A correction factor accounting for discrepancies between the area of the slot and flatjack

U - Displacement

$\Delta_{C\text{-}D}$ - Closure of the crack between Pins C and D

$G_{C\text{-}D}$ - A factor relating the in-situ stress to the closure and modulus of a setup of a particular geometry

F - Force

φ - Internal friction angle

UCS - Unconfined Compressive Strength

LVDT - Linear Variable Differential Transducer

ASTM International - Formerly American Society for Testing and Materials. As of 2001, ASTM International is the operating name

ISRM - International Society for Rock Mechanics

MTS - MTS Systems Corporation

ACKNOWLEDGEMENTS

I would like to say thank you to all those who help me, my supervisor Dr. Andrew Corkum, and mentors Dr. Pedram Sadeghian, Dr. Hany El Naggar, Dr. Donald Jones and Dr. John Newhook for all their guidance. I would also like to thank the technicians who helped bring my vision to reality, Brian Kennedy, Jesse Keane and Blair Nickerson. June Ferguson and Shelley Parker for their perpetual reminders of important dates without which I would have been lost. My wife Courtney and my family for their kind support. Finally, I would like to thank Halifax Fire Department for saving all my hard work and Pioneer Coal Limited for their contributions and access to their site.

1.0 INTRODUCTION

In-situ stresses are stresses that are pre-existing within the Earth's crust prior to any disruption. These stresses impact the structural integrity of engineering works such as dams, mines, tunnels and oil wells. In addition, the stress field is one factor that controls the direction of crack propagation in rock, an important factor in oil and gas extraction. In-situ stresses are too often only estimated using existing measurements that can be tens to hundreds of kilometers away or by using the depth to determine stress. This means that stresses used in excavation designs may not be representative of the actual environment. In addition, rock stress measurements are often highly variable due to rock mass heterogeneity. A variety of different techniques have been developed to measure these stresses such as overcoring, hydraulic fracturing and back analysis techniques but these methods require the use of specialised equipment and mobilisation of heavy machinery such as a drill rig (Hoek, 2008).

The flatjack test is one of the simplest and lowest cost in-situ stress measurement techniques. It begins by inserting pins into the rock and measuring the initial distance between them. A slot is cut between these pins and their relative displacement is measured. The flatjack is inserted into this slot and pressurized until the pins return to their original location. The fluid pressure in the jack can then be correlated to the stress in the ground. The flatjack was first patented in 1940 by Eugene Freyssinet although the design has since been modified (US patent US 2226201 A). One of the first uses of the flatjack in rock mechanics was by the Mayer, Habib and Marchand in collaboration with Tincelin in 1951 where he conducted a lab test in loaded concrete to determine the theoretical viability of the flatjack test in both the plastic and elastic range (Mayer, Habib, & Marchand, 1951; Tincelin, 1951) Over the next couple of decades this test was used extensively, however, the results were often anomalous, leading people to question the effects of inelastic behavior on the test (Moye, 1958; Hoskins, 1966). In 1966, Hoskin's conducted a laboratory test in which he tested the performance of the flatjack on various types of rock and concrete under known biaxial and uniaxial loads both with and without time allowances for creep. He found the tests to be accurate within the margin of error of his measurements (-1.5% to +5.5%). Despite Hoskin's results, the flatjack test fell out of favor in the rock mechanics field in favor of other tests such as overcoring and hydrofracking due to the following limitations (Amadei & Stephansson, 1997):

1. A flatjack test only measures near surface stresses. Stresses in the near surface can be significantly impacted by topography and, weathering and disturbance (e.g., excavation).
2. A flatjack test only measures stresses in a single direction normal to the cut axis.

Despite falling out of favor in rock mechanics, the flatjack became popular in the 1980's when it was modified for masonry structural evaluation by Palo Rossi (Gregorczyk & Lourenço, 2000). The test remains popular in masonry (ASTM International, 2003; Atkinson & Schuller, 1990; Carpinteri, Invernizzi, & Lacidogna, 2005; Gregorczyk & Lourenço, 2000) because it has significant advantages over other in-situ stress measurement tests such as (Amadei & Stephansson, 1997):

1. Nearly direct measurement of stress value (as opposed to indirect calculation based on strain).
2. Involves a fairly large volume of rock or masonry, reducing sensitivity to small-scale characteristics.
3. Can be used to determine Young's modulus.
4. Relatively straight-forward to execute and interpret results.
5. Cost effective method compared to most others.

While the test is simple in principle, it can be difficult to make a slot that matches the dimensions of the flatjack. Often the jack must be grouted which limits the recoverability of the jack and increases waiting time resulting in a higher test cost. This research hopes to reduce the cost of the flatjack method for in-situ stress testing by using a saw cut that is different in shape to the jack and eliminating the use of grout. The reduced cost and reusability of the modified flatjack test could allow for many measurements allowing for statistical analysis of the highly variable results.

Prior to developing the research section of this thesis, a detailed literature review was completed. In the literature review, the fundamental principles governing stresses were reviewed to ensure a solid foundation to discuss more complex topics. Once a solid foundation was established, the types of stress fields encountered in a rock mass were explained along with the factors that cause in-situ stresses. These stresses have been measured in various locations around the globe and incorporated into the World Stress Map (Heidbach et al., 2008) which was briefly discussed. Observations for estimating stress in the field or in a borehole were examined and prove useful for both setting up measurement tests and validating the results. Then, the different types of stress measurement methods along with their strengths and limitations were examined to demonstrate why the flatjack test is a good candidate to reduce the cost of determining in-situ stresses. The flatjack testing method is then described in detail to provide the reader a detailed understanding of its principles, advantages and limitations. Numerical modeling plays an important role in this thesis and multiple types of numerical modeling was summarised to explain why finite element modeling and specifically Plaxis3D was selected for the modeling components of this thesis.

There are two main research sections in this thesis, (1) a lab component and (2) a field component, each of which incorporate numerical modeling. In the lab component a 2 MN load frame was designed and built to subject a 1 m by 0.8 m by 0.5 m concrete specimen to an axial load on the smallest face. The flatjack test was then conducted on the loaded specimen using a variety of different slot geometries such as plunge cuts, drag cuts and overlapping boreholes. This was done to determine correction factors based on the cancelation pressure for slot geometries that deviated from the ASTM specifications. It was also used to determine if any relationships existed between relative slot area and this correction factor. In addition, closure data of the slot after cutting was examined for each of the slot geometries and a relationship between Young's modulus, closure and axial stress was determined. These closure results were plotted versus the surface area of each slot to determine if a broader relationship existed. The tests conducted in the lab were numerically modeled using *Plaxis3D*[1] to gain further insight into the internal stresses of the sample and to create a validated numerical model. This model set up can then be used with confidence to determine correction factors and closure relationship constants for geometries that were not performed in the lab.

The field component took place in Stellarton, Nova Scotia at Pioneer Coal Limited (Pioneer Coal) open pit. While the flatjack test could not take place in an area of significant in-situ stress, it did demonstrate the variations to the flatjack test explored in the lab could be scaled to the larger flatjacks used in the field. The slot closure for a location at the bottom of the pit in a continuous stratum was used to determine the stress in the pit. This closure was then related to the stress using the method created during lab testing and a numerical model of the slot. This result was then

---

[1] Plaxis3D is a program by the company Plaxis in Delft, Netherlands. It is available for purchase from https://www.plaxis.com/product/plaxis-3d/.

corrected using a numerical model of the open pit to provide the pre-mining state of stress at the location of measurement.

This thesis aimed to show it is possible to reduce the cost of the flatjack in-situ stress test using a saw cut slot and eliminating the use of grout. It is hypothesised that the errors created by the variation between slot shape and flatjack shape can be corrected using a correction factor specific to the slot geometry.

2.0 LITERATURE REVIEW

This literature review aims to inform the reader of the fundamental principles of in-situ stresses, their causes and what influences them. This knowledge emphasises the difficulty of getting a true measure of in-situ stress and some of the many techniques used to do so. This information will help the reader understand why the flatjack was selected to reduce the cost of in-situ stress measurement, how the changes made will affect the test and what its limitations are when used.

2.1 Fundamental Principles of Stress

In-situ stress, also known as far field stress, is the stress naturally occurring within an undisturbed rock mass. Knowing these stresses is important when designing underground tunnels, caverns, mines and large open pits. Stress is a tensor consisting of nine parameters, six of which are independent of each other, shown in Equation 1. These independent tensors define the shear and normal stress in three dimensions shown in Figure 1. In rock mechanics, the convention is to have compressive stress as a positive and tensile stress as a negative. This is opposite to the convention used in other engineering disciplines, and allows geotechnical and mining engineers to work with positive numbers when dealing with rock masses (Hoek, 2008).

$$[\,1\,] \qquad |\boldsymbol{\sigma}| = \begin{vmatrix} \boldsymbol{\sigma_{xx}} & \boldsymbol{\tau_{xy}} & \boldsymbol{\tau_{xz}} \\ \boldsymbol{\tau_{yx}} & \boldsymbol{\sigma_{yy}} & \boldsymbol{\tau_{yz}} \\ \boldsymbol{\tau_{zx}} & \boldsymbol{\tau_{zy}} & \boldsymbol{\sigma_{zz}} \end{vmatrix};\ \boldsymbol{\tau_{xy}} = \boldsymbol{\tau_{yx}}, \boldsymbol{\tau_{xz}} = \boldsymbol{\tau_{zx}}, \boldsymbol{\tau_{zy}} = \boldsymbol{\tau_{yz}}$$

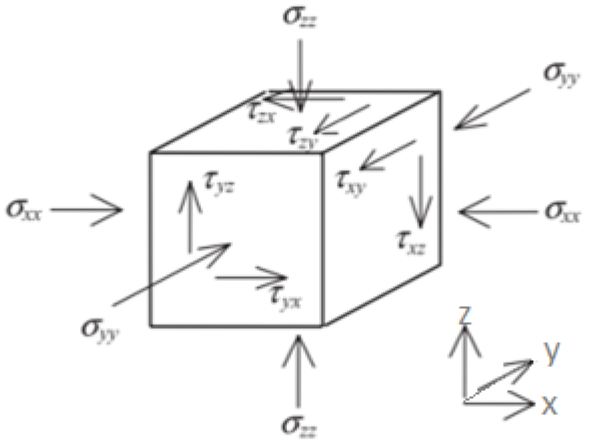

Figure 1: Stress tensor components existing within an infintesimally small cube of any material *(Aiyeru, 2014)*.

There are several properties which are important in the determination of rock stress states. Young's modulus is a value that relates the stress applied to a material to its strain by Hooke's law, as shown in Equation 2. Another important parameter is Poisson's ratio, shown in Equation 3. It is the relationship between the axial compression (strain) and the radial expansion (strain). Although plastic deformation can occur within a rock mass, the flatjack test when carried out properly typically takes place in the elastic region.

[2]

$$\boldsymbol{\sigma = \varepsilon \times E}$$

[3]

$$\boldsymbol{\nu = \frac{\varepsilon_{axial}}{\varepsilon_{radial}}}$$

Another concept important to measuring stress is permanent set hysteresis. Hysteresis is when a body is exposed to a load that deforms it and once that load is remove it returns along a load displacement path to an unloaded state that is different than the original state. A micromechanical model of rock attributes hysteresis to the effects of sliding crack friction (Jaeger, Cook, & Zimmerman, 2009). To explain what sliding crack friction is, consider a sample with many randomly oriented elliptical cracks. An applied compressional stress begins closing these cracks. As the cracks close the Young's modulus increases. When unloaded, the modulus is the intrinsic modulus of the rock, but as the stress decreases cracks with progressively smaller angles relative to the loading direction begin to open thus decreasing the modulus. The hysteresis occurs when there is a lateral confining stress that prevents these cracks from reopening and the friction of the crack stores some of the strain energy resulting in a permanent "set" where the deformation permanent.

2.2 Rock Stress Fields and Their Causes

In-situ stresses are often simplified as the vertical stress, estimated from weight of the rock above, and the horizontal maximum and minimum stress. This concept, however, does not necessarily provide the principle stresses, which could be at an angle relative to the vertical and horizontal, as shown in Figure 2. This simplification is made because many measurement techniques can only measure stress in one or two dimensions and therefore one test cannot provide an estimate for the full in-situ stress field. To get a complete stress field, it may be necessary to take multiple differently oriented measurements to create a system of equations, to solve for the principle stresses.

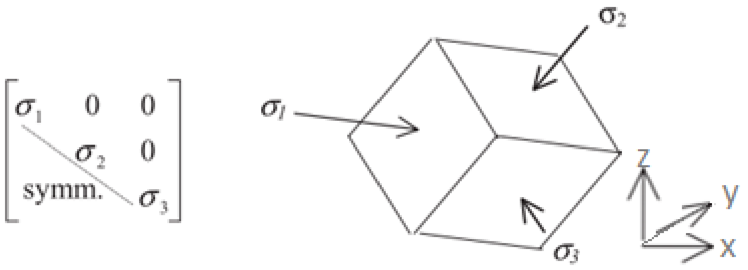

Figure 2: The vertical and horizontal stresses (left) and the principal stresses that correspond to no shear (right) ***(Aiyeru, 2014)*****.**

A variety of different types of stress fields can occur in a rock mass and are outlined in Figure 3 by the ISRM. This Figure shows the types of stress distribution in a rock mass are divided into four main categories; in-situ, perturbed in-situ, structural, and perturbed structural. In-situ stress is broken down into four causes; gravity loading, tectonic, residual and terrestrial. The tectonic stresses are further sub-divided into three different scales of tectonic stresses; first order which are the largest and are on the scale of tectonic plates, second order which is isostasy and on the scale of mountain ranges. Finally, the third order stresses which are the smallest and are on the scale of local faults. These categories are more thoroughly explained in the subsequent sections, however, there is sometimes overlap between them.

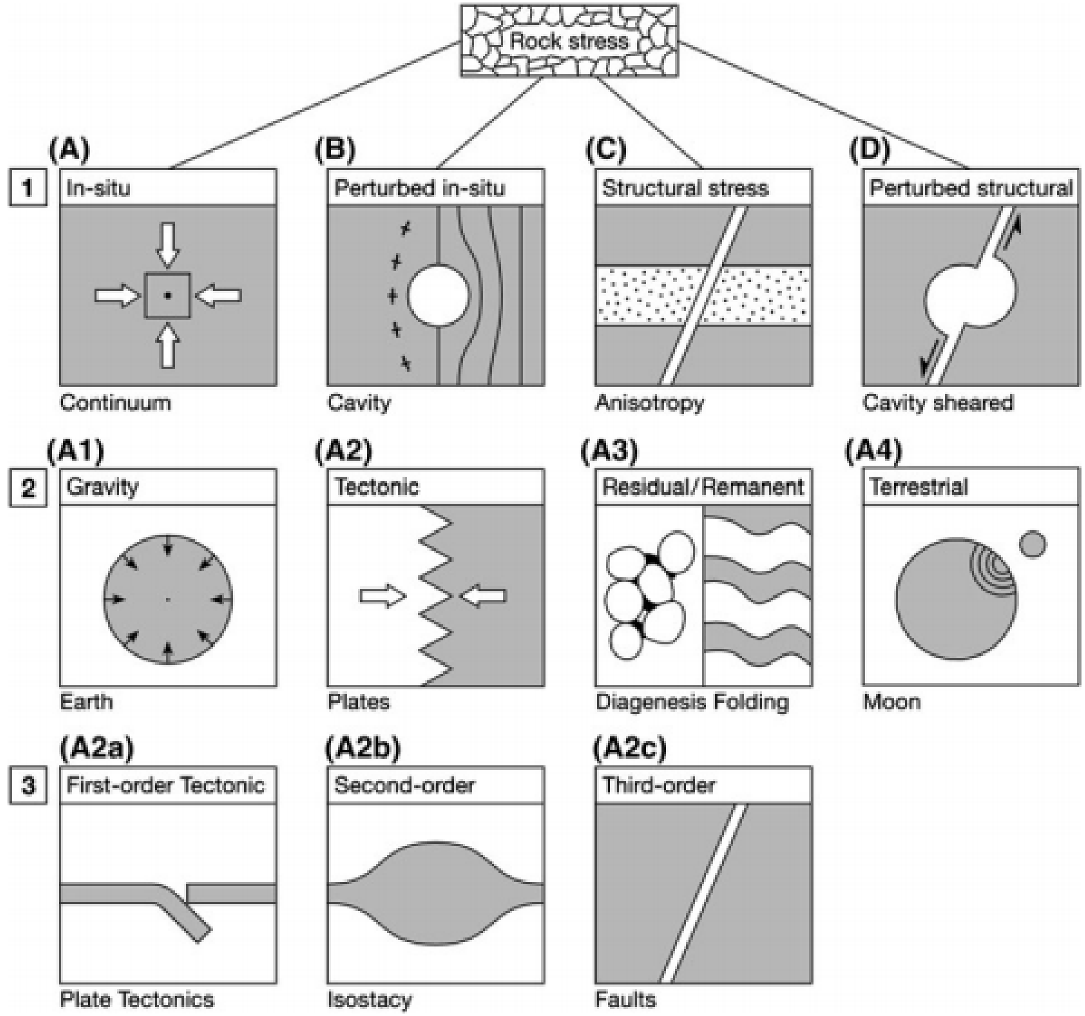

Figure 3: Rock stress scheme and terminology at three hierarchical levels. Level categorises the types of stress fields in a rock mass. Level 2 separates in situ stress components according to their origin forces. Level 3 separates tectonic stresses according to their coherent domains *(Ulusay, 2015).*

2.2.1 Continuous In-Situ Stress Fields

The continuous in-situ stress field is the simplest stress field. It assumes a homogenous and undisturbed rock mass on which a variety of stresses are applied. The possible stress causes are divided into four categories; gravity, tectonic, residual and terrestrial.

Gravity Stress

Gravity plays a large role in causing in-situ stresses, the vertical stress is often approximated as the stress due to the weight of the rock above that point and is relatively accurate, as shown in Figure 4 (left). The ratio between the vertical stress and the horizontal stress is often represented by a capital K. Figure 4 (right) shows this relationship as a function of depth and the value of K is less variable in relation to both depth and Young's modulus with increasing depth.

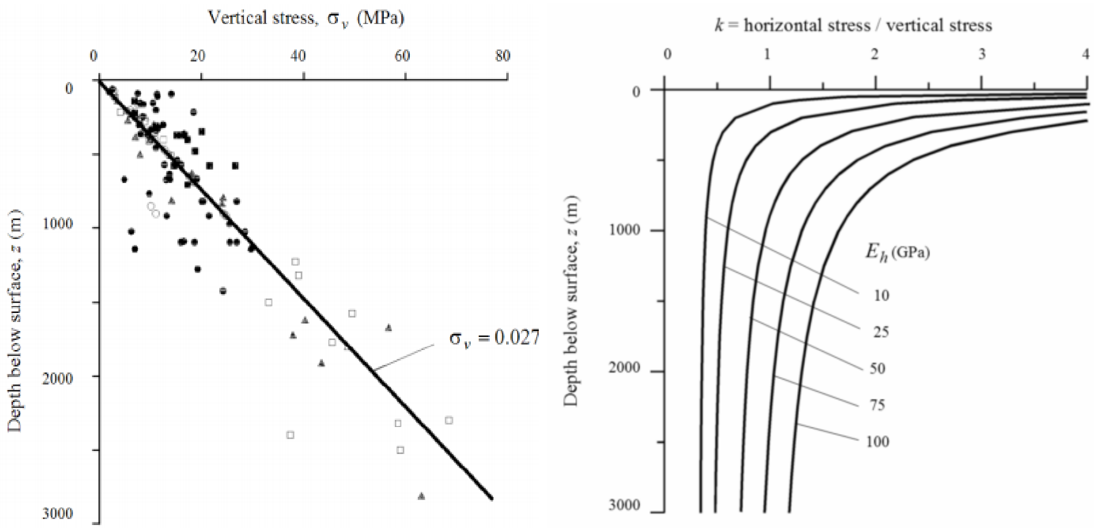

Figure 4: Vertical stress measurements form mining and civil engineering projects from around the world (left) and the ratio of horizontal to vertical stress as a function of depth (right) *(Brown & Hoek, 1978)*.

Tectonic Stresses

Tectonic stresses are stresses caused by tectonic forces in the lithosphere. The ISRM sub-divides tectonic stresses into three orders based on the scale of the influence.

First Order: Plate Scale Tectonic Stresses

The main cause of high horizontal in-situ stresses are the interactions between plate boundaries(M. Lou Zoback & Magee, 1991). The current model of plate tectonics suggests that plate movement is driven by convection currents within the outer mantel (shown in Figure 5).

These currents cause tectonic plates to move, rotate, collide and split apart generating tremendous forces in the crust resulting in horizontal stresses even when vertical stress is low or non-existent.

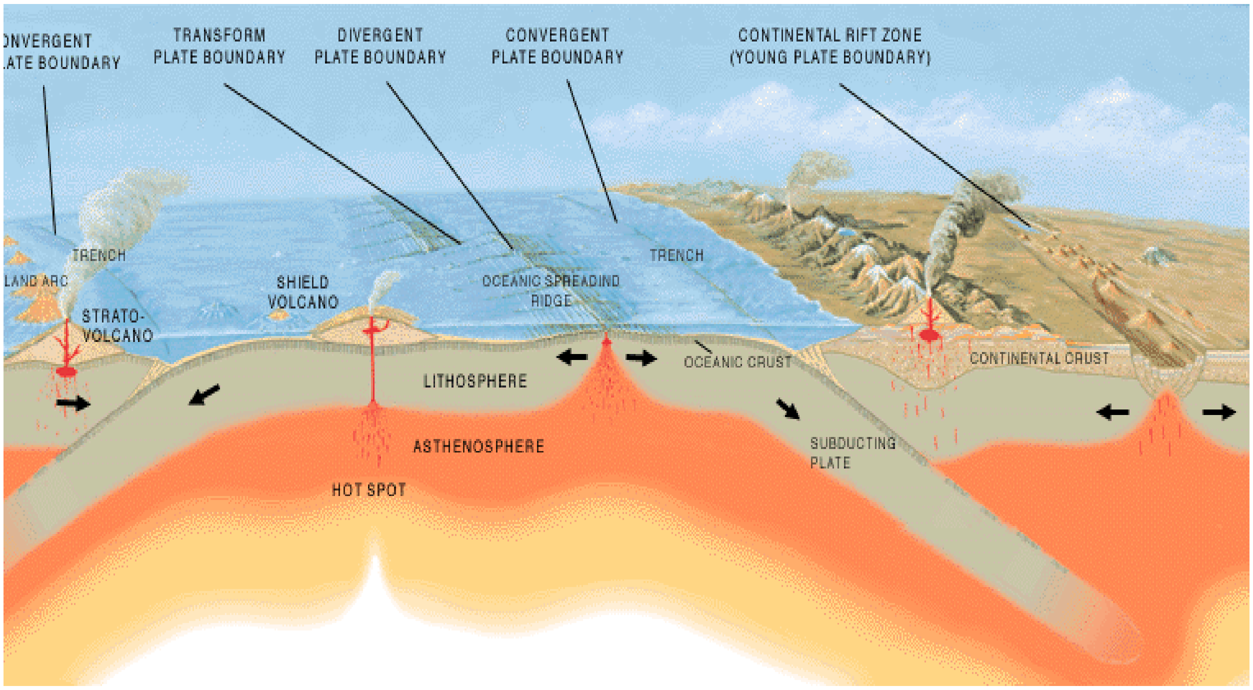

Figure 5: Tectonic plate movement and related geological features *(Simkin, Unger, Tilling, Vogt, & Spall, 1994)*.

Second Order: Isostatic Stresses

Isostasy is the gravitational equilibrium between the Earth's crust and mantle that allows the crust to “float” on the mantel. Both mountain building processes and glaciation can shift this equilibrium so that the bottom of the crust is deeper into the mantel. Rapid removal of material due to erosion can cause uplift. The higher initial stress field coupled with the non-instantaneous transmission of stress within the crust result in high near surface residual horizontal stress once the rock or ice sheet is removed (M. Lou Zoback & Magee, 1991).

Third Order: Fault Stresses

The presence of faulting is caused by the in-situ stress field. According to Fjaer et al. (2008) normal faults typically form when the vertical stress is the highest and the horizontal stress perpendicular to the strike of the fault is the lowest in the stress field. Thrust slip faults are formed when the horizontal stress perpendicular to the strike is the largest and the vertical stress is the lowest. Strike slip faults are formed when the highest horizontal stress is parallel the strike of the fault and the lowest stress is perpendicular to it. This is illustrated in Figure 6 below.

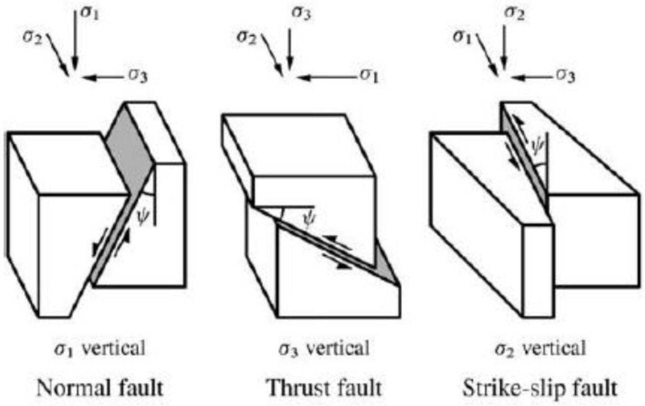

Figure 6: Normal, thrust and strike-slip faults in relation to their respective vertcal and horizontal maximum and minimum stresses *(Aiyeru, 2014)*.

Residual Stresses

Residual stresses are stresses locked in equilibrium inside a free body with tractionless and momentless boundaries (Engelder & Sbar, 1984). In rock this can result from changes in temperature, applied stress that has since been removed of or previous changes to the configuration of the body (R. Holzhausenab & M. Johnson, 1978).

Terrestrial Induced Stress

Terrestrial forces are forces induced in the Earth by the moon and are small relative to tectonic and gravity forces. They are ignored in engineering design (Ulusay, 2015) and are only mentioned to acknowledge their existence but are neglected in the rest of this thesis.

2.2.2 Perturbed Stress Fields

Perturbed stresses are stresses that have been affected by some disruption to the rock mass, this could be alteration of the rock mass due to weathering or removal of material by erosion, tunneling or the creation of an open pit. Weathering, topography and pit effects are examined in the subsequent subsections.

Weathering

Weathering changes the shape and physical properties of the rock near surface. This change does not have one clear effect on the stresses in the ground because the properties that change depend on the type of rock and the environment of weathering. Erosion and rock joints creates a free surface that releases strain thus reducing stress. These openings can be infilled with either precipitate minerals or water that freezes increasing stress. Typical thermal fluctuations due to weather are not large enough to cause significant expansion to change the stress level on the large scale but much larger thermal changes such as the proximity to magma can. Chemical weathering in rock causes alteration of the minerals to a form that is more stable on the earth's surface. These minerals include clay minerals and oxides which expand when forming and cause a volumetric change leading to swelling that can resulting in heaving and raveling or stress increases depending on confinement. Some other minerals are stable on the surface, such as quartz, do not change and minerals such as calcite dissolve leading to voids which release strain (Nelson, 2011).

Topography

Topography relieves horizontal stresses within mountains or ridges. The ridges in Figure 7 can be thought of as the removal of strips of material in one direction. This removal of material has the effect of relieving the horizontal stress perpendicular to the ridges, re-aligning the maximum horizontal stress to coincide with the strike of the ridges and valleys within the ridges.

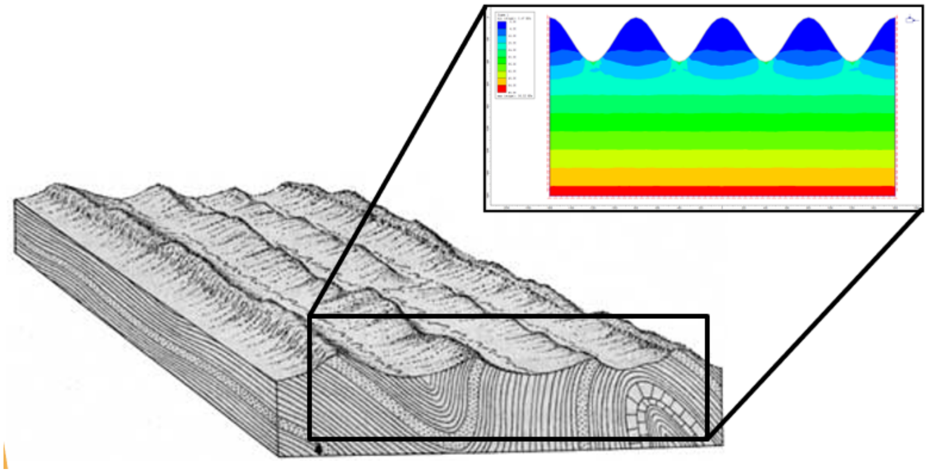

Figure 7: A diagram of a series of ridges and mountains with an inset of the Plaxis2D model showing stress concentration changes with erosion similar to that done by Pariseau *(Matthes, 2006)*.

A simulation was done by Pariseau (1971) and again by Martel (2016) to illustrate the internal stress changes. Pariseau's simulation the initial state of the land mass was assumed to be flat and through a series of seven cuts repeating valleys were cut into the land mass so that the final landmass has a saw tooth shaped series of mountains and valleys. The result of this study found that significant uplift took place throughout the land mass with more uplift in the valleys and less on the mountain tops. The mountain tops had significant stress relaxation bordering on tensile stress while there was stress concentration near the valley floor. The effect of the topography on the stress field was found to extend a similar distance below the valley floor as the height of the mountains. Martel's model used low amplitude sinusoidal hills and found similar results but the effects on the stress field extended deeper relative to the smaller hills.

A more refined model of the experiment performed by Pariseau (1971) was made to help gain further insight into the effects of topography. This model replaced the chevron shape excavations with a rounded sinusoidal pattern to better reflect the real-world hills and eliminate the localised effect of the sharp points in the model. The model was initially set as a flat surface and erosion was simulated by removing seven successive layers. These layers were sinusoidal in shape, equal in period and increasing in amplitude with the peak of each period occurring at the original surface level.

It was found that the tensile stresses in the mountain tops found by Pariseau (1971) were eliminated while the stress concentration at the valley floor remained as shown in Figure 8. Like Pariseau (1971), the effects of the topography were found to be similar with the influence of topography extending below the valley floor equidistant to the height of the mountains. Thus, real-world near surface environments are not accurately modeled by the linear stress gradient due to the presence of residual stress and topography.

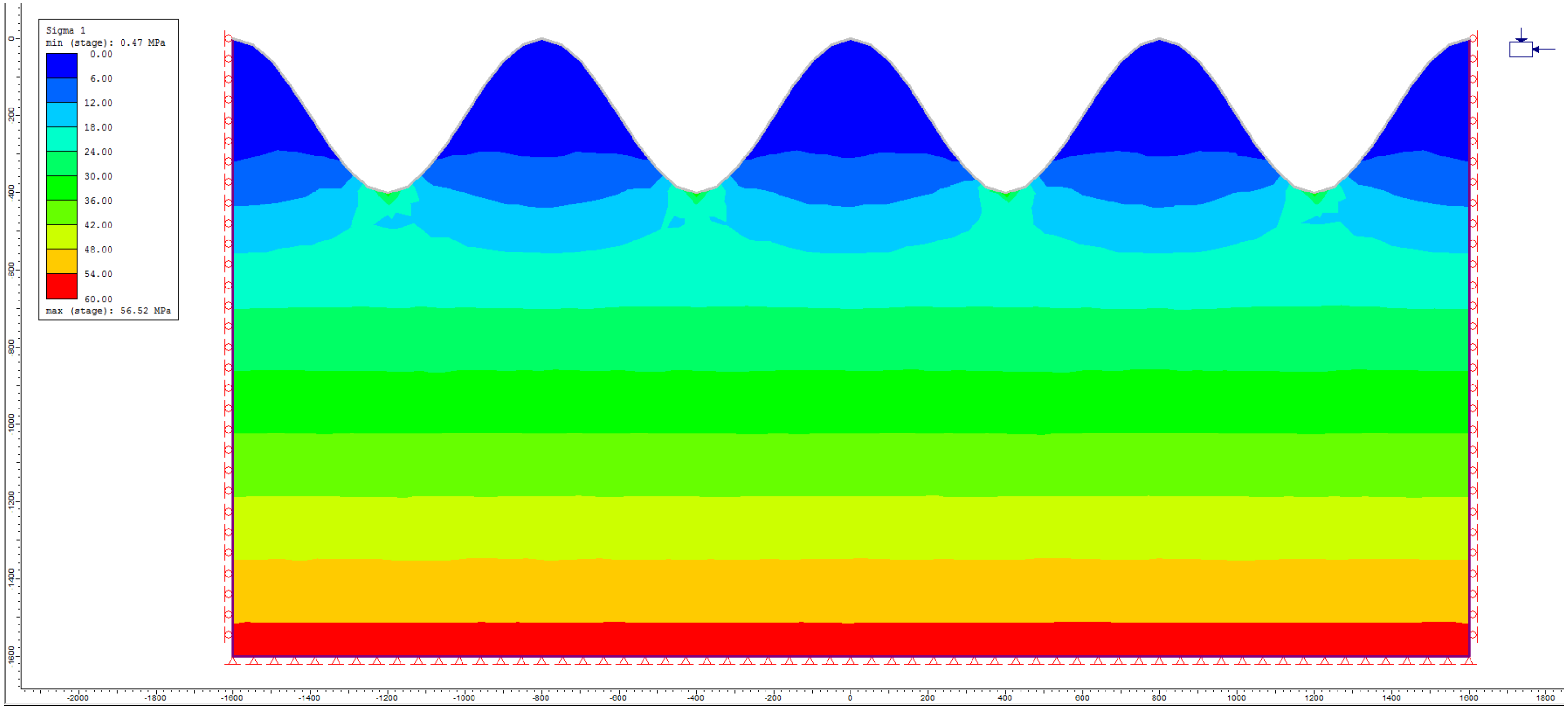

Figure 8: Model representing the erosion of a series of parallel valleys through 7 steps of erosion.

Excavations

Excavations perturb the stress field around their boundaries. In an elastic medium, the stress around circular tunnels can be approximated using the Kirsch equations resulting in the stress distribution shown in Figure 9. More complex shapes often require the use of numerical modeling to determine the resulting stress distribution. This thesis will focus on the measurement of in-situ stress field in the form of an open pit mine so a pit was modeled to predict the effects on the in-situ stress field.

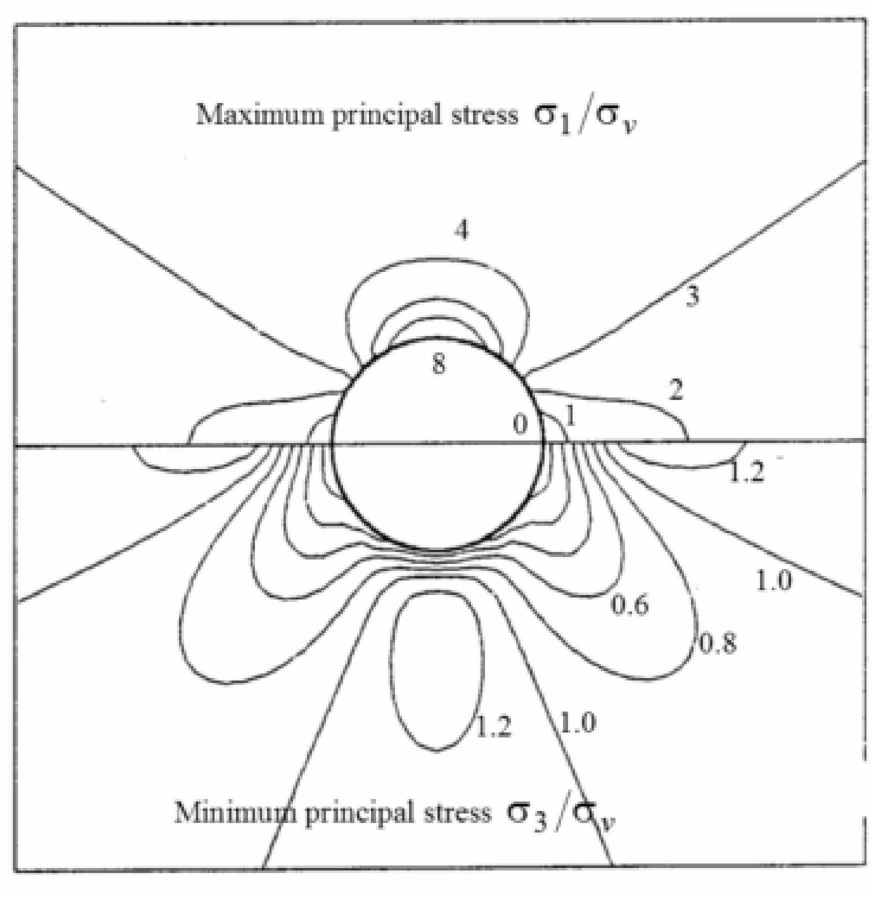

Figure 9: Relative maximum and minimum horizontal stress around a circular opening based on the Kirsch equations (Hoek, 2008).

This model examined the corner effect of benches in an open pit. The model, a 200 m by 200 m footprint open pit in a 1000 m by 1000 m by 500 m block was conducted using the numerical modeling software Plaxis3D. The pit was two benches deep with a bench height of 15 m of and a bench width of 20 m. The horizontal (σ_1 and σ_2) stresses were represented by a K factor of 2 (i.e. twice the vertical stress).

Figure 10 shows the maximum principal effective stress to be concentrated near the toe of the bench while the stress is relaxed near the crest of the bench. The stress concentration near the toe is much more significant than the stress relaxation near the crest. Similar to the maximum principle effective stress, Figure 10 shows the minimum principal effective stress concentrated in near the toe of the bench while the stress is relaxed near the crest of the bench. The stress concentration near the toe is less pronounced for the minimum stress than the maximum stress however the stress relaxation in the crest is more pronounced and is in tension.

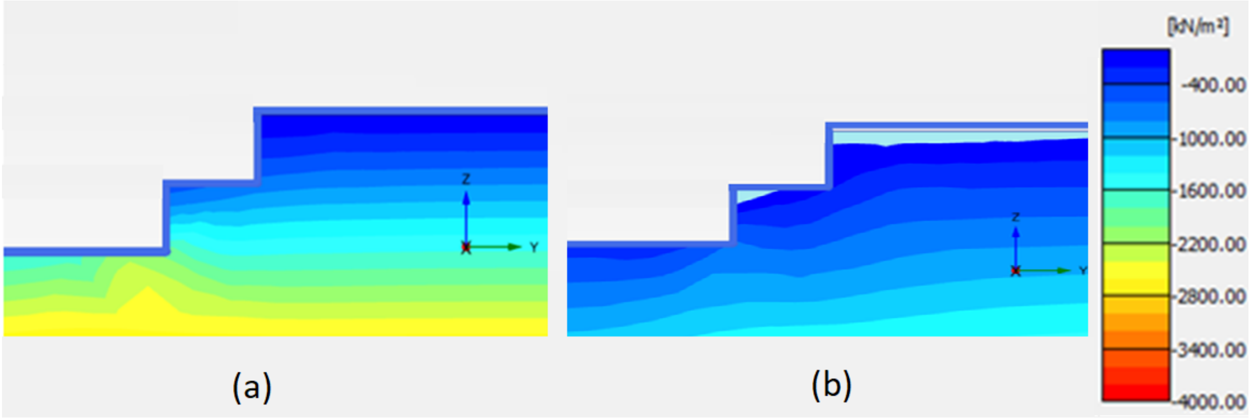

Figure 10: The effect of an open pit on the maximum (a) and minimum (b) principal stresses modeled using Plaxis3D.

2.2.3 Structurally Controlled Stress Fields

Structural features such as joints, bedding or rock of varying material properties can influence the stress distribution in a rock mass. Under equal strain, stiffer rock layers are subject to higher stress than the surrounding softer rock due to their higher Young’s modulus. In addition, joints cause regions of low, or no, shear stress redistributing the stress in their vicinity and the petrogenic history for different stratigraphic layers can contain different residual stresses. The effect of these facts can result in principle stresses that vary in direction and magnitude as a function of depth. Figure 11 shows the borehole breakout direction (minimum horizontal stress) as a function of depth at various locations in the United Kingdom has been graphed by Harper and Szymanski (1991) and demonstrates that not only does the orientation of principle stress change but these orientations can be specific to a particular geologic layers . As seen in the figure the directions of maximum stress can vary significantly with depth, notably between lithographic units.

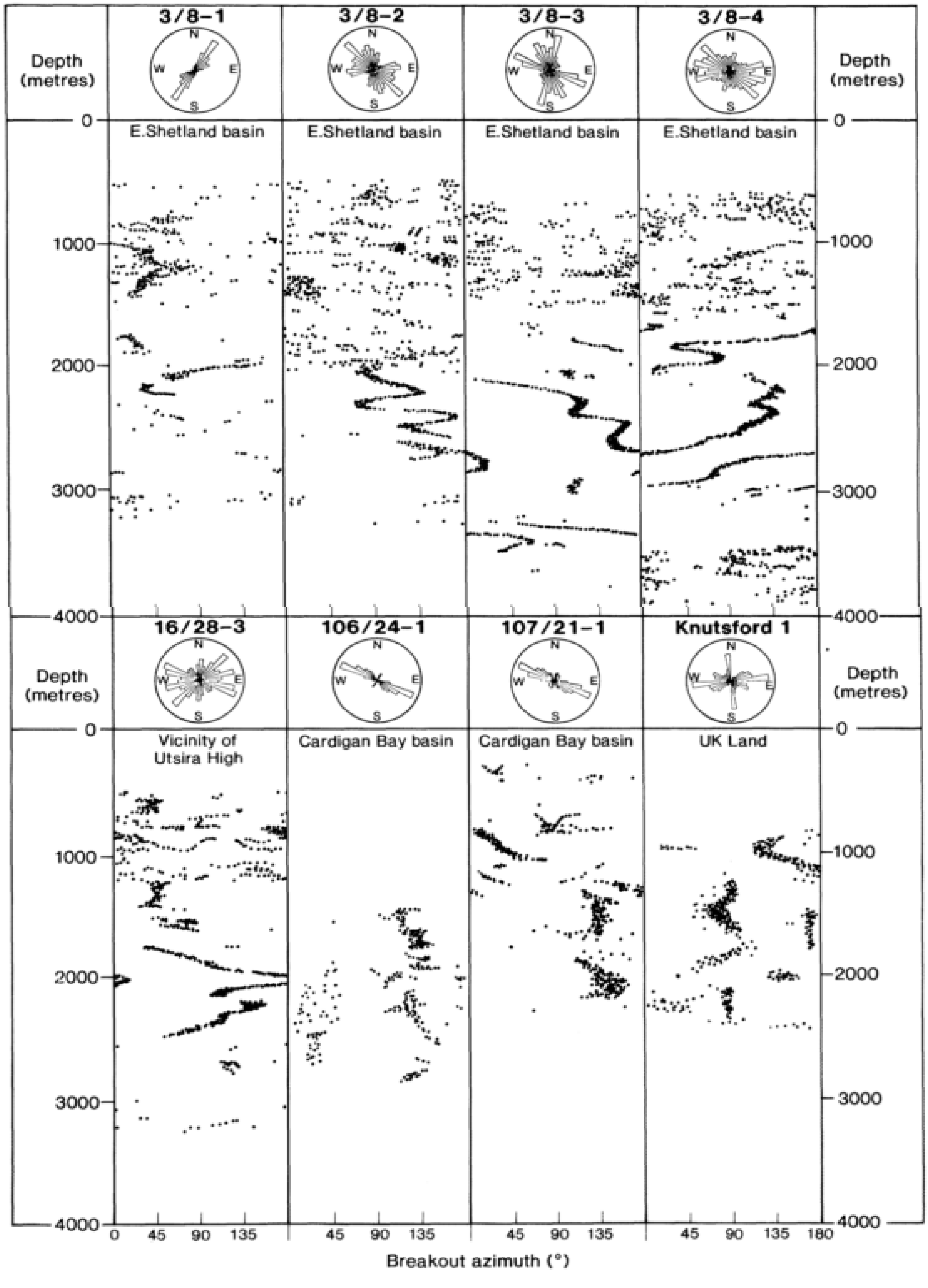

Figure 11: Break out direction with depth for various boreholes in the United Kingdom, the borehole label is at the top of each column. The breakout orientation and by extension the principle stress direction shifts sharply across certain depths *(Harper & Szymanski, 1991)*.

2.2.4 Perturbed Structurally Controlled Stress Fields

A perturbed structurally controlled stress field is a combination of both structurally controlled and perturbed stress fields. This type of stress field cannot be represented by a simple homogeneous model governed by an in-situ stress field and analysis of this type of stress field does not lend itself to closed form solutions of stress. A more detailed analysis is required than the other types of stress fields described here to determine the stress around the perturbation due to the complex rock mass.

2.3 In-Situ Stress Maps

The accurate determination of in-situ stresses is often difficult and expensive (Figueiredo, Lamas, & Muralha, 2010). This analysis resulted in the desire to create a global database of in-situ stresses by collaborating with industry and governments around the world. The results of these efforts is the World Stress Map shown in Figure 12 which is used for studying plate movement and estimation of in-situ stresses (M. Lou Zoback & Magee, 1991).

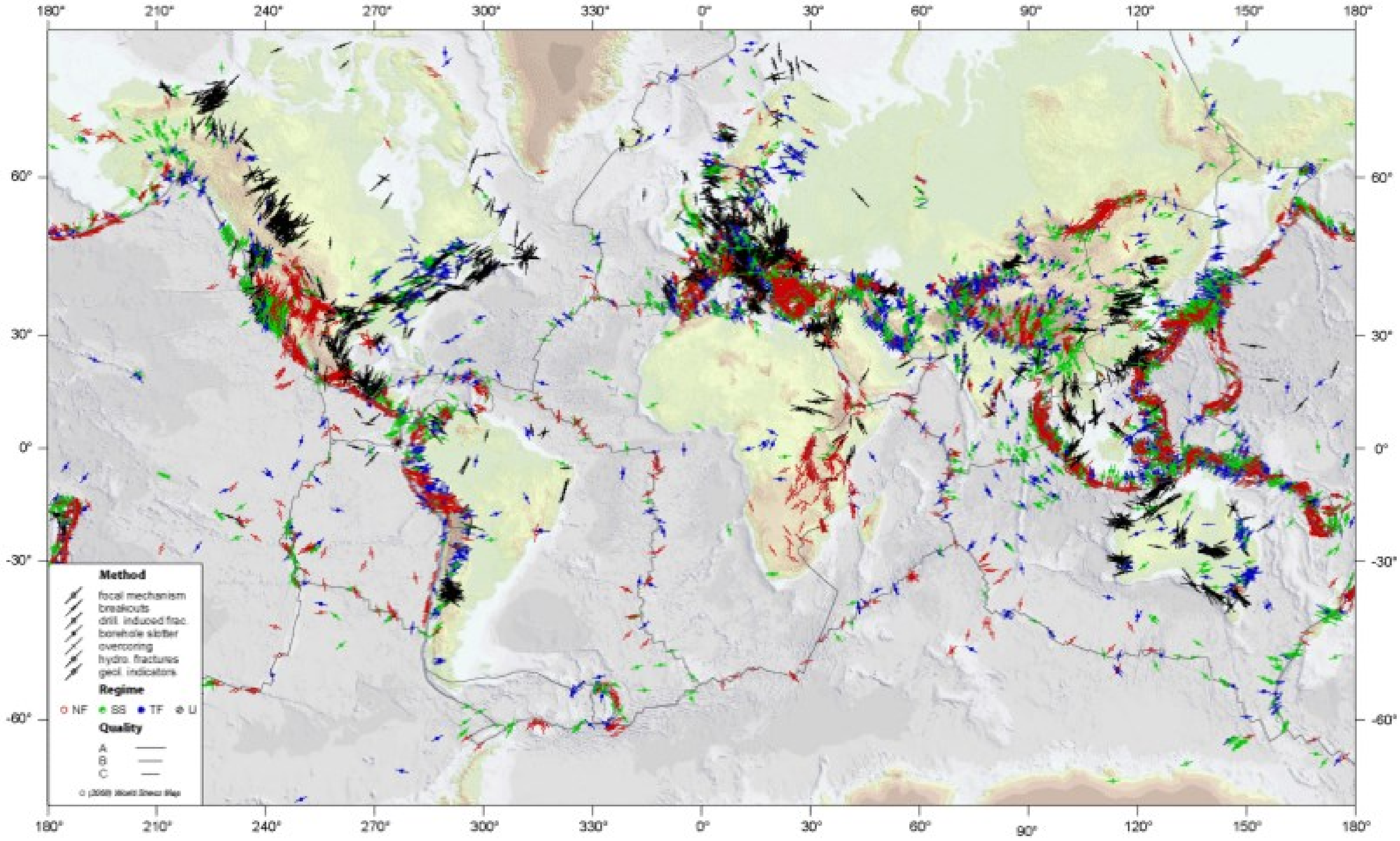

Figure 12: The World Stress Map showing arrows representing the stresses at a specific points on the earths surface *(Heidbach et al., 2008)*.

2.4 Field Observations for Preliminary Stress Estimation

Various field observations can be used to approximate the direction of maximum and minimum horizontal stresses. These observations include valley orientation, the presence of pop ups and folds in the lithographic units. The information obtained from these observations is often inexpensive and therefore attractive as a preliminary method. While field observations can be useful, they do not provide a reasonably accurate magnitude or direction for engineering design, as such they should only be used for an initial estimate of in-situ stresses for positioning further tests or for data validation after performing further tests.

Valley orientation usually coincides with the direction of maximum horizontal stress near the earth's surface. This feature is because the formation of the valley releases stress in the direction perpendicular to it while the remaining ridges maintain some of the existing stress parallel to the valley. This method is qualitative in nature but is usefully for a first estimate when positioning other tests or validating their results. Results of this method are only applicable in the near surface stress field because stress relief does not extend to great depth (Froidevaux, Paquin, & Souriau, 1980).

Figure 13 illustrates a phenomenon known as "pop ups", which are caused when high near surface stress buckle intact surface rock on the free face. This creates a rock ridge that can extend for hundreds of meters along its strike and can have a depth up to several meters (White & Russell, 1982). These pop ups indicate two things about the near surface in-situ stresses, firstly they are high in magnitude and secondly that the highest horizontal stress is oriented perpendicular to the strike of the pop up fold axis. Pop ups are relatively uncommon but in areas where pop-ups occur this feature can be a useful indicator for near surface stresses much like valleys.

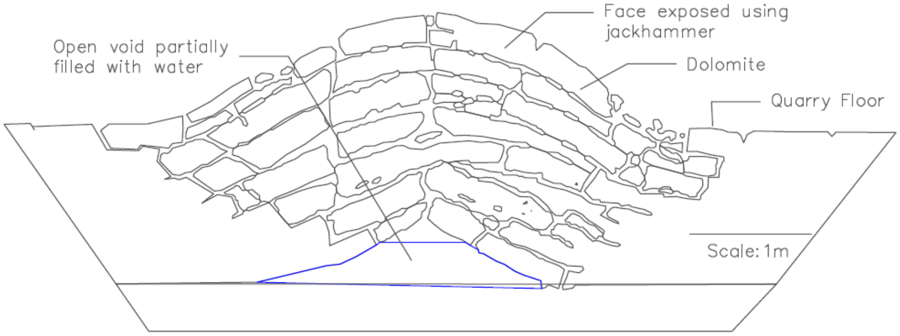

Figure 13: Cross section of a typical pop modified from Roorda (1995).

Folds in the lithography are caused by high in-situ stress. At the time of folding, the major principle stress was oriented perpendicular to the fold axis. This observation can provide the orientation of the maximum principal stress provided the stress field did not change significantly between folding and the present time. In addition, the magnitudes of principles stresses cannot be determined using this method (Yamamoto, 2009).

Diamond drill cores can be useful in predicting in-situ stress fields through observation of features such as those shown in Figure 14. When stresses are sufficiently high, drilling can cause breakouts or deformations in the borehole wall which is useful for not only determining the direction of horizontal stresses, but also demonstrate the horizontal stress is likely high. When measuring only the breakout, the ratio of the maximum to minimum stress can be calculated as shown by M. D. Zoback, Barton, Brudy, Castillo, and Finkbeiner (2003). Measurement of borehole deformations can provide an inexpensive estimation of in-situ stresses (Panek, 1966). Heterogeneity in the rock mass can affect results in both methods (Harper & Szymanski, 1991). Another useful observation that can be obtained from boreholes is the presence spalling (disk like sections) core in competent rock. Spalling indicates very high in-situ stresses but provides no information on the orientation but is reported to occur only in competent rock (Eberhardt & Stead, 2011).

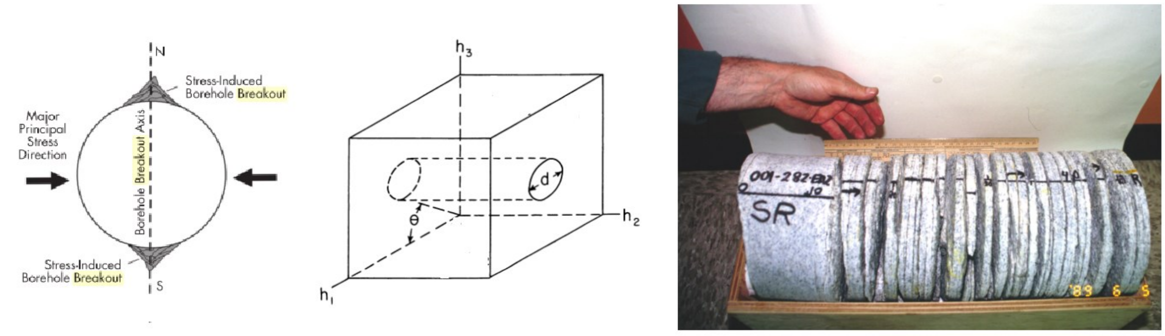

(a) (b) (c)

Figure 14: Three Pictures showing (a) breakouts *(Eberhardt & Stead, 2011)*, (b) deformation (Panek, 1966), and (c) disking *(Hoek, 2008)*.

2.5 Rock Stress Measurement Methods

There are many methods to measure the in-situ stress in a rock mass and these methods are continuously being improved (Mortazavi & Saati, 2016) (Nezhadshahmohamad & Moosazadeh, 2015) (Dongshen et al., 2015). This section summarizes some of the more popular methods of in-situ stress measurement, how they are preformed and some of their advantages and disadvantages.

2.5.1 Overcoring

The overcoring method of in-situ stress determination involves drilling a hole to the depth of the desired measurement. Then a smaller diameter bit is used to drill out a smaller hole at the bottom of the original borehole. Strain gauges are then attached to the walls of the smaller hole using a Council of Scientific and Industrial Research (CSIR) or United States Bureau of Mines borehole deformation gauge (USBM) type cell or the bottom of the hole using a doorstopper type cell and an overcoring bit (the same diameter of the original bit) is inserted into the hole. The overcoring section is then extended beyond the depth of the strain gauges. During this process shown in Figure 15, the strain caused by the release of the in-situ stress due to overcoring is measured and recorded. The sample is then retrieved and the modulus of elasticity is determined from it in the lab. Finally, the in-situ stresses can be determined using Hooke's law (Ljunggren qt al. , 2003).

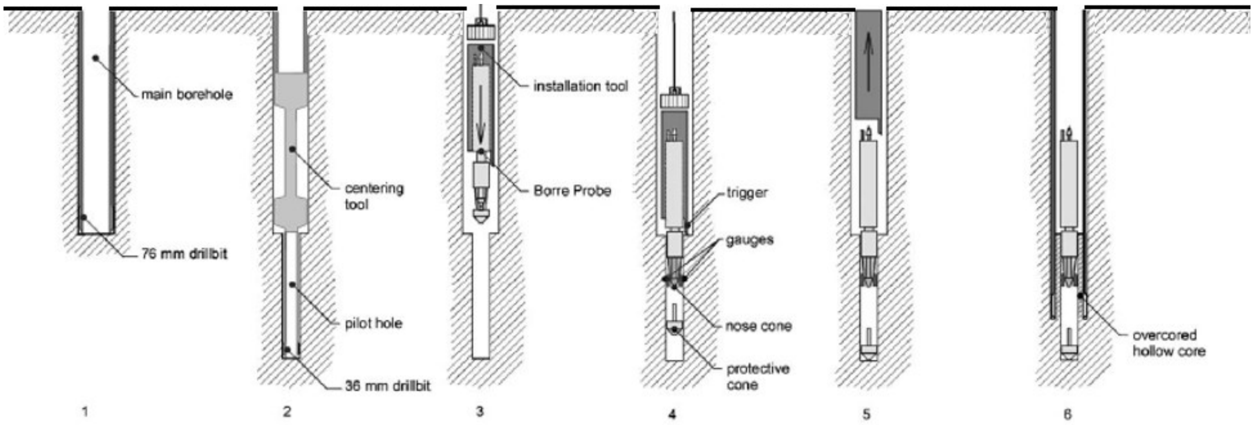

Figure 15:The step by step process of overcoring using a USBM gauge *(Hoek, 2008).*

This method is recognized as being the most direct method of in-situ stress measurement as well as being able to resolve 3D stresses (Eberhardt & Stead, 2011). The use of strain gauges allows for the recording of time dependent strain release as overcoring takes place and placement of several strain gauges allows for multiple readings (Vreed, 1981). Furthermore the 3D stress field can be determined from just one sample (Vreed, 1981). However, overcoring is relatively difficult to perform at depths less than 15m or in areas with fracture spacing less than 13cm (ASTM International, 2005). In addition, the strain gauge can be difficult to adhere to the borehole wall (Kim & Franklin, 1987) and large grain sizes can affect the reading due to the small size of the strain gauge (Christiansson & Janson, 2003). The determination of Young's modulus is done in a lab with core samples; while lab results gives a good result for an intact specimen, it may not be representative of the rock mass (ASTM International, 2005).

2.5.2 Hydraulic Fracturing

Hydraulic fracturing makes use of the principal that the confining pressure around a borehole is less in one direction. Therefore, under uniform pressure the rock will deform the most in that direction causing a fracture perpendicular to the minimum stress. To perform a hydraulic fracturing test, a section of the borehole in unfractured rock is selected and isolated by packers from the rest of the borehole as shown in Figure 16. This section is then pressurized with fluid until the pressure begins to drop, indicating the formation of a fracture. The pump is then turned off and the pressure is monitored until the rate of pressure drop decreases indicating the closing of the fracture, also called the shut-in pressure. This process is then repeated to obtain the fracture re-opening pressure and additional shut in pressure values; additional repetitions can be done, but are often found to be redundant. The directions of the maximum and minimum horizontal stresses are determined by the orientation of the fracture, which is parallel to the maximum horizontal stress and perpendicular to the minimum horizontal stress. The magnitude of the minimum stress is assumed to be the shut-in pressure while the maximum horizontal stress is determined by Equation [4] (ASTM International, 2009).

$$\boldsymbol{\sigma_H = T - 3\sigma_h - P_{c1} - P_0} \qquad \textbf{[4]}$$

Where σ_H = Maximum normal stress

σ_h = Minimum normal stress

T = Tensile strength of the rock

P_{c1} = Break down pressure at the test horizon

P_0 = Fluid pressure at the test horizon

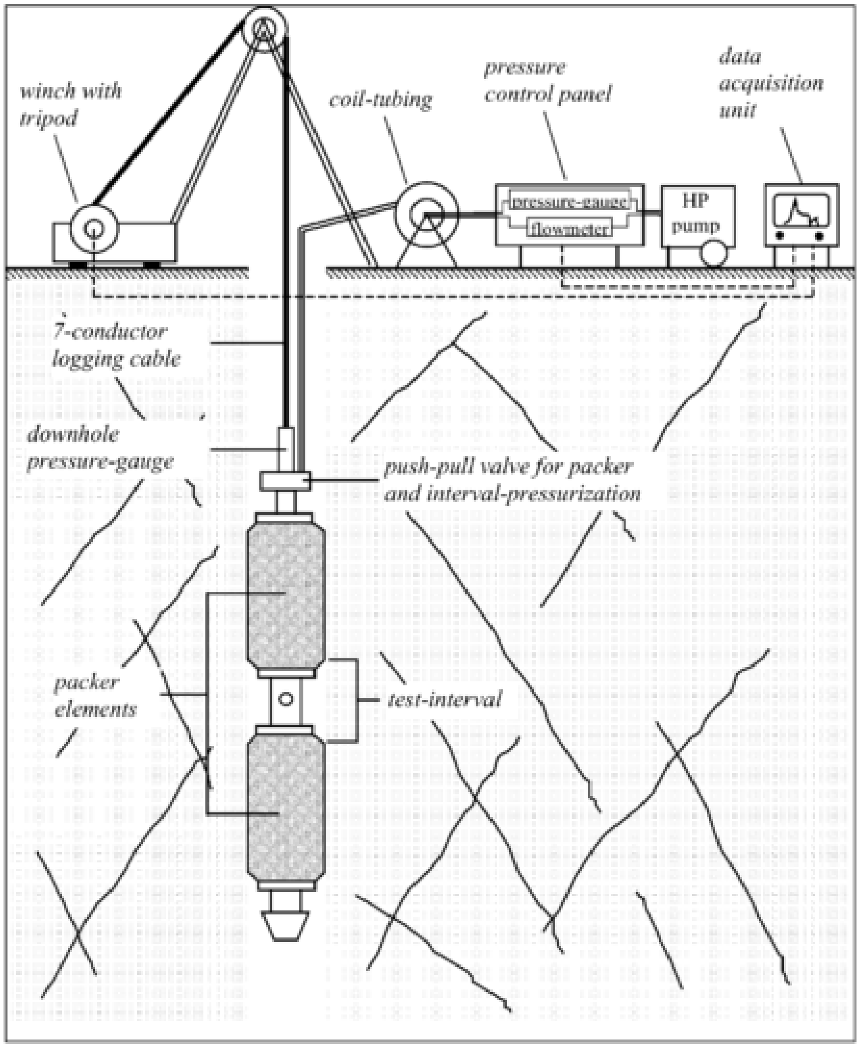

Figure 16: A simplified hydraulic fracture set up where pressure is increased between the packers until a fracture is initiated *(Rummel et al. , 2002)*.

Hydraulic fracturing is a well understood method and is a widely accepted choice for in-situ stress measurement (ASTM International, 2009). It can be performed at great depth and directly measures the minimum stress normal to the borehole. This method relies on the assumption that the fracture initiated perpendicular to the normal stress and not along some natural plane of weakness in the rock such as schistosity. While this assumption is only an issue in some types of rock, the determination of the maximum horizontal stress by Equation [4] is done for all tests and only provides an estimation of the maximum horizontal stress not a direct measurement. Finally, borehole hydraulic fracturing measurements are required in three different orientations to determine the 3D stress field.

2.5.3 Modified Hydraulic Fracturing

The use of hydraulic fracturing for deep in-situ stress measurement have led to many attempts to improve the technique with varying degrees of success. One method, instead of using an unfractured section of rock, uses a section with fractures that have known orientations. The pressure reopens the existing fractures which allows for the determination of stress that is perpendicular to the fracture surface. This process is repeated along different sections of the borehole with differently oriented fractures. From this sequence of measurements, the 3D stress field can be determined using only one borehole. While this method is excellent in theory it relies on having a specific density of cracks since too many or too few cracks make the test impossible. These cracks need to vary in orientation and the orientation must be measured which can be difficult when they are tightly closed or strong foliation is present (Serata et al., 1992).

Another promising variation is the double fracture technique developed by Serata et al. (1992). This method contains the fracking fluid within a membrane. The membrane acts on the borehole walls uniformly much like hydraulic fracturing and initiates a fracture perpendicular to the minimum normal stress. Due to the geometry of the borehole wall and the first crack, the membrane then acts in the direction perpendicular to the initial fracture which is the direction of maximum principle stress as shown in Figure 17. The increasing pressure eventually initiates a fracture perpendicular to the first and the pressure in the membrane is released. The process is repeated several times to get the reopening pressures for both sets of cracks. The pressure vs.

dimetral deformation graph can be analyzed to get the maximum and minimum normal stress. Their orientations can be determined by using an imprint on the outer side of the pressure membrane or by using a borehole scope, both of which can be difficult to assess due to the small size of the cracks formed. Despite the promising results of this method it remains underutilised and therefore information on its reliability, accuracy and cost are not well defined (Serata et al., 1992).

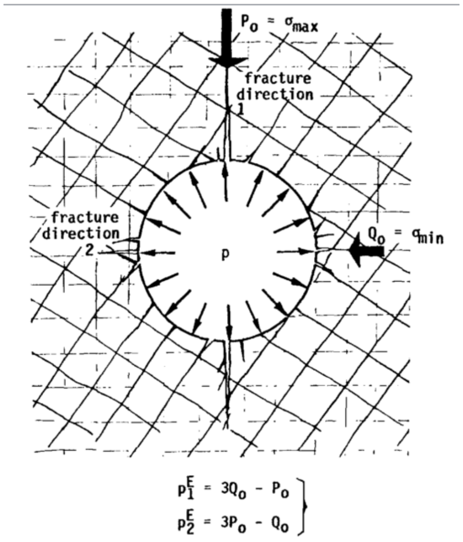

Figure 17: The fractures caused by the double fracture technique. The larger fracture is the first to form and is perpendicular to the minimum normal stress. The smaller fracture is formed 90° relative to the first fracture (Serata et al., 1992).

2.5.4 Cylinder Jacking

Cylinder jacking uses a jack to initiate a fracture in a chosen plane in a borehole as seen in Figure 18. Strain gauges in the jack record the tangential strain change perpendicular to the crack orientation. This measurement is then repeated in two different orientations so that the maximum and minimum stresses normal to the borehole can be calculated. This method allows the user to select the orientation of the measurement helping to offset the effect of anisotropy associated with other fracturing methods. The main technical issue with this method is that varying diameters between the contact plate and the borehole wall can lead to contact issues. It was also found that if the ratio of in-situ stresses perpendicular to borehole wall was greater that 3:1 then the test was invalid (Yokoyama et al., 2014).

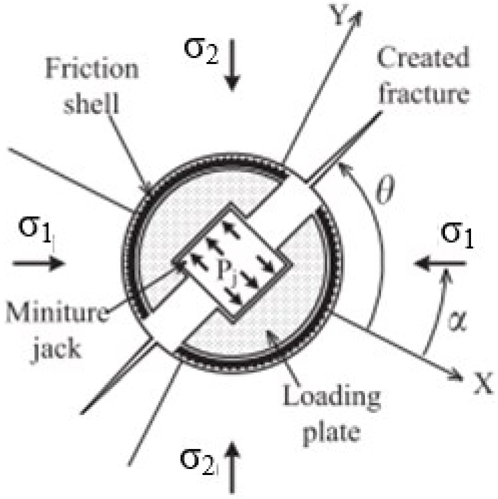

Figure 18: A cylinder jack set up and the maximum and minimum normal stress components σ_1 and σ_2 (Yokoyama et al., 2014).

2.5.5 Slot Cutting

Slot cutting, shown in Figure 19, uses a probe equipped with several frictional strain gauges around its circumference and a diamond saw. The probe is inserted into a borehole and the strain gauges are applied to the borehole wall. The strain is then recorded and the diamond saw portion of the probe makes several cuts between the strain gauges. The change in strain can then be compared to a standard to determine the stresses normal to the borehole. This method has the advantage of being fully reusable and provides multiple cuts and measurement points that can be used to validate the data. Furthermore, the 3D stress field can be determined by a single borehole with 6 differently oriented cuts. The reusability of the friction strain gauges can however result in slipping during measurement and the method assumes continuous homogeneous rock with deviant rock requiring numerical analysis (Corthésy, He, Gill, & Leite, 1999).

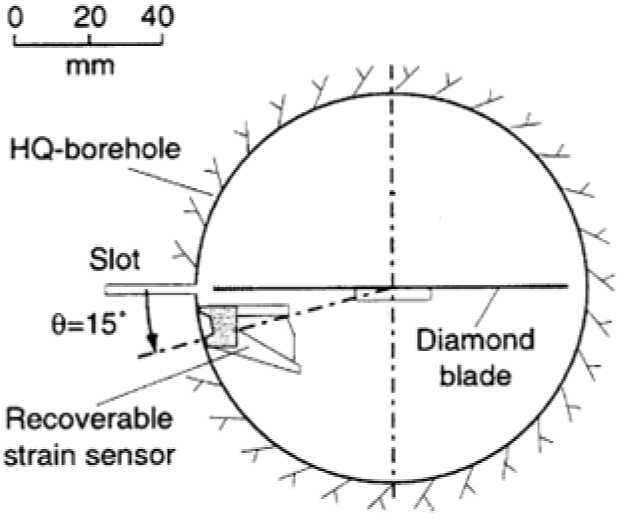

Figure 19: Cross Section of the borehole slotter (Ljunggren et al. 2003).

2.6.6 Back Analysis

In back analysis, holes are drilled ahead of an advancing drift and strain gauges are installed. The drift is driven past the strain gauges and the resulting strain is recorded. Using the strain, the stress can be determined using Young's modulus. This method has the advantage of including a large sample area giving a result that is more representative of the stresses in the rock mass rather than being beholden to material properties in a small area around a single or rosette of strain gauges (Eberhardt & Stead, 2011). The main disadvantage with this system is that a drift must be driven meaning construction must have begun or a test drift was driven incurring significant cost.

2.5.7 Focal Methods

Relationships between occurrences of fault slips and the state of stress have been made by correlating the magnitude of stress to data from earthquakes. While it is possible to use the method to estimate the directions of principle stress, earthquakes often occur at great depth often below the depths which engineering projects take place and are therefore of little engineering use (Ljunggren et al., 2003).

2.5.8 Acoustic Methods

Acoustic methods use the Kaiser effect to estimate in-situ stress. The Kaiser effect is when a rock is loaded there is a significant increase in the acoustic emissions once the applied load exceeds the previous load to which the rock was exposed. It is thus possible to determine the maximum load that a rock was exposed to by stressing a rock sample until there is an increase in acoustic emissions (Ljunggren et al., 2003). The main downside of this technique is that the maximum stress the rock was exposed to may not match the modern day in-situ stress (Holcomb, 1993).

2.6 Flatjack Testing Methodology

The flatjack technique, the subject of this thesis, is less popular than overcoring, hydraulic fracturing and slot cutting but does have some promising advantages. It is a simple method, shown in Figure 20 where a series of six pins is inserted into the rock on a prepared surface, then the distance between the pins is measured. A slot is then cut between the middle pins and the movement between the pins due to the stress relief is measured. A flatjack is then inserted into the slot and is pressurized until the pins return to their original location. The internal fluid pressure required to do this is directly proportional to the stress in the ground and is related by the factor K in Equation [5] (ASTM International, 2008). Factor K is provided by the flatjack manufacturer and its value is specific to each jack.

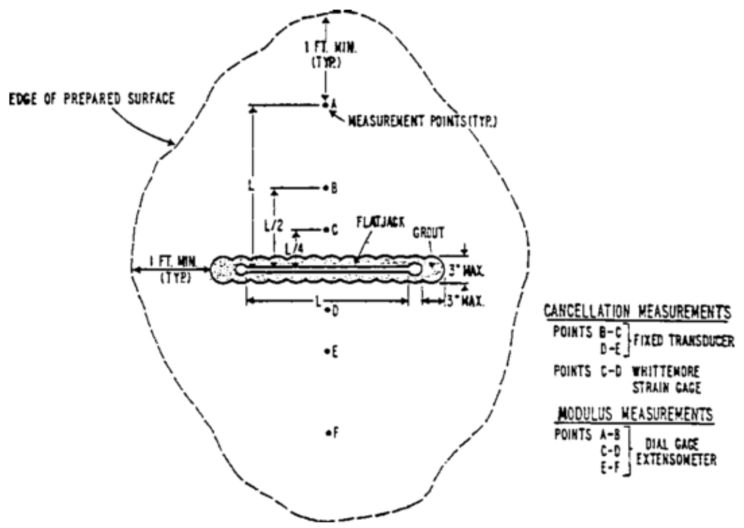

Figure 20: The ASTM international setup for a flatjack. The slot in this example is created using overlapping boreholes (ASTM International, 2008).

[5] $$\sigma = KP$$

The flatjacks to be used are square having an edge of no less than two feet (0.6 m) according to the ASTM standard test procedure and the slot must extend no more than three inches beyond the edge of the flatjack. The top of the flatjack must be at least three inches below the prepared surface. Although this is the standard, there is a specific note in the ASTM procedure for flatjack testing that variation in flatjack shape and size is allowable for specific applications. The creation of the slot can be done by either overlapping drill holes which produces a very rough but square hole or by saw cutting which produces a smooth slot with a variety of possible slot shapes all with rounded corners as shown in Figure 21.

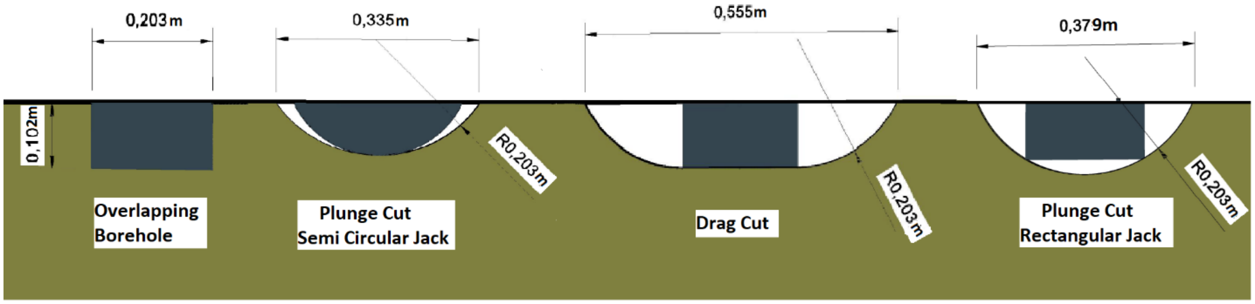

Figure 21: Various types of slots that can be made with overlapping borehole and with a saw. The shaded area within the slot shows flatjack location and shape

Mortar is recommended to secure the flatjack when the surface is rough to prevent deformation and movement. It was found by Gregorczyk & Lourenço (2000) that carbon paper could be inserted between the flatjack and the slot wall and a light pressure applied to determine how well the flatjack was making contact. In their tests, they found that the saw cut was sufficiently smooth that mortar was not required while overlapping boreholes required mortar. The use of mortar makes the flatjack difficult to recover and therefore the cost of the test increases significantly. In addition, the overlapping hole method is much more time consuming while a saw cut is quick and effective. The disadvantage with the saw cut is that it can be difficult to get a deep cut and the rounded corners require a non-square flatjack or the slot to extend more than three inches from the flatjack which deviates from the ASTM.

The flatjack test directly measures the in-situ stress perpendicular to the slot. This is extremely beneficial because the field conditions at the time of measurement are entirely captured in the stress determination because it is performed solely in the field. Errors associated with determining Young's modulus on a lab specimen instead of the rock mass and indirectly calculating the stresses are eliminated. In addition, the large size of the flatjack eliminates the impact of large individual grains on the test and allows for testing in fractured rock.

One of the major drawbacks to the flatjack technique is that it is limited to the near surface testing or testing in tunnel walls. Not only does this limit where it can be performed but it also locates the test in areas where there can be significant blast damage or heavy weathering (Palmström & Singh, 2001). This damage to the rock can release some of the in-situ stress resulting in inaccurate magnitudes or directions of in-situ stresses. The prepared surface helps eliminate some of this uncertainty but blast damage can extend several feet into a surface making it difficult to be confident of results in areas of significant blast damage (Hoek, 2008).

Since the flatjack only restores the stress perpendicular to the slot, the lateral and shear stresses are not restored. This outcome can cause issues when the flatjack is not aligned with a principal stress. This effect can be mitigated by using field observations and the world stress map to provide an initial first estimate of the principle stress orientation. Three tests are required to determine the horizontal principle stresses and the ASTM recommends using Alexander's method to determine the in-situ stresses as shown below(ASTM International, 2008).

[6]

$$\boldsymbol{W_0 = \frac{SC}{E}\left\{(1-v)\left[\left(1+\frac{Y^2}{C^2}\right)^{\frac{1}{2}} - \frac{Y}{C}\right] + \left[\frac{(1-v)}{\left(1+\frac{Y^2}{C^2}\right)^{\frac{1}{2}}}\right]\right\}}$$

[7]

$$\boldsymbol{W_1 = \frac{SY_0}{E}\left\{(-2v)\left[\left(1+\frac{Y^2}{C^2}\right)^{\frac{1}{2}} - \frac{Y}{C}\right] + \left[\frac{(1+v)}{\left(1+\frac{Y^2}{C^2}\right)^{\frac{1}{2}}}\right]\right\}}$$

[8]

$$\boldsymbol{W_2 = W_1\frac{Q}{S}}$$

[9]

$$\boldsymbol{W = W_0 + W_1 + W_2}$$

Where:

W_0 = Displacement on one side of the slot during cutting an infinitely thin slot (mm)

W_1 = Displacement on one side of the slot due to a slot of finite width slot (mm)

W_2 = Displacement on one side of the slot due to biaxial stress. (mm)

S = Rock stress perpendicular to the jack (MPa)

Q = Rock stress parralel to the jack (MPa)

C = Half length of the slot (mm)

Y = Distance from measuring point to the centerline of the slot (mm)

Y_0 = Half width of the slot (mm)

E = Young’s modulus (GPa)

ν = Poisson’s ratio of the rock mass

The deformation due to the flatjack is given by

[10]

$$\boldsymbol{W_J = \frac{PC_0}{E}\left\{(1-v)\left[\left(1+\frac{Y^2}{{C_0}^2}\right)^{\frac{1}{2}}-\frac{Y}{C_0}\right]+\left[\frac{(1-v)}{\left(1+\frac{Y^2}{C^2}\right)^{\frac{1}{2}}}\right]\right\}}$$

Where:

W_J = Displacement on one side of the slot from the flatjack

P = Pressure in the flatjack (MPa)

Co = Half length of the jack (mm)

To determine the modulus of the rock mass we evaluate at the when the displacements cancel (W=Wj) also known as the cancelation pressure. When measurement is made on one side of the slot the modulus is given by the following equation.

[11] $$\boldsymbol{E = \frac{PLR}{2\pi(\Delta Y)}}$$

Where:

L = Distance between the two measurement points

R = Stress distribution factor

Delta Y = Deformation between 2 measurment points.

[12] $$\boldsymbol{R = \left(A_q + \sin A_q\right) - \left[v\left(A_q + \sin A_q\right) + \left(A_z + \sin A_z\right) - v\left(A_z - \sin A_z\right)\right]}$$

Where: A and A_z are shown in .

When deformation is measured across the slot, the modulus is given by the equation

[13] $$\boldsymbol{E = \frac{KP}{\Delta Y}}$$

Where K is a correction factor for the geometry of the test.

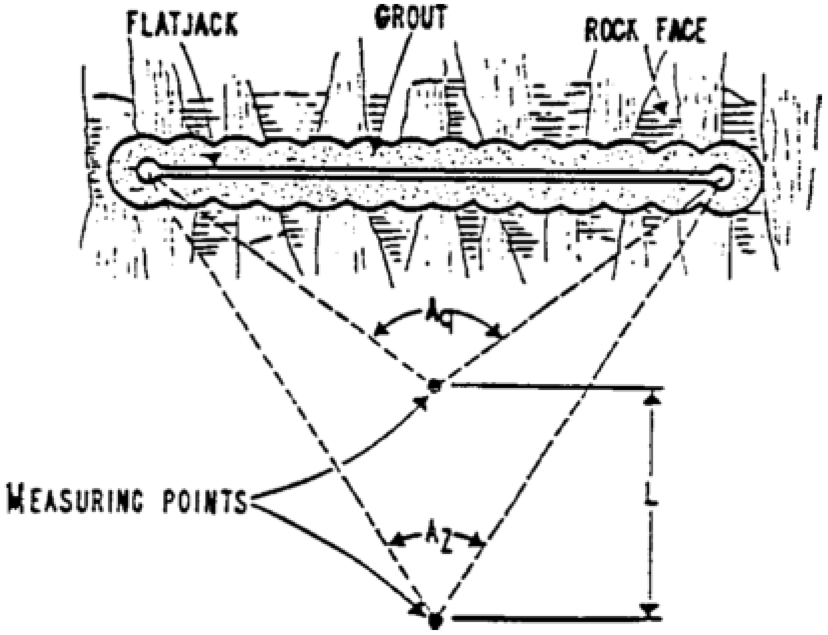

Figure 22: Dimension relative to the flatjack for use in Equation [12] (ASTM International, 2008).

2.7 Numerical Modeling

Numerical modeling methods use the principle of dividing a complex real-world situation into discrete sections that are relatively easily solved. The smaller these sections are, the more accurate the solution as system approaches the continuous solution. These methods are frequently used to deal with complex situations where close form solutions are either impractical or impossible. There are several different types of numerical modeling techniques, including but not limited to, finite element method, finite boundary method and distinct element method.

2.7.1 Finite Boundary Method

Finite boundary methods are frequently used in tunnel analysis. In this method, all boundaries are divided into elements. These include tunnels, rock types, fault boundaries, etc. and the surrounding rock mass is considered infinite. The resulting models can be solved by one of, or some combination of, the following three methods; 1) indirect (fictitious stress) which applies fictitious stresses to satisfy the boundary conditions and then uses them to calculate displacement and actual stress, 2) direct in which the results are calculated directly, and 3) displacement discontinuity which the fundamental solution of an elongated elastic slit superimposed with the shear and normal displacements of that slit (Hoek, 2008)

2.7.2 Distinct Element Method

Distinct element models such as the program Flac3D use solid blocks that interact with one another. These blocks can collide, slide past one another, support each other and depending on the program even fracture. This type of modeling excels at modeling fractured rock masses and rock failure along grains boundaries (Hoek, 2008).

2.7.3 Finite Element Method

Finite element modeling sub divides a system into a series of nodes, each of which is connected to its neighboring nodes. The connections between nodes are mathematical relationships. In the context of linear elasticity these connections can be represented as spring. Using static nodal analysis where the sum of the forces acting on node must equal zero and the forces are related to relative displacements of nodes it is possible to determine the net movement of each node and the force in each element. This method excels when stresses are within the elastic region of the material and when displacements are expected to be small as heavily distorted meshes can result in erroneous results (Hoek, 2008) (Brinkgreve, Kumarswamy, & Swolfs, 2015).

2.7.4 Plaxis

Plaxis is a geotechnical and rock mechanics numerical modeling software package with both two dimensional and three-dimensional capabilities called Plaxis2D and Plaxis3D respectively. Both software tools are based on finite element models. Plaxis3D uses 10 nodded three dimensional elements to solve for solutions and interactions between nodes can be based on a variety of relationships and failure criterion such as linear elastic, Hoek-Brown, Mohr Coulomb. These criteria can be set based on material layer (i.e.: one stratigraphic layer could be linear elastic and another in the same simulation could be Mohr-coulomb). Meshing in Plaxis is automatic and can be done by selecting one of five coarseness (very coarse to very fine) and/or by applying a coarseness factor to each volume or surface. In addition, mesh parameters can be set for relative element size, polyline angle tolerance, and surface angle tolerance (Brinkgreve et al., 2015).

3.0 LAB TESTING

This lab program took place inside the Heavy Structures Lab which has a specialised floor that can handle heavy objects and high forces. A new 2 MN actuator was commissioned in collaboration with Dr. Sadeghian and Mr. Khorramian for the test. The actuator exerted a known uniform static load onto a concrete specimen that simulated a rock mass and the modified flatjack testing procedure was performed on this loaded specimen to determine suitable correction factors to use to account for slot shapes that did not correspond to the flatjack shape.

3.1 Purpose

The purpose of this lab testing program was to establish the corrections factors (J) shown in Equation [14], between the external jack pressure required to negate the slot deformation caused by the in-situ stress for specific slot geometries. In addition, the slot closure factor ($G_{C\text{-}D}$), which relates the slot closure to in-situ stress as shown in Equation [15], will be determined for each of these slot shapes. These equations where developed using a combination of numerical modeling, experimental results and linear elastic theory. The relationships between slot area, slot closure and cancellation pressure was examined to determine if any broader trend exists.

[14] $$\boldsymbol{\sigma = KPJ}$$

Where:

σ = In-situ stress

K = Correction factor for the internal fluid pressure to external (output pressure)

P = The internal fluid pressure

J = The proposed slot geometry correction factor (specific to each slot geometry)

[15] $$\sigma = G_{C-D}\Delta_{C-D}E$$

Where:

σ = In-situ stress

$G_{C\text{-}D}$ = The slot closure factor that relates, modulus, applied stress and the measured closure between pins C and D (specific to each slot geometry)

$\Delta_{C\text{-}D}$ = Measured closure between pins C and D

E = Young's modulus of the rock mass

Several different parameters were considered for the lab test; however, due to space, time and budget considerations only four 0.4 m^3 specimens could be prepared. It was decided to complete tests that were the most likely to be encountered in the field environment. These include; slot shapes with different diameter saw blades, overlapping boreholes, plunge cuts and the drag cut all shown in Figure 23. The different diameter blades were selected for testing because in industry the test would most likely be carried out using whatever equipment is available and the different slot shapes were those which were simplest to perform. Since the tests were carried out in the linear elastic range of the concrete, the samples could be reused by filling the slot with a grout with a similar modulus.

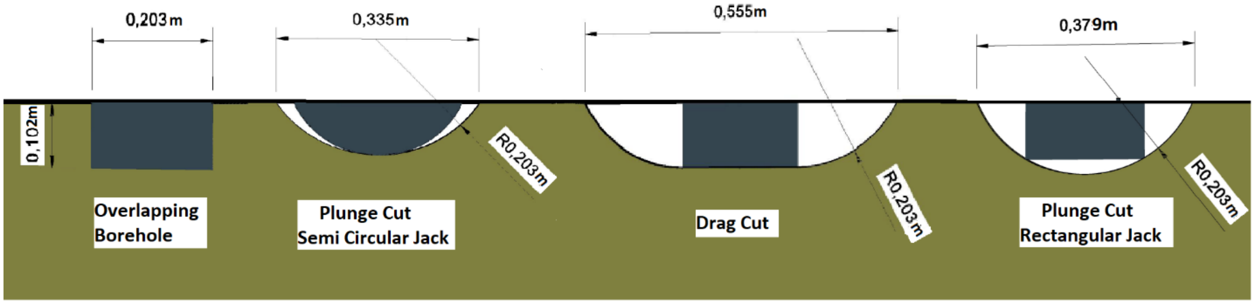

Figure 23: Various types of slots that were tested in the lab. Note: Dimensions change based on saw blade diameter

3.2 Equipment

The test equipment used during the lab test consisted of the following:

- 2 000 000 N capacity MTS actuator
- Concrete end blocks
- Force distribution plate
- Swivel plate
- 16” Concrete saw
- 406-mm (16”), 356-mm (14”) and 305-mm (12”) diamond saw blades
- Flatjack Apparatus (oil used)
- 203-mm (8’) by 102-mm (5”) rectangular flatjack
- 152-mm (6”) radius circular segment flatjack
- Concrete samples
- Hoskins multilength strain gauge set
- Mechanical cement bolts 9.5 mm (3/8”) with tapered tops
- Hammer Drill
- Hilti Rotary Hammer
- Various wrenches
- Camera
- Masonry bits (12.7 m (1/2”) and 7.9 mm (5/16”))

3.3 Setup

The load frame end blocks used in this test were developed in collaboration with Ph.D. student Koosha Khorramian and Dr. Pedram Sadeghian. This was done to reduce both overall cost and reduce required space in the lab for the test set up. The concrete form design and construction was completed as part of this project while the size and rebar design of the end blocks was completed by Mr. Khorramian.

Two reinforced concrete end blocks, 1 m by 0.5 m by 0.8 m, were prepared using the mold shown in Figure 24. The mold was created using one 19-mm (¾”) plywood sheet as the base and 19-mm (¾”) plywood walls reinforced with 2”x4” wooden framing on 30.5 cm centers. This framing was further supported with two sets of 2”x4” strapping and four, 2”x4” bracing across the top for added stability from bulging. A bulkhead was inserted in the middle to separate the two end blocks. Pipes of 102 mm (4”) diameter polyvinyl chloride (PVC) were used to create vertical holes in the blocks on a 61-cm (2’) grid centered in each block. These holes align with holes in the concrete floor of the Heavy Structures Lab and were used to prevent the end block from sliding when pressure was. Four 63.5-mm (2.5”) PVC pipes were used to create horizontal holes in the blocks. These are used to secure the actuator to the load frame end blocks.

The end blocks were reinforced with 19-mm (¾”) rebar spaced with 51 mm (2”) centers in three dimensions. The rebar was pre-bent into three different sized rectangles so they could be nested within one another and were assembled on steel saw horses for maximum access. The design called for 14 rebar rectangles of each size however it was anticipated that during construction this would be impossible to accomplish due to the installation of PVC pipes, especially for the horizontal rebar that required 14 bars in only 0.8 m compared to 1 m in the other 2 dimensions. The design had a safety factor of 1.67. In addition, 9 steel bars where inserted in a grid pattern through the center of each block to resist internal shear. The internal structure of the end blocks is shown in Figure 24.

Figure 24: The internal reinforcement of the end block with the PVC tubes for the internal voids to secure samples to the block and the block to the floor. Note: at this point, one of each type is missing but was later added in.

One block (block 1) was fitted with a 25-mm (1") steel plate to distribute the load and the actuator using 25-mm (1") threaded rod and 152-mm (6") square washers on the back side. A thin layer of grout was applied between the steel plate and the block to ensure good contact. The other block (block 2) was not fitted with anything as the sample distributed the load sufficiently. Both blocks where attached to the Lab floor using 75.2 mm (3") diameter threaded rod.

A 203 mm (8") diameter 2 MN swivel plate was installed on the actuator to correct for minor deviations in parallelism between actuator and the specimen

The specimen was placed near block 2 with a sheet of 1.6 mm (1/16") thick tar paper on both sides (later replaced with butyl rubber, see Appendix F). A reinforced steel load distribution plate was positioned between the swivel and the specimen to distribute the load applied to the specimen. This set up is shown in Figure 25.

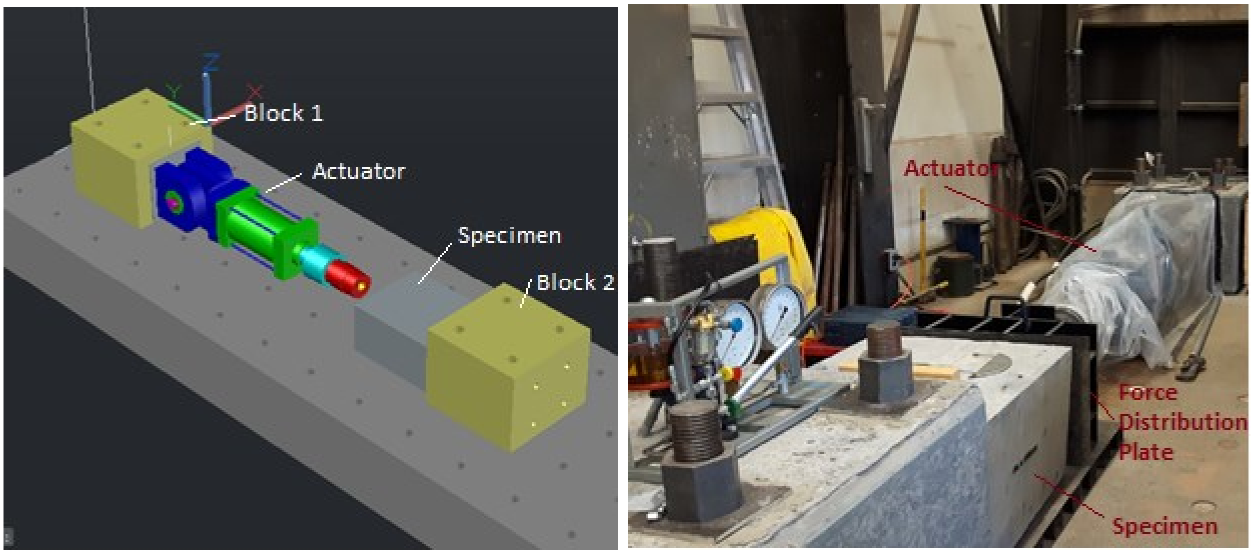

Figure 25: An AutoCAD drawing of the designed (left) and an as built picture (right).

The specimens were prepared as pairs in mold and a total of four specimens where prepared shown in Figure 26. The specimens were 0.8 m wide 1m long and 0.5 m high. The 0.8 m by 0.5 m side was the side to which the load was applied. An oversight during creating the specimen is the positioning of the lifting hooks. These were positioned along the center axis and may serve to reinforce the plane in which the slot is cut. These hooks were cut off once the blocks were positioned prior to testing. The blocks where later moved using concrete bolts inserted into the top in the corners.

The flatjacks used in the lab tests were attached to a Glotzl pump using hydraulic connectors and then blead to remove air from the system. Adapters were required to convert the metric pump to the Imperial fittings on the jack.

Figure 26: Pouring of the four specimens and end blocks.

3.4 Procedure

Since the actuator was new, initial trials were conducted prior to testing of the first specimen. To do this one of the samples was used and the specimen loaded with progressively large loads to identify any potential issues with the actuator, hydraulics or end block. Loads of 10 kN, 25 kN, 50 kN, 100 kN, 250 kN 500 kN, 1000 kN, 1500 kN, and 2000 kN were applied and held for 5 minutes while the elements of the actuator where inspected.

Once the actuator was tested for proper functioning, tests where completed as per the below procedure.

1. Position the sample with the 0.8 m x 0.5 m end facing the actuator.
2. Place butyl rubber on both ends of the sample to ensure good contact.
3. Slowly apply a small load to the sample to seat it on the end block.
4. Remove Load
5. Install measurement pins as shown in Figure 27
6. Record distance between pins 3 times

7. Slowly apply load of 1 900 000 N over 5 minutes
8. Wait 15 minutes to allow for any time dependant movements
9. Record distance between pins 5 times using measurement device
10. Cut slot
11. Record measurement between pins immediately after cutting and again every 5 minutes for 15 minutes
12. Position flatjack centered in the slot
13. Begin inflating Flatjack recording the pin position and pressure every 0.7 MPa
14. Hold peak pressure for 15 min recording every 5 min
15. Depressurise jack recording the pin position and pressure every 0.7 MPa
16. Hold zero pressure for 15 min recording every 5 min
17. Repeat three times to account for hysteresis.
18. Regrout the slots in the specimens with a grout of similar Young’s modulus for reuse.

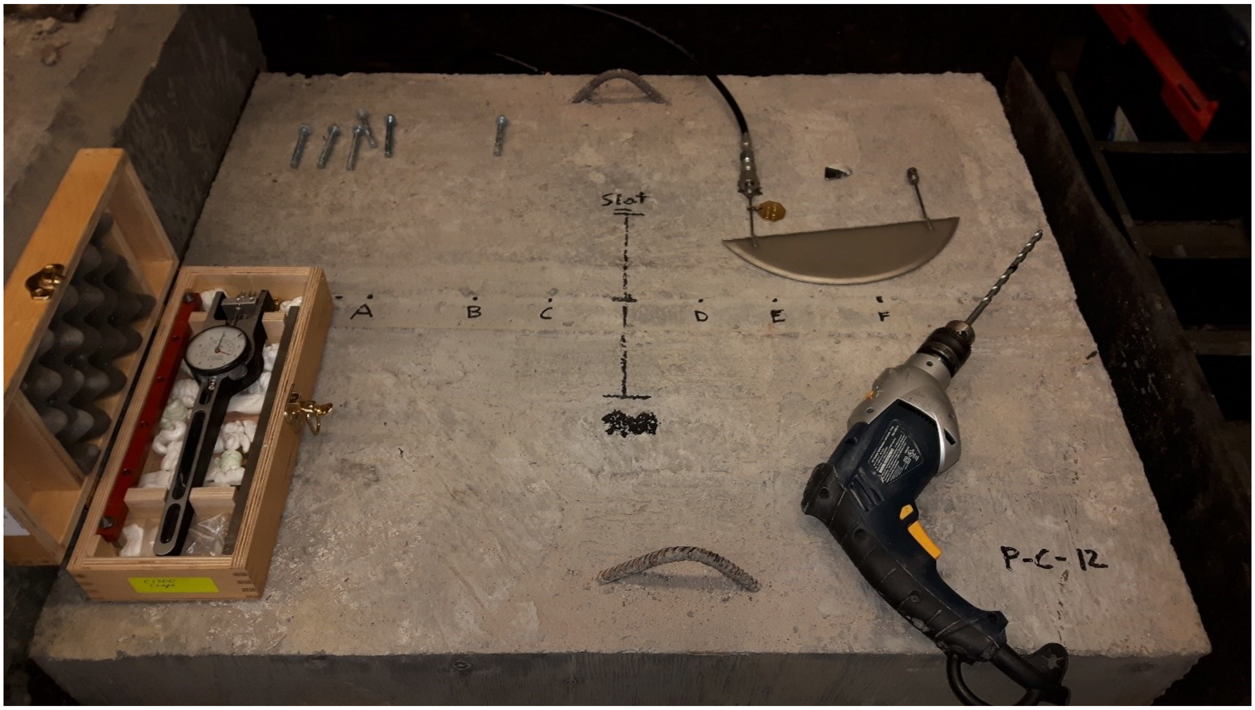

Figure 27: Pin locations in test specimen P-C-12.

The slot was prepared differently for each test shown in Table 1. The overlapping borehole was completed using a series of overlapping holes created using a 1/2-inch masonry bit in a Hilti rotary hammer. The plunge cuts where prepared using a Hilti DSC800 concrete saw with either a

305 (12”), 356 (14”), or 406 mm (16”) diameter blade. The wheels of the saw where set to a stationary setting and the saw was rotated so the blade cut to the depth required to fully insert the flatjack. For the drag cut the wheels of the saw were set to the rotate setting and the saw was rotated into the specimen to a depth of 102 mm (4”) it was then moved the required horizontal distance of 203 mm (8”) and rotated up out of the cut. This was done with either a 305, 356, or 406-mm blade depending on the test being performed. Errors in measurement are ±1.27 µm (±0.00005 in) for displacement measurements and ± 0.05 MPa (±0.5 Bar) for internal flatjack pressure measurement.

Table 1: List of the tests to be performed. All tests are labelled such that the first letter represents the type of jack, rectangular (R) or circular segment (C) then the type of cut, plunge (P) or drag (D), and finally the diameter of the blade in inches. ASTM_OB is created using overlapping boreholes

Test	Load (MPa)	Specimen	Variables Determined	Test Order
C-P-12	4.75	3	J, $G_{C\text{-}D}$	1
C-P-14	4.75	3	J, $G_{C\text{-}D}$	3
C-P-16	4.75	3	J, $G_{C\text{-}D}$	5
R-D-12	4.75	4	J, $G_{C\text{-}D}$	2
R-D-14	4.75	4	J, $G_{C\text{-}D}$	4
R-D-16	4.75	4	J, $G_{C\text{-}D}$	6
R-P-14	4.75	4	J, $G_{C\text{-}D}$	7
R-P-16	4.75	4	J, $G_{C\text{-}D}$	8
ASTM-OB	4.75	4	J, $G_{C\text{-}D}$	9

In addition, specimens were numerically modeled as ¼ the actual specimen since the specimen is symmetric in both the x and y axis to maximise computational efficiency. The models were normally constrained on the x, y and z minimum boundaries and free on all remaining boundaries. The actuator or “in-situ” load was simulated using an area load of 4.75 MPa on the entire y-maximum surface and jacks were simulated using an area load in the shape of the applicable jack at varying loads. Since the models are linear elastic the slots were created all at once by removing a 3 mm thick slot in the shape required for each test. The material used had a Young's modulus of 27.2 GPa and a Poisson's ratio 0.26 as determined by testing cylindrical samples of the same concrete shown in Appendix E. Mesh density was selected by iteratively increasing the density until the C-D closure results from the previous mesh density where less than 1% different from the results of the new mesh. Measurement locations where selected as close as possible to the actual measurement points.

3.5 Lab Results

All tests are labelled such that the first letter represents the type of jack, rectangular (R) or circular segment (C) then the type of cut, plunge (P) or drag (D), and finally the diameter of the blade in inches. For example, R-D-12 is a drag cut using a 12-inch blade and a rectangular saw. The exception to this is the ASTM standard test (ASTM-OB) using a rectangular jack with a slot made from overlapping drill holes. The pins in the test are labelled A through F as shown in Figure 27. The raw data from each test are provided in Appendix A and the results for the commissioning tests are in Appendix B. To determine the relative displacement of the pins, the average of 5 pre-cut measurements was taken and this value was subtracted from all future measurements to provide the displacement of the pins relative to the precut position. In the following graphs of the results, convergence is represented as a positive number while divergence is negative. Figure 28 shows the displacement path of span C-D for test R-D-12 and shows there is significant scatter in the data between sequential loading cycles. Since no hysteresis was observed, a trend line was fitted to all data points instead of just the first loading cycle as specified in the ASTM to reduce the impact of random error in the test. Test R-D-16 was the only test to exhibit permanent set hysteresis and observation occurred was on the final unloading cycle. Consequently, the final unloading cycle for test R-D-16 was not included in the trend line calculation shown later in Figure 38.

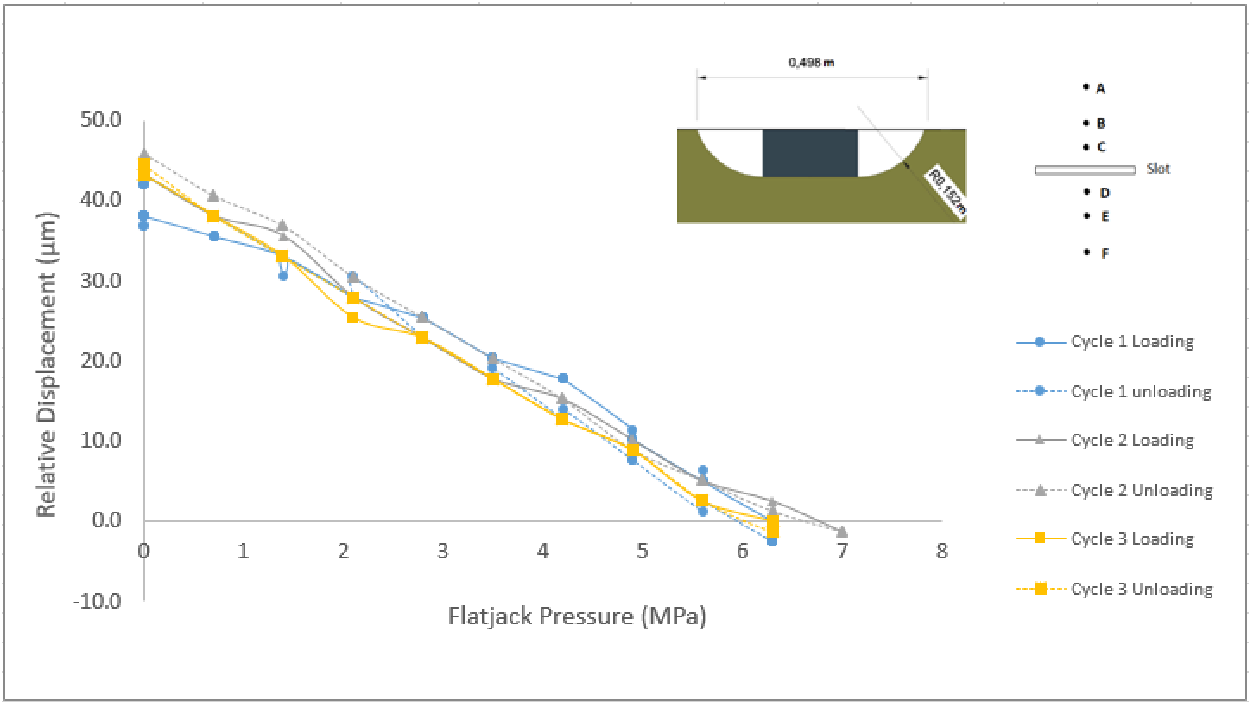

Figure 28: The loading path for span C-D of test R-D-12. No hysteresis is present but there is some minor scatter in the data.

A sample of the graphed results (R-D-14) are shown in Figure 29. It is clear from this figure that the error in relative displacement measurements is too large to be of use for spans A-B, B-C, D-E, and E-F. In addition, span A-B should have identical measurements to span E-F due to symmetry and likewise for spans B-C and D-E. Since the symmetrical spans do not have similar measurements, it is further indicated these measurements have sufficiently large error that they should not be considered reliable. Plots of the complete data including spans, A-B, C-D, D-E and E-F are available in Appendix C for the reader but are not plotted in subsequent graphs. The most important span (C-D) has sufficiently large closure so that the error was small enough relative to the measurements to be considered reliable.

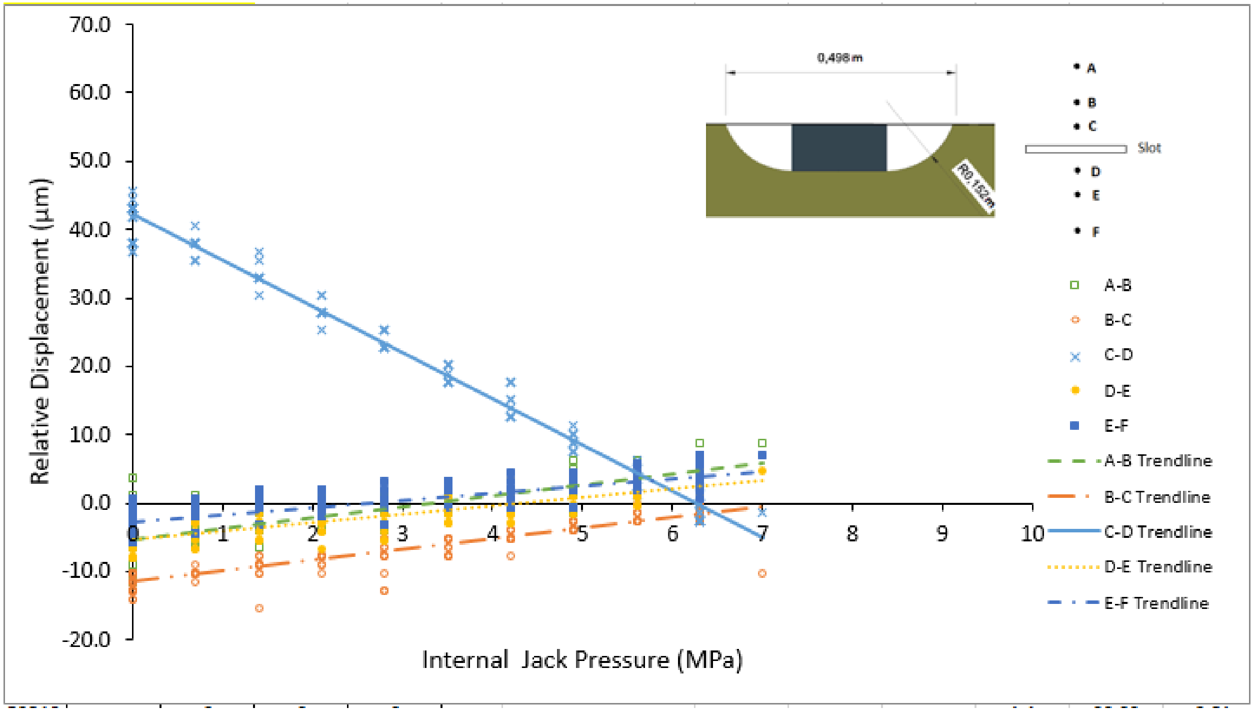

Figure 29: The relative displacement (µm) of pins C-D as a function of measured pressure in the flatjack (MPa) using the rectangular flatjack in a drag cut with a 356 mm diameter blade (R-D-12). The trend lines are the mean of each data set.

The span C-D results were plotted in the subsequent figures along with the numerical modelling results using Plaxis3D.

3.5.1 Overlapping Borehole

Figure 30 shows the lab and numerical modeling results for the ASTM-OB test. The lab results gave a slot closure of 40.92 µm and cancelation pressure of 6.01 MPa compared to numerical model predictions of 42.00 µm and 5.86 MPa. The numerical modeling trend line lies centered within the data points obtained from the lab results and agrees well with the lab results best fit line. These results have no additional correction factors ($G_{C\text{-}D}$ or J) and is used as a baseline to show that the numerical model parameters such as Young's modulus, Poisson's Ratio, boundary conditions and loadings are an accurate representation of the lab set up.

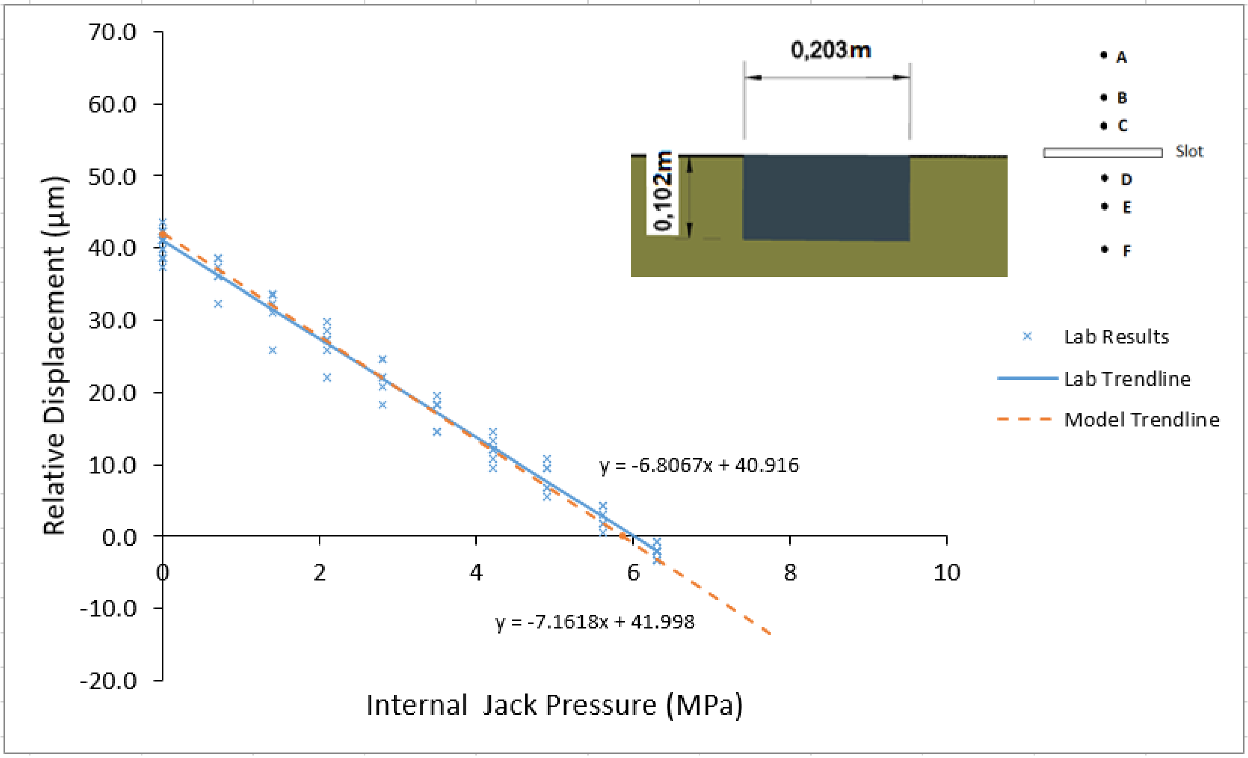

Figure 30: The relative displacement (µm) of pins C-D as a function of measured pressure in the flatjack (MPa) using the rectangular flatjack in a grouted slot made from overlapping boreholes (ASTM-OB) compared to the numerical modeling results for same scenario corrected for the K value of the flatjack (0.81).

3.5.2 Plunge Cuts

Figure 31 shows the lab and numerical modeling results for the C-P-12 test. The lab results gave a closure of 25.90 µm and cancelation pressure of 6.37 MPa compared to numerical model predictions of 29.93 µm and 6.09 MPa. The numerical modeling trend line lies centered within the data points obtained from the lab results and agrees well with the lab results best fit line.

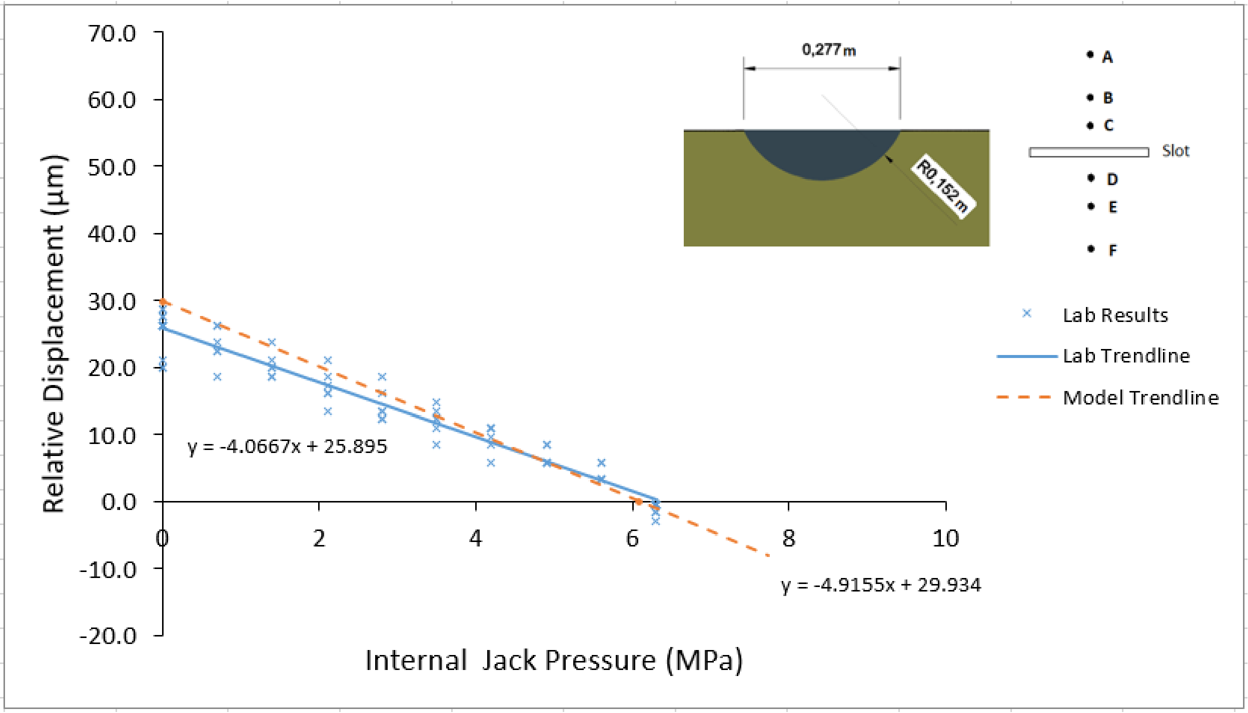

Figure 31: The relative displacement (µm) of pins C-D as a function of measured pressure in the flatjack (MPa) using the circular segment flatjack in a plunge cut with a 12-inch diameter blade (C-P-12) compared to the numerical modeling results for same scenario corrected for the K value of the flatjack (0.78).

Figure 32 shows the lab and numerical modeling results for the C-P-14 test. The lab results gave a slot closure of 30.08 µm and cancelation pressure of 7.06 MPa compared to numerical model predictions of 33.02 µm and 6.24 MPa. The numerical modeling trend line lies mostly centered within the data points obtained from the lab results and agrees fairly well with the lab results best fit line.

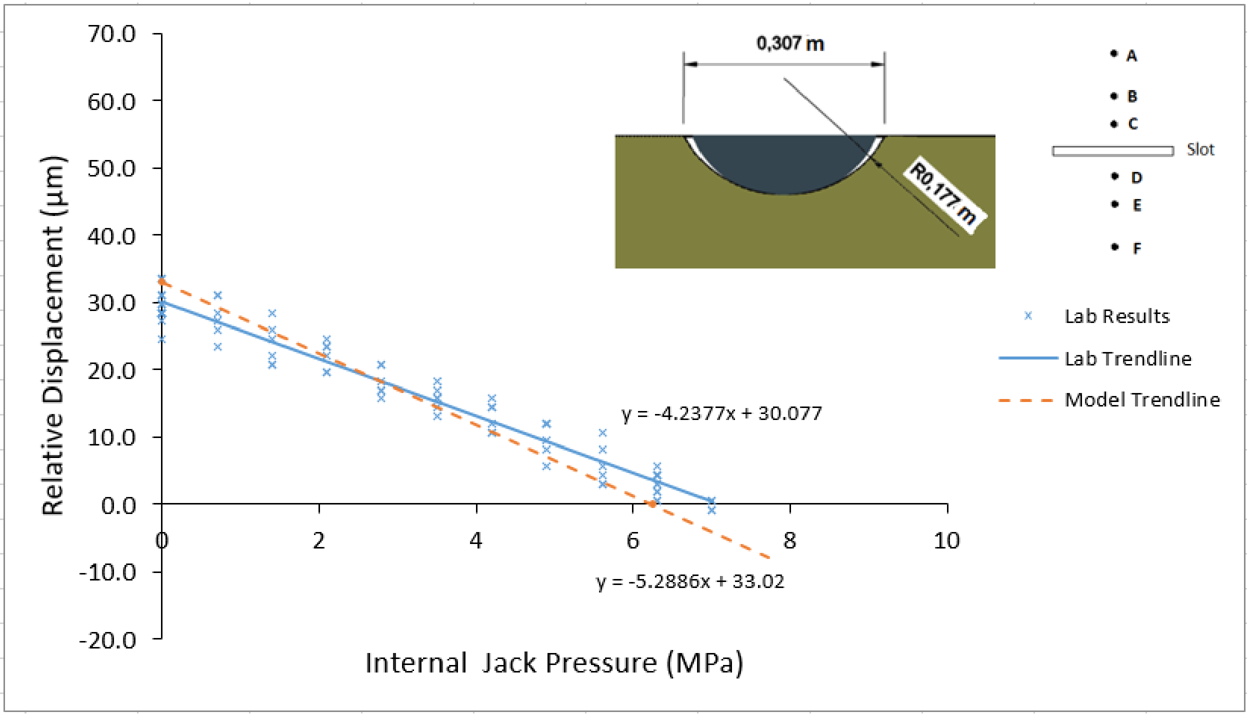

Figure 32: The relative displacement (µm) of pins C-D as a function of measured pressure in the flatjack (MPa) using the circular segment flatjack in a plunge cut with a 356 mm diameter blade (C-P-14) compared to the numerical modeling results for same scenario corrected for the K value of the flatjack (0.78).

Figure 33 shows the lab and numerical modeling results for the C-P-16 test. The lab results gave a slot closure of 29.85 µm and cancelation pressure of 7.49 MPa compared to numerical model predictions of 33.91 µm and 6.33 MPa. The numerical modeling trend line lies centered within the data points obtained from the lab results and agrees well with the lab results best fit line.

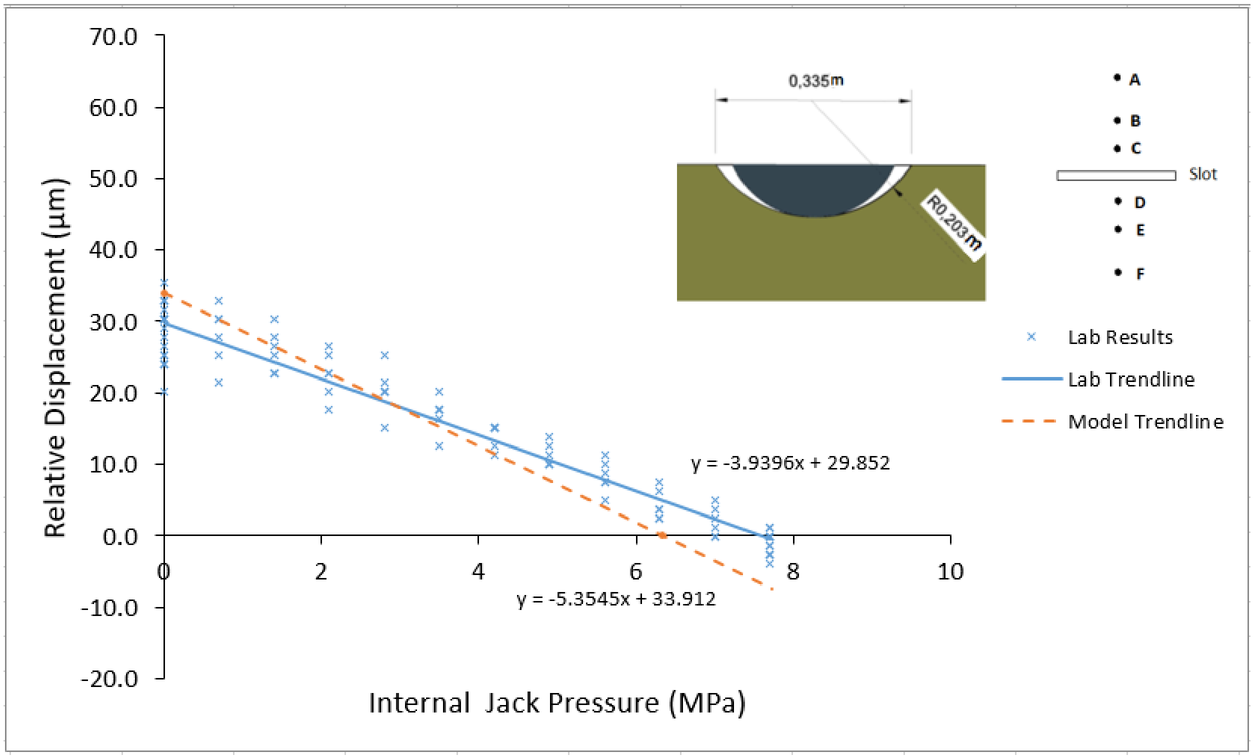

Figure 33: The relative displacement (µm) of pins C-D as a function of measured pressure in the flatjack (MPa) using the circular segment flatjack in a plunge cut with a 406 mm diameter blade (C-P-16) compared to the numerical modeling results for same scenario corrected for the K value of the flatjack (0.78).

3.5.3 Plunge Cut with a Rectangular Jack

Figure 34 shows the lab and numerical modeling results for the R-P-14 test. The lab results gave a slot closure of 42.38 µm and cancelation pressure of 5.30 MPa compared to numerical model predictions of 64.62 µm and 6.93 MPa. The numerical modeling trend line's slope agrees with lab results trend line but it has a larger initial closure and cancelation pressure. This discrepancy is examined further in the discussion section.

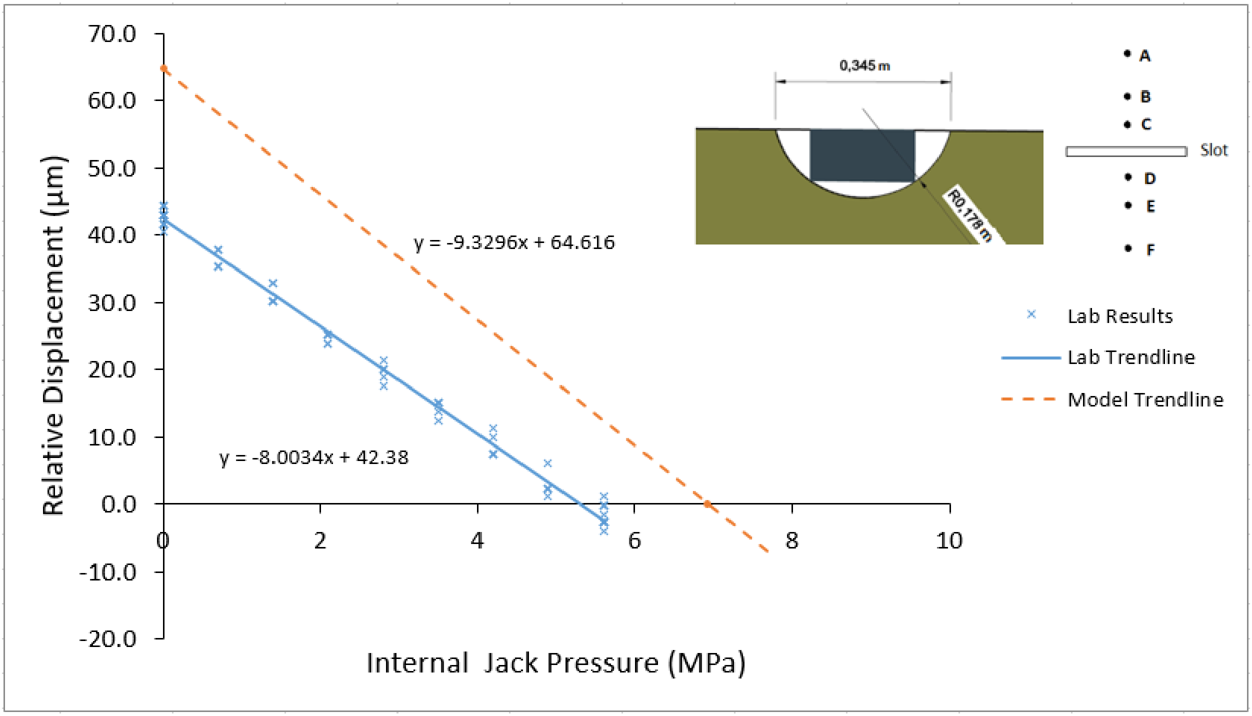

Figure 34: The relative displacement (µm) of pins C-D as a function of measured pressure in the flatjack (MPa) using the rectangular flatjack in a plunge cut with a 356 mm diameter blade (R-P-14) compared to the numerical modeling results for same scenario corrected for the K value of the flatjack (0.81).

Figure 35 shows the lab and numerical modeling results for the R-P-16 test. The lab results gave a slot closure of 46.95 µm and cancelation pressure of 7.47 MPa compared to numerical model predictions of 65.65 µm and 5.71 MPa. The numerical modeling trend line agrees with the cancelation pressure but differs significantly in its prediction of the slot closure. This discrepancy is examined further in the discussion section.

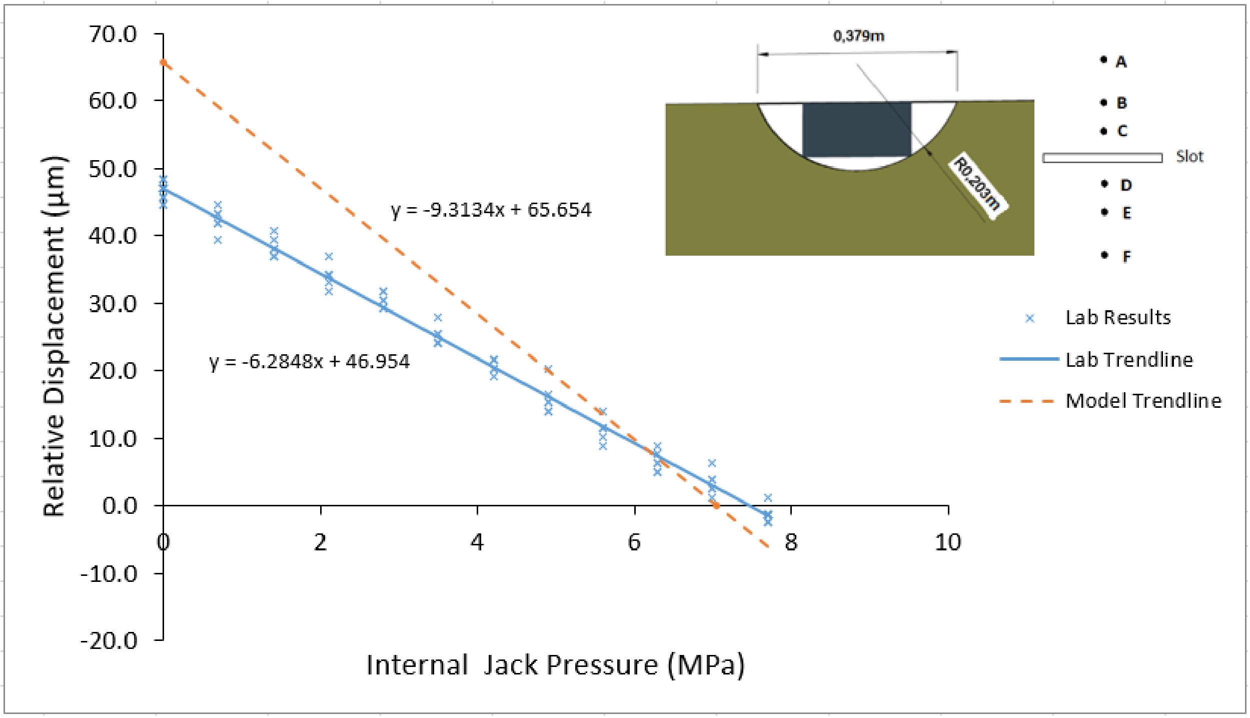

Figure 35: The relative displacement (µm) of pins C-D as a function of measured pressure in the flatjack (MPa) using the rectangular flatjack in a plunge cut with a 406 mm diameter blade (R-P-16) compared to the numerical modeling results for same scenario corrected for the K value of the flatjack (0.81).

3.5.4 Drag Cut

Figure 36 shows the lab and numerical modeling results for the R-D-12 test. The lab results gave a slot closure of 42.10 µm and cancelation pressure of 7.25 MPa compared to numerical model predictions of 42.00 µm and 7.54 MPa. The numerical modeling trend line agrees somewhat with the lab results best fit line.

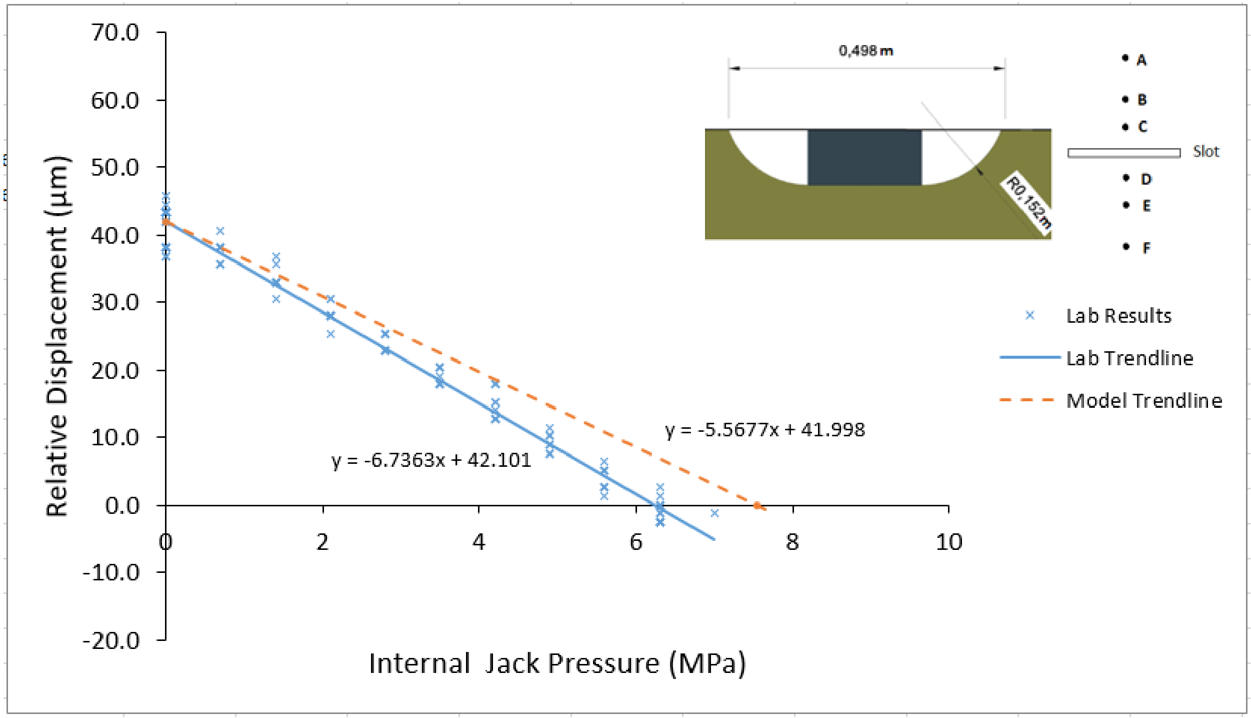

Figure 36: The relative displacement (µm) of pins C-D as a function of measured pressure in the flatjack (MPa) using the rectangular flatjack in a drag cut with a 12-inch diameter blade (R-D-12) compared to the numerical modeling results for same scenario corrected for the K value of the flatjack (0.81).

Figure 37 shows the lab and numerical modeling results for the R-D-14 test. The lab results gave a slot closure of 55.08 µm and cancelation pressure of 7.29 MPa compared to numerical model predictions of 62.06 µm and 7.67 MPa. The numerical modeling trend line is lies above the data points but the slope agrees well with the lab results best fit line indicating a slight initial closure error.

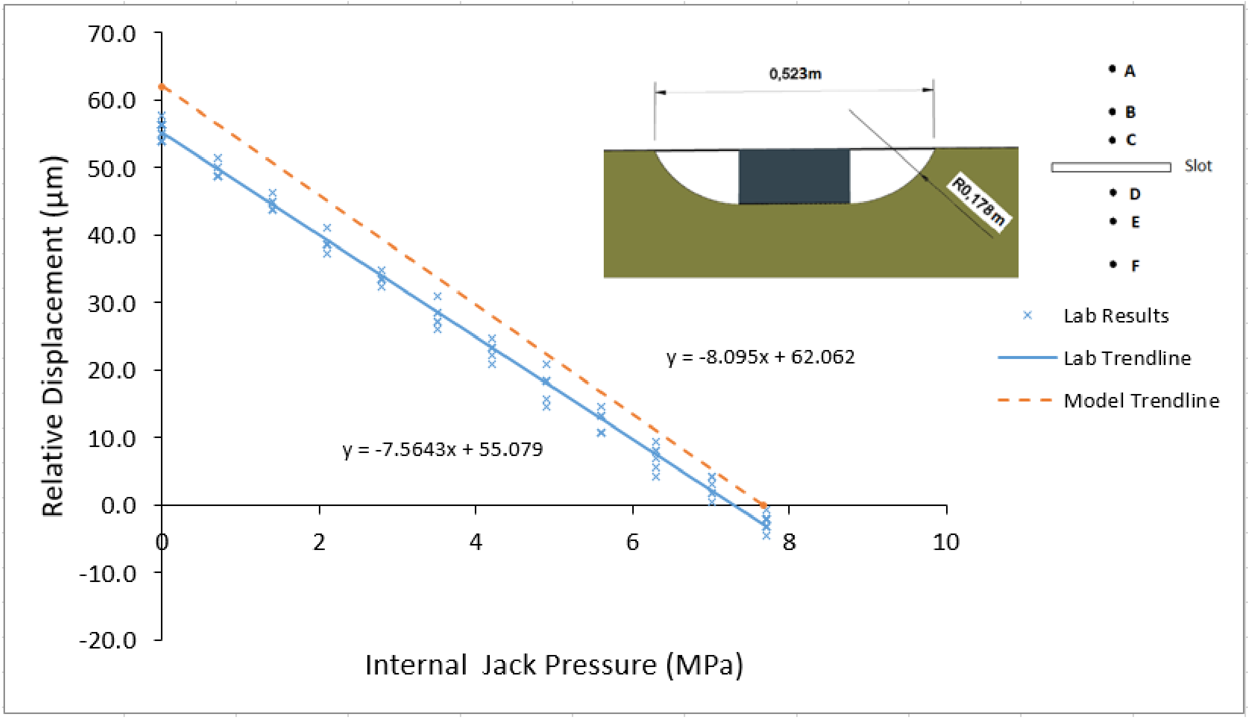

Figure 37: The relative displacement (µm) of pins C-D as a function of measured pressure in the flatjack (MPa) using the rectangular flatjack in a drag cut with a 356 mm diameter blade (R-D-14) compared to the numerical modeling results for same scenario corrected for the K value of the flatjack (0.81).

Figure 38 shows the lab and numerical modeling results for the R-D-16 test. The lab results gave a slot closure of 59.66 µm and cancelation pressure of 8.68 MPa compared to numerical model predictions of 63.31 µm and 7.73 MPa. The numerical modeling trend line lies mostly centered within the data points obtained from the lab results and agrees somewhat well with the lab results best fit line.

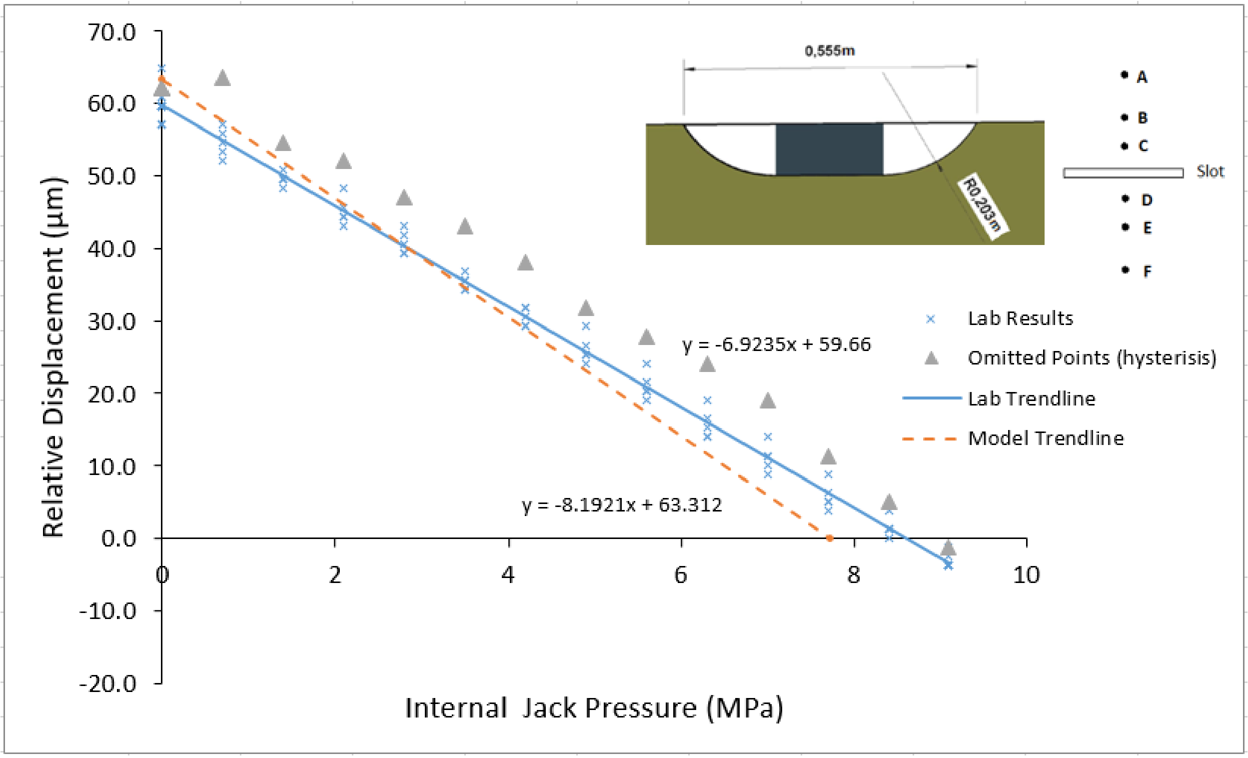

Figure 38: The relative displacement (µm) of pins C-D as a function of measured pressure in the flatjack (MPa) using the rectangular flatjack in a drag cut with a 406 mm diameter blade (R-D-16) compared to the numerical modeling results for same scenario corrected for the K value of the flatjack (0.81). The data points with the shaded background were not used to calculate the trend line due to hysteresis.

3.6 Area Relationships

Analysis of the data from all the tests in Figure 39 shows a trend for increasing closure with increasing area, however, the geometry affects the closure as well. The effect of the geometry can be seen on the ASTM test which is similar in size to the C-P-x series tests but produced a larger closure in both the models and the lab tests. The rectangular plunge tests produced significantly different results compared to the numerical model. The results from the lab test fall on the trend line more accurately however upon detailed inspection of the numerical model no issues where detected. With exception to the two R-P-X series tests, the results between the numerical model and the lab tests are within 11.86% and the model gave larger closures as shown in Table 2. Both results indicated a correlation between the slot area and the closure however the lab results had a stronger correlation with an R^2 value of 0.786 vs 0.618. This indicated that the effect of shape of hole is larger in the numerical model than in the lab tests.

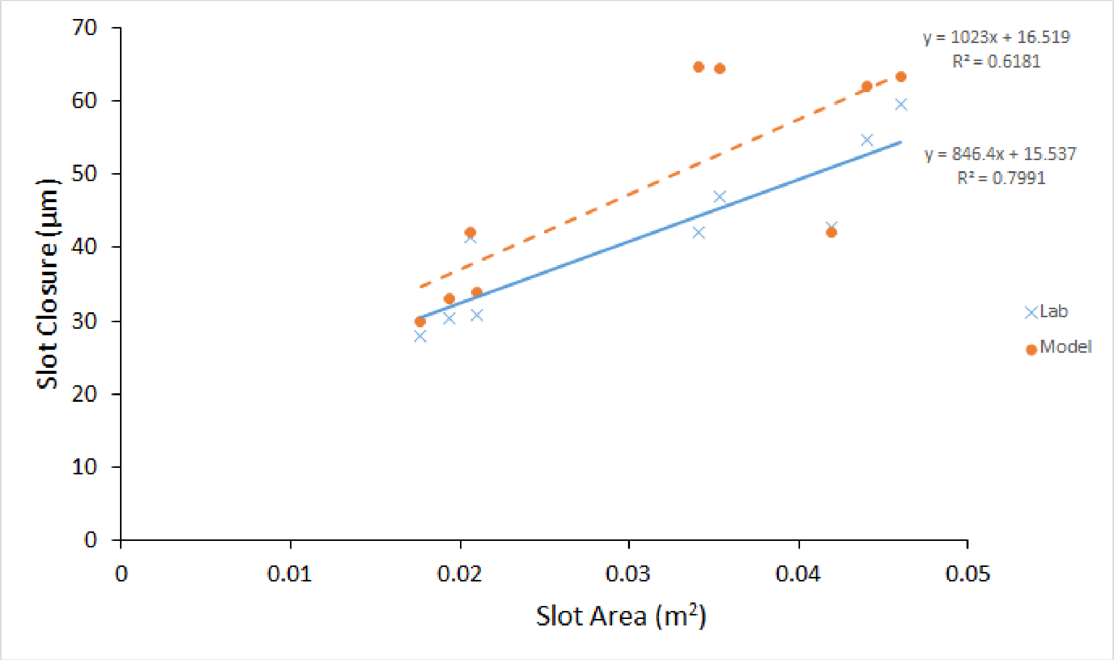

Figure 39: Lab closure (µm) at zero flatjack pressure versus slot face area compared to model predictions for pin span C-D.

Table 2: Summary of the numerical model and lab closure data and their error.

Test	Slot Area (m^2)	Lab Closure (μm)	Model closure (μm)	Error (%)	$G_{C\text{-}D}$ Lab	$G_{C\text{-}D}$ Model
C-P-12	0.017704	26	30	-6.49	5.81	5.43
C-P-14	0.019416	30	33	-7.78	5.34	4.93
C-P-16	0.020989	30	34	-8.79	5.26	4.80
R-D-12	0.041936	42	42	1.72	3.81	3.87
R-D-14	0.04406	55	62	-11.86	2.97	2.62
R-D-16	0.046005	60	63	-5.77	2.73	2.57
R-P-14	0.034065	42	65	-34.86	3.86	2.52
R-P-16	0.035321	47	64	-26.95	3.46	2.53
ASTM-OB	0.020645	41	42	-1.54	3.93	3.87

Comparison of the cancelation pressure in Figure 40 reveals a stronger correlation between relative area of the slot to the flatjack and cancelation pressure in numerical modeling. The trend in the lab tests is similar to that of the numerical modeling. The results between the numerical model and the lab tests are within 23.48% in Table 3. The lab results have a very poor correlation between the slot area and the closure however the model results had a stronger correlation with an R^2 value of 0.989 vs 0.163. In addition, blade size has a large influence on the cancellation pressure in the lab tests compared to numerical modeling. However, this could be attributed to the error associated with the lab experiments.

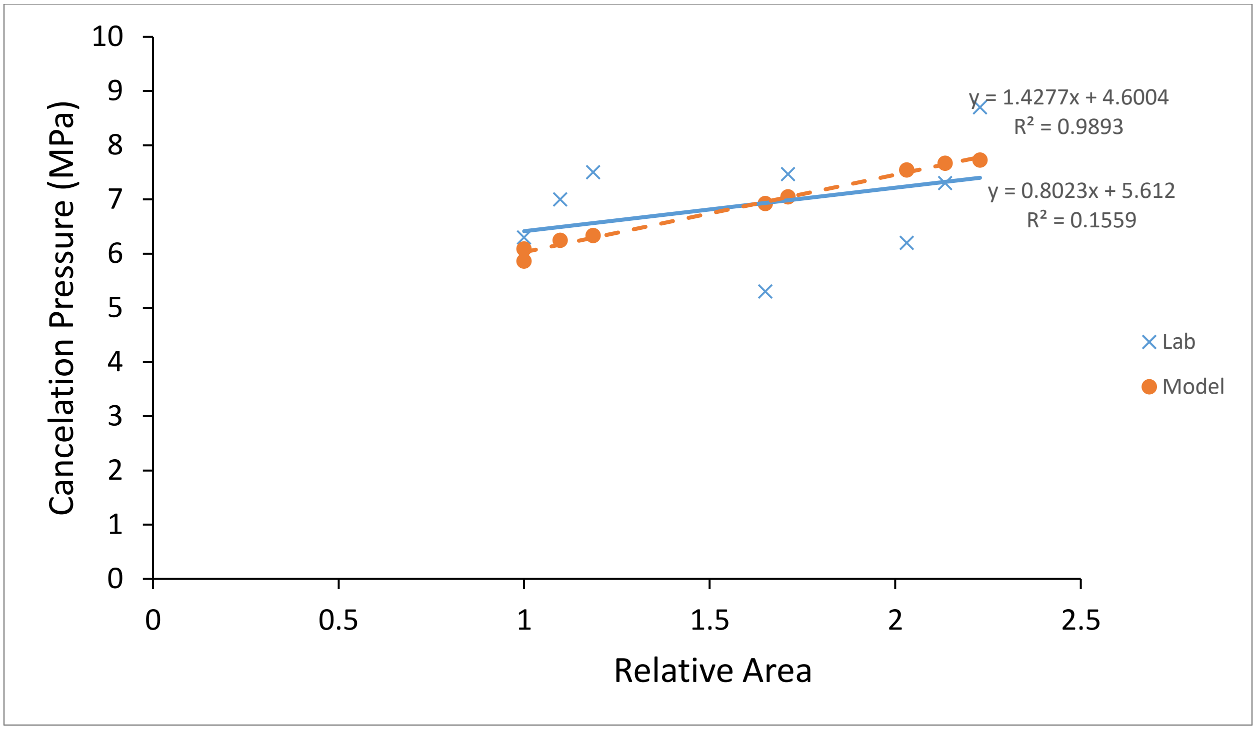

Figure 40: Cancelation pressure (numerical model results were corrected for the k value) versus the relative area of the slot compared to the jack for both lab and model predictions in pin span C-D.

Table 3: Summary of the numerical model and lab cancelation pressure data points and their error.

Test	Slot Area (m^2)	Lab Cancelation (MPa)	Lab Corrected Cancelation (MPa)	Model Cancelation (MPa)	Error (%)	*J*-lab	*J*-model
C-P-12	0.017704	6.3	4.97 (K=0.78)	4.75	-4.60	0.956	1.000
C-P-14	0.019416	7.0	5.51 (K=0.78)	4.87	-13.08	0.863	0.975
C-P-16	0.020989	7.5	5.84 (K=0.78)	4.94	-18.26	0.813	0.962
R-D-12	0.041936	6.2	5.06 (K=0.81)	6.11	17.14	0.938	0.777
R-D-14	0.04406	7.3	5.90 (K=0.81)	6.21	4.91	0.804	0.765
R-D-16	0.046005	8.7	7.03 (K=0.81)	6.26	-12.31	0.676	0.759
R-P-14	0.034065	5.3	4.29 (K=0.81)	5.61	23.48	1.106	0.847
R-P-16	0.035321	7.5	6.05 (K=0.81)	5.71	-5.97	0.785	0.832
ASTM-OB	0.020645	6.0	4.87 (K=0.81)	4.75	-2.49	0.976	1.000

3.7 Summary of Lab Results and Discussion

It was observed that the spread in the lab displacement data is larger than the instrument tolerance. This spread has the largest impact on the measurement of spans A-B, B-C, D-E, and E-F because the instrument error is large (up to 50%) compared to the relative displacement of these spans. This impact is compounded by their relatively shallow trend line slope (a little more than 1:1) which gives a larger change in cancelation pressure for small variations in the trend line slope. When comparing these spans to span C-D, span C-D has a smaller instrument error of (1.9%-4.7%) and a steeper slope of between -4 and -8 which results in a smaller change in cancellation pressure for small variations in the trend line slope. In addition, span A-B and E-F should produce identical results as they are symmetric, however, they were only within instrument tolerance (±1.27 μm) in three out of nine tests while spans B-C and D-E which are likewise symmetric produced results within tolerance three out of nine tests. Finally, the results disagree on which of the two span pairs (A-B/E-F or B-C/D-E) had the larger relative displacement. The results of these measurements were considered unreliable due to the large errors associated with their measurements. These values could be useful in future tests if one of three changes were made 1) increase the in-situ stress, 2) decrease the stiffness of the material or 3) create a larger slot. Each of these changes would result in a larger initial displacement and thus a smaller relative error.

Span C-D is the focus of this experimental evaluation and produced useable results with sufficiently low error but still not within instrument error. This indicates another source of error most likely associated with experimenter as the actuator force and room temperature were constant and the error was random in nature. Hysteresis was rarely observed.

The results from the numerical modeling agreed extremely well for the ASTM test and the best fit lines matched very closely. For the drag cut and the plunge cut with the circular segment flatjack the numerical model produced results that were reasonably close to the lab results with the numerical model predictions being fully or mostly contained within the data points and thus within the error associated with the experiment. Numerical modeling results from the plunge cut with the rectangular jack did not agree well with the lab results. The relative displacements in the models were much higher than the observed results and the closure pressures were in accurate. Overall, the error in cancelation pressure between numerical modeling and lab tests are ±23% and there was no indication that either type of flatjack produced results with larger errors than the other.

To further investigate the cause of the error in the R-P-x series tests, a series of numerical models was made. In these, a 356 mm diameter cut was made into a lab specimen to increasingly large depths which revealed a linear increase in closure as the depth increased as shown in Figure 41. The closure results from the model used in R-P-14 agrees well with the trend line created in Figure 41. In addition, the J factor in Table 3 is greater than 1 for the lab results which is illogical since the factor is correcting for a slot larger than the jack (i.e. it should be less than 1). It can therefore be concluded that the source of error was in the lab.

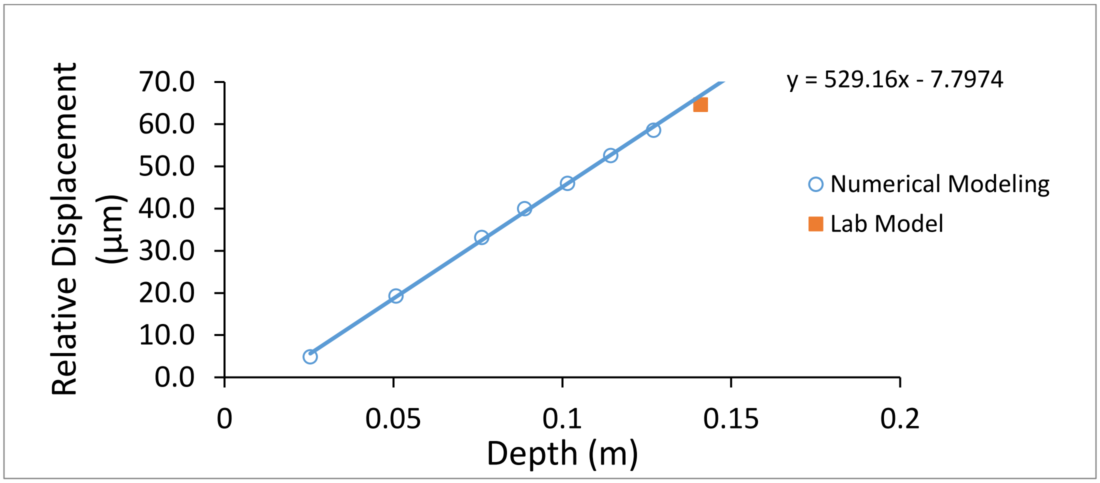

Figure 41 : Numerical modeling results of a 356 mm diameter slot at varying depths. The square is the result of the lab set up for R-D-14.

These lab tests had several sources of potential error. Reusing the blocks could result in both degradation of the block due to the formation of micro crack and a variation in the stiffness of the material that was used to fill in the slot. The latter was minimised by using a grout with a similar modulus to that of the concrete after setting for two days. Degradation of the block was also unlikely since the last test to take place, ASTM-OB had the most accurate results. Another potential source of error is that the larger block could have a different Young's modulus than the cylinders used to determine the modulus due to scale effects, however good agreement between most modeled closures and their measured results indicate that this is unlikely. The large variation in closure between the model and measured values in tests R-P-14 and R-P-16 cannot be explained using any of these sources of error as the results for ASTM-OB were not affected and it took place in the same block after R-P-14 and R-P-16 tests were conducted.

The only variable that seems significantly different to the other tests is the depth of the cut as all other tests were no deeper than the jack. R-P-14 was at the limit of the depth of what the saw could cut and therefore the slot could be shallower than modeled. Since the flatjack has rounded corners, this smaller than modeled slot could have been able to still accept the flatjack without the experimenter becoming aware of the shallow slot. Although this may have had an effect, Figure 41 indicates that the slot would have had to have been half of the depth to account for all the error and it does not explain the error in R-D-16 which was sunk to a known depth.

In lab testing, all jacks where recovered by inserting a screwdriver or similar tool under one side of the jack and prying up. In instances when the jack was particularly difficult to remove, a file with a blunt end was used on side with a hammer to tap the jack rotating it and lifting one side. A screwdriver was inserted into that side of the slot and the other side of the jack was tapped to rotate jack while the screwdriver prevented the other side from re-entering the slot. Repeating this procedure successfully extracted the flatjack with no significant damage.

4.0 FIELD TESTING

Pioneer Coal operates the Stellarton Open Pit Coal Mine which is in the town of Stellarton, Nova Scotia, Canada approximately 160 km north of Halifax as shown in Figure 42. It is an open pit coal mine that has been in operation since 1996. This mine consists of four main coal seams, the Foord, the Cage, the Third and the Flemming/McGregor seams. These seams dip 24° towards North North-East. There is a thick sandstone/claystone layer below the Cage seam that presents difficulty when mining due to its strength and lack of joints. In addition, these seams have all been mined from 1798 until 1967 ("Men in the Mines: A History of Mining Activity in Nova Scotia, 1720-1992," 2017) using surface and underground room and pillar methods affecting the in-situ stress field.

Stress measurement at the Stellarton site was attempted using the flatjack method based on the ASTM specifications and were focused on the sandstone layer for this project. Alterations to the hole shape and flatjack size where made to reduce the time and cost to perform the test. The slot shape was a drag cut while the flatjack was rectangular and measured 400 mm by 200 mm. The slot was cut using a 26-inch diameter wall saw mounted to the bedrock.

Figure 42: Location of the Stellarton open pit and the town of Stellarton (Modified from Google Maps, 2018).

4.1 Site Geology

To determine the stratigraphy in the Stellarton open pit, a desktop study carried out using exploratory borehole logs retrieved from the Nova Scotia Department of Natural Resources (NSDNR) as well as 'Open File Reports' conducted by the NSDNR. This stratigraphy was then compared to the exposed walls in the Stellarton open pit.

The Stellarton basin is a late Paleozoic pull apart basin consisting of about 3 km of clastic sediment (Waldron, 2004). The basin is approximately 165 km^2 and bounded by two faults, the Hallow fault and Cobequid fault, both of which are dextral strike slip faults (Morris, 2002). The basin consists of eight geologic members, the Thorburn, Coal Brook, Albion, Plymouth, Westville, Skinner, Brook and Middle River. Only the Coal Brook, Albion and Plymouth members are relevant to the Stellarton open pit. The Ford seam is the boundary between the Coal Brook and the Albion members. Meanwhile, the Plymouth member exists concurrently with both of the other members (Gillis, Naylor, & Waldron, 1996).

The Coal Brook member is interlayered mudstone, sandstone, shale, oil shale and coal. The Albion sequence consists primarily of mudstones interlayered with sandstones, shales, oil shales and coal seams dipping 24° to north north-east. These layers range from 3–30 m thick and vary in composition and thickness laterally. In order of increasing age, the coal seams are McLeod, Foord, Cage, Third, Purvis, New, Oil Coal and Norah which are shown in plan view and cross section in Figure 43 and Figure 44 respectively (George Wimpy Canada LTD, 1977).

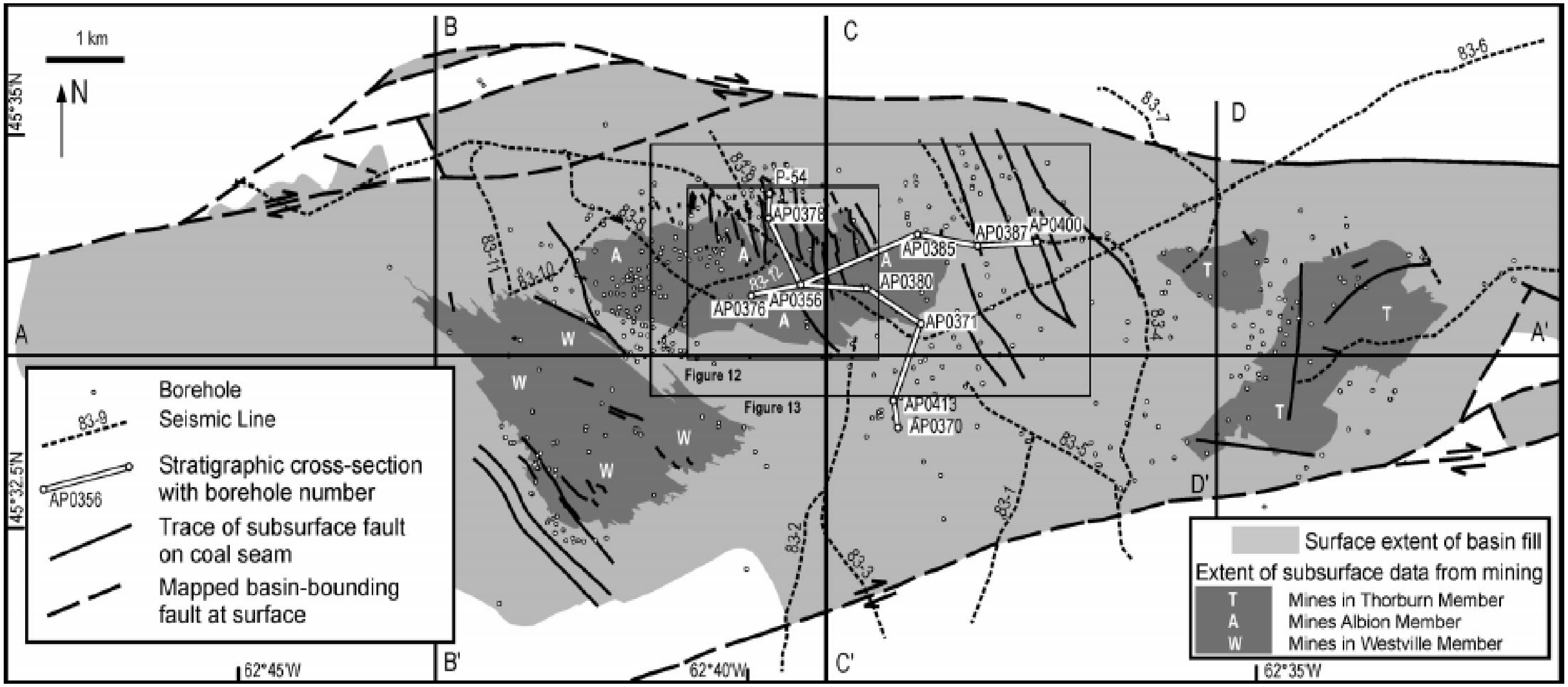

Figure 43: Map showing coal outcrops and boreholes in the Stellarton area notably those used to develop Figure 44.

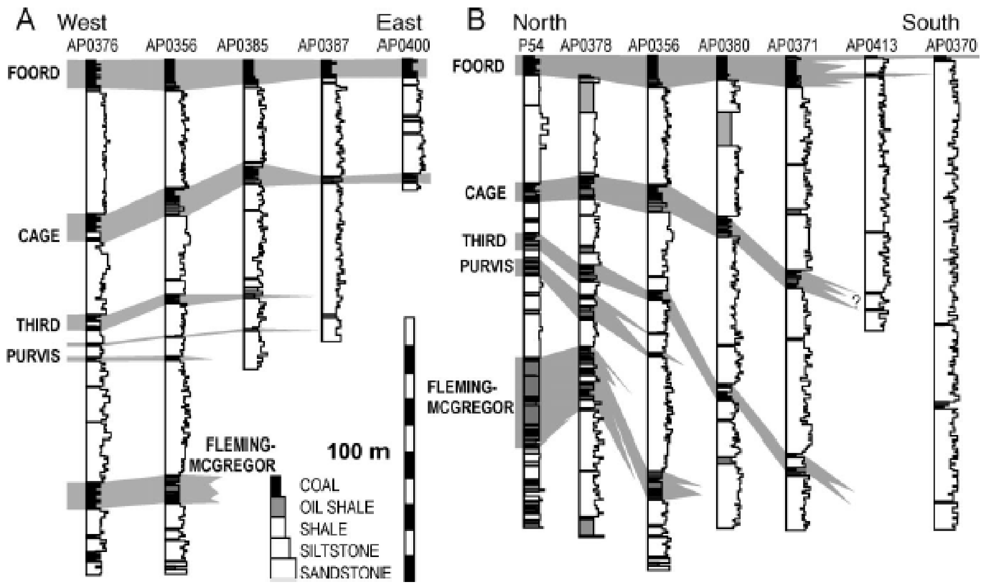

Figure 44: Stratigraphic columns for representative holes in the upper Albion member of the Stellarton formations. Thicknesses are dip corrected true stratigraphic thicknesses. Location of the holes are shown in Figure 43 (Waldron, 2004)**.**

4.2 Site History

Coal was first discovered in Stellarton, then Albion Mines, in 1798 and was locally mined in small pits. Formal mining first began in the Stellarton area in 1827 by the General Mining Association and both surface and later underground methods were used. Mining in the region intensified after the monopoly that the General Mining Association had was revoked in 1858 which resulted in the creation of the Acadia Coal Company in 1866 and the Intercolonial Company's Drummond mine in 1867. Mining remained prominent in the region until World War II that saw a decrease in coal demand due to rising use of oil (Ellerbrok, 1998). Although there have been many mines in the Pictou coal field, it is the Storr, Bye, Cage Foorde, Foster and Westray test pits that that influence the in-situ stresses the immediate area of the Stellarton pit shown in Figure 45 (Gillis & Dewolfe, 1992).

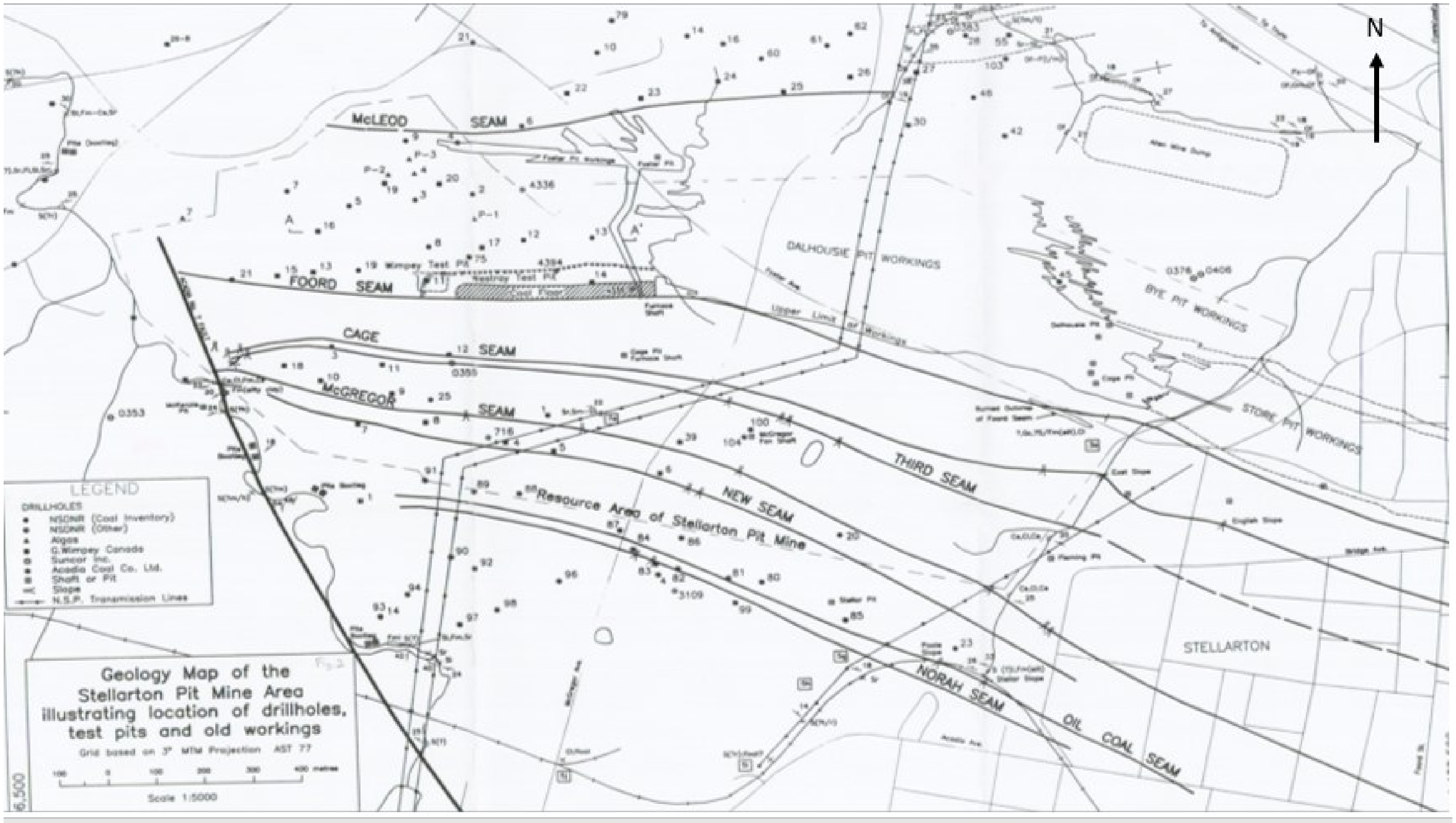

Figure 45: A map of the coal seam outcrops, historic mining locations and Stellarton resource pit mine area ***(Gillis et al., 1996)*** **.**

Due to extensive mining in the area around the Foord and Cage seams, cave-ins were common with subsidence reaching the surface and fires occurred intermittently in the Cage seam workings. In 1996, Pioneer Coal reached an agreement to remine the Foord, Cage, Third and Flemming/McGregor seams to both extract the resource and remediate the effects of historic mining. The effects of previous mining can be seen in the pit wall in Figure 46.

Figure 46: A photo of the side wall of the active open pit the day of testing. Historic underground mining can be seen in the cage seam and the sandstone layer that was to be used to determine the in-situ stress is shown below a layer of coaly shale.

4.3 Test Site Description

The in-situ stress field test site was selected to have a geological stratum that was uninterrupted along strike by mining or erosion so the in-situ stresses were not relieved. The layer of interest was a massive sandstone below the cage seam. The mining on-site proceeds in strips mining down dip. Once one strip is finished another begins in adjacent to the previous cut. Up to three strips may be open prior to the oldest being backfilled. This sequence is shown in Pioneer Coal's mining schedule in Figure 47.

The test sites, shown in Figure 48, were prepared in advance by the mining company. These sites included four pits dug partially through a layer of shale and coal to reach the sandstone layer, unfortunately this was not achieved. In addition, one section of exposed sandstone in the sidewall of the mine was used. These locations are shown in Figure 49.

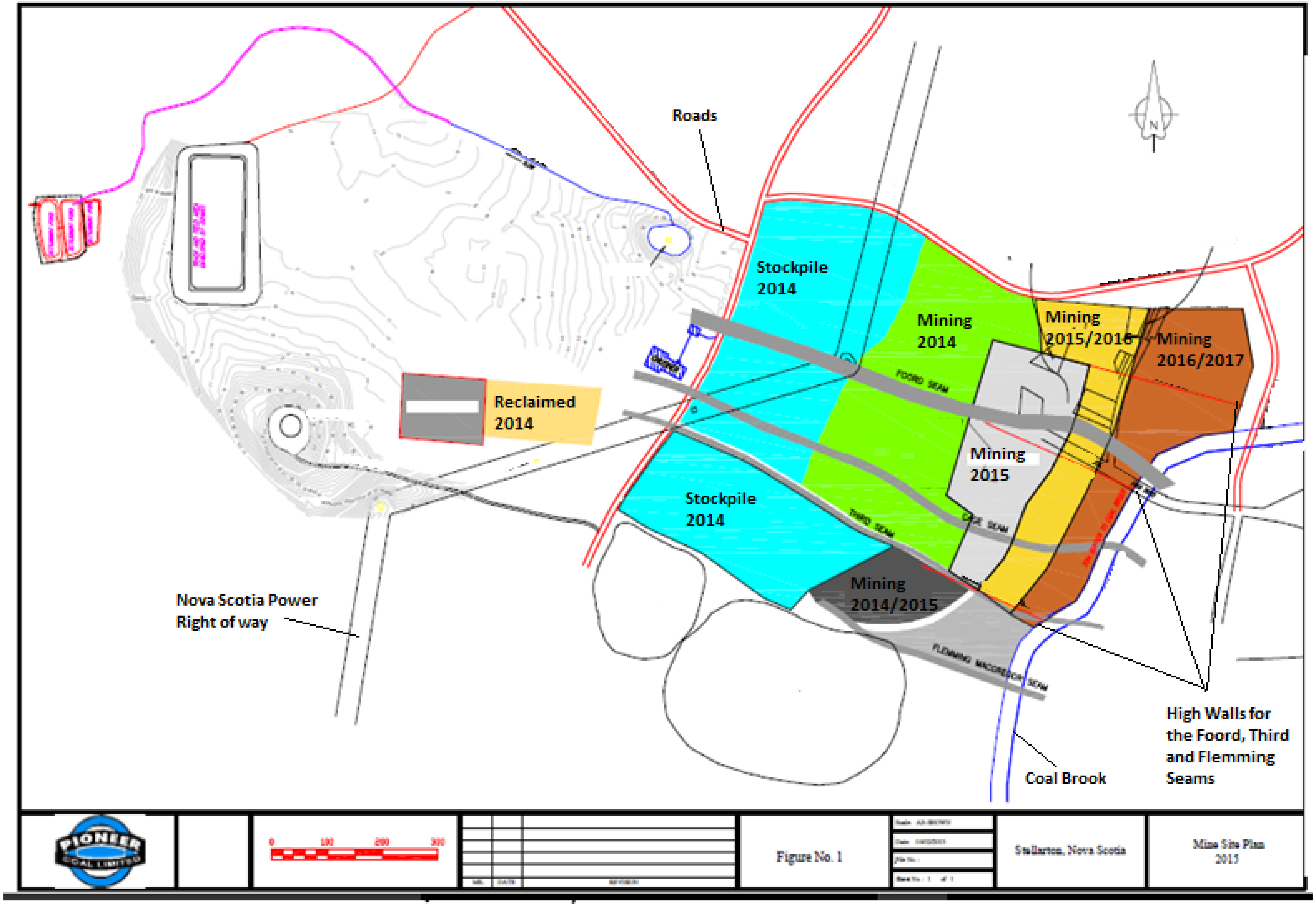

Figure 47: The Stellarton open pit mining schedule.

Figure 48: Image of the test sites in the coal/shale mix.

Figure 49: The testing locations

4.4 Test Equipment

The test equipment used during the field test consisted of the following:

- Glotzl M2H16 Hand Pump with pressure gauges (60 MPa and 6 MPa)
- 2 Glotzl Flatjacks (400 mm x 200 mm x 6 mm)
- Hilti wall mounted 22-inch diameter Diamond Saw provided by contractor
- Mechanical cement bolts 3/8-inchwith tapered tops
- Hydraulic oil
- Hoskins multilength strain gauge set
- Shovel
- Broom
- Calipers (back up)
- Hammer
- Adjustable wrench
- Paint
- Camera

4.5 Test Procedure

The following procedure was used in the test pits created by Pioneer coal. This procedure is based on the ASTM standard testing procedure for flatjacks (ASTM International, 2009).

1. Clean and label test site
2. Install measurement pins
3. Record distance between pins
4. Allow contractors to install and create slot using the specialised saw
5. Record measurement between pins immediately after cutting
6. Position flatjack
7. Begin inflating Flatjack recording the pin position and pressure every 0.7 MPa
8. Hold peak pressure for 15 min recording every 5 min
9. Depressurise jack recording the pin position and pressure every 0.7 MPa
10. Hold zero pressure for 15 min recording every 5 min
11. Repeat 3 times to account for potential hysteresis.

4.6 Test Results

The tests in the pits where mostly unsuccessful because the saw could not be safely anchored to the friable coal and shale layer. Only one slot, in pit 3, was successfully cut and this arrangement is shown in Figure 50. Further, the flatjack would not fit into the slot and thus only the closure measurement could be made. Attempts were made to widen the slot and insert the jack using steel wedges however this only damaged the rock and the slot could not be enlarged as the saw would no longer safely anchor to the rock. There was 241um (0.0095 in) of closure between pins C-D at this location. The slot was then excavated on one side to expose the surface of the cut to evaluate the smoothness of the cut surface which appeared to be satisfactory except for where the saw became loose near end of the cut. This outcome is shown in Figure 51 and the ridge near the outer radius of the cut was caused by the saw vibrating as it loosened in the rock.

Figure 50: Test pit 3 where the 26-inch diameter saw was installed and the slot was successfully cut. This saw and mounting hardware could be pulled easily out of the ground after vibrations due to cutting.

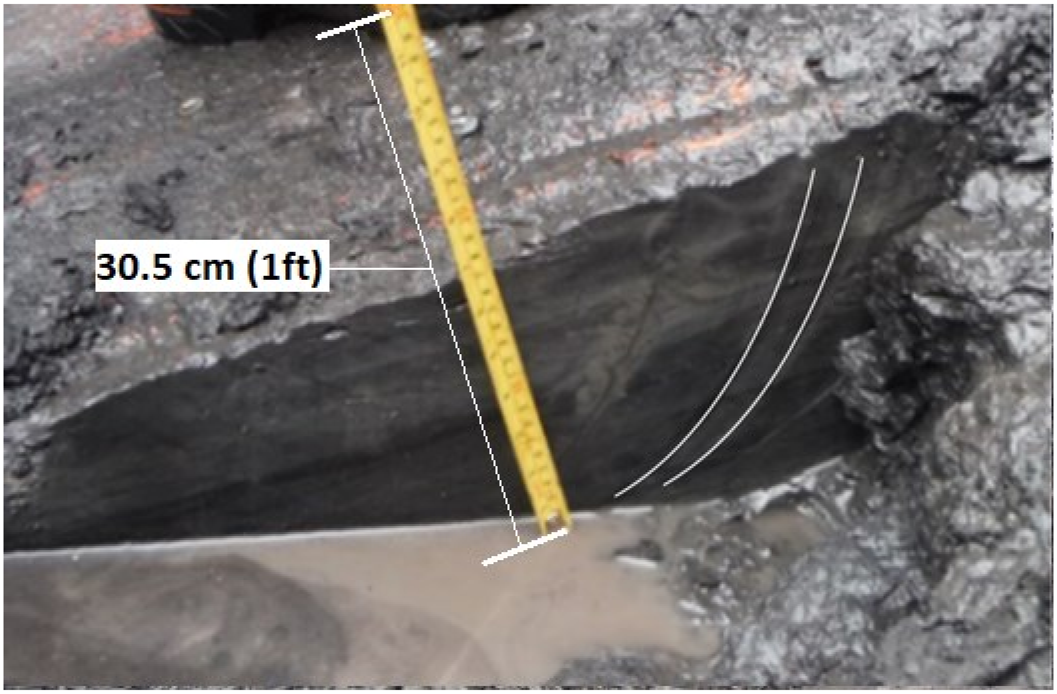

Figure 51: The excavated slot showing the smooth sides of the slot. The two curved white lines highlight the location where the saw became loose and wobbled cutting grooves into the side of the slot

The side wall measurement in the sandstone shown in Figure 52 was more successful. The saw had sufficient anchorage and the cut proceeded smoothly. After the saw cut, the pins were measured and it was found that they dilated indicating the rock was in tension which is consistent with the location as the rock was unconfined and could therefore have no compressive forces. This meant that further testing would not produce meaningful results as pressurising the flatjack would only separate the pins further. Despite this, the test was performed to evaluate the safety and reusability of the field sized flatjack in an ungrouted slot. The installation of the flatjack was difficult as the jack fit tightly into the slot and needed to be hammered in. A steel spacer was used between the hammer and the jack to avoid damaging the jack. The pin locations were measured before and after installing the flatjack to account for the pressure exerted by the tight fit. The installation of the jack was found to spread pins C-D by 25.4 μm (0.001 in) and the jack was off centred in the slot after installation by 9 cm. Due to the time constraints, uncertainty on the recoverability of the jack and the lack of stresses it was deemed acceptable to continue as only the reusability of the jack would be evaluated. Due to time constraints, only the measurement C-D (the pins closest to the slot) were measured. The jack was pressurized to 2 MPa for an initial test, allowed to deflate and then pressurised to 5 MPa. Recovery of the jack was successful by using a wrench and prying up on the hooks of the jack with a progressively larger spacer between the rock face and the wrench. No damage to the flatjack was observed.

Figure 52: The wall test location. The cut was made directly behind where the engineer is standing.

4.7 Numerical Modeling

Two numerical models where used to gain insight into the in-situ stresses in the Stellarton pit using a closure measurement obtained from a single flatjack located at the bottom of the pit. The first model was used to determine the stress at the slot location using the closure measurement for the given slot geometry. The second model was of the open pit and used to determine the effect of the open pit on the stress at the measurement location.

The first model was of the slot (test scale) and was used to find the relationship shown in Equation [16] between stress, slot closure and Young's modulus of the material and a closure correction factor ($G_{C\text{-}D}$). The closure correction factor for a particular geometric configuration, $G_{C\text{-}D}$, was easily determined using known values of applied pressure and Young's modulus, then using the first numerical model to solve for the closure at a particular point. The values were then inserted into in Equation [16] and the $G_{C\text{-}D}$ value was determined. This value of $G_{C\text{-}D}$ was then used with the closure obtained in the field to determine the stress at the location of the measurement.

The Plaxis3D model for this slot shown in Figure 53 was 6 m by 6 m by 6 m to minimise edge effects. In addition, only a quarter slot was modeled to maximise computational efficiency and normally constrained boundaries along the axis of symmetry of the slot. The slot was a drag cut 20 cm deep and 40 cm long along the bottom edge of the slot with "wings" corresponding to a 26-inch diameter blade. The $G_{C\text{-}D}$ value was found to be 1.373 using the closure contours caused by a known load, shown in Figure 53, and Equation [16].

[16]

$$\boldsymbol{\sigma = G_{C-D}\Delta_{C-D}E}$$

Where: σ is the stress perpendicular to the slot

$G_{C\text{-}D}$ is a factor accounting for the geometry of the slot and the position of measurement relative to it

$\Delta_{C\text{-}D}$ is the closure between pins C and D

E is the Young’s modulus of the material

The resulting stress using this equation and the closure of 241 µm are shown in Figure 54 as a function of Young’s modulus. The rock on site was a very friable shale/coal and thus the value of Young’s modulus is likely between that of a weak shale (10 GPa) (Al-maamori, Hesham, Naggar, & Micic, 2014) and strong coal (4.74 GPa) (Ming, Yi, & Tiedemann, 2005). This results in a stress between 1.56 MPa and 3.31 MPa.

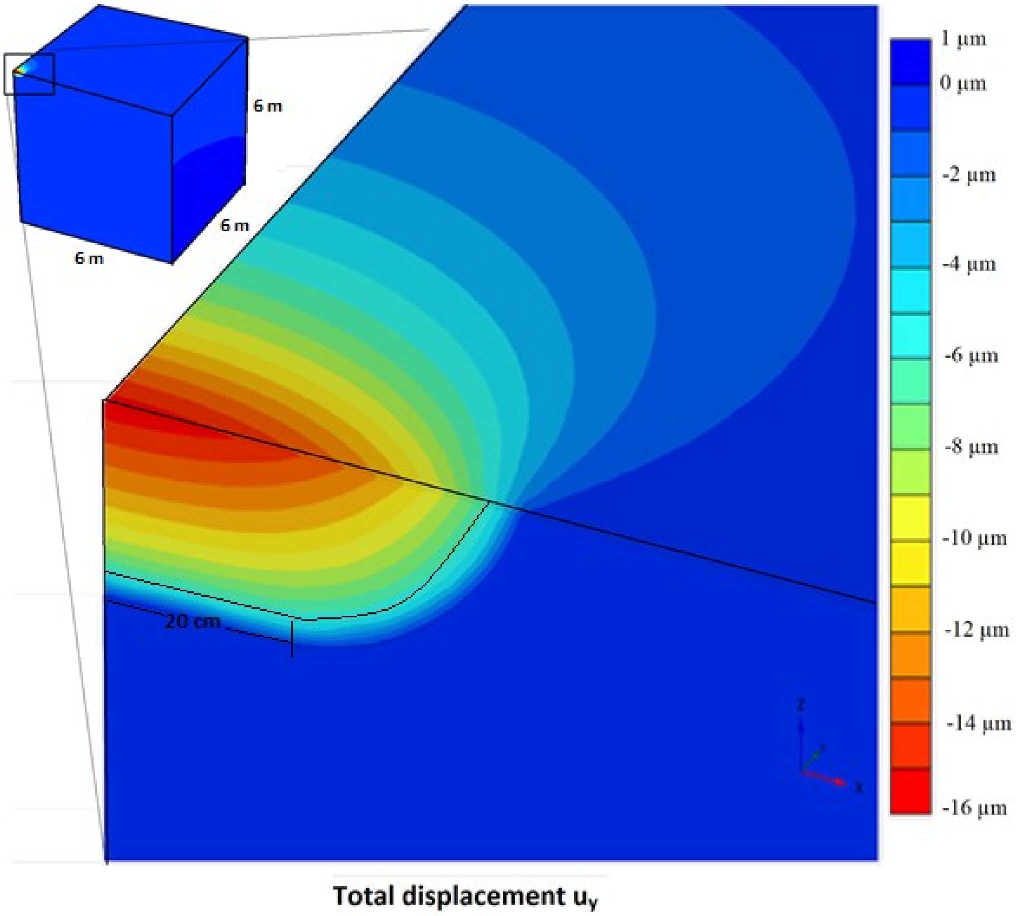

Figure 53: The Plaxis3D model used to develop the G_{C-D} factor used for the 26-inch drag cut. Negative numbers indicate movement toward the slot centerline. The left and front sides of the model, as shown in the image, are planes of symmetry with normally constrained boundary. The bottom and right sides are also normally constrained and the top and the back are free surfaces. The load was applied to the back of the model as a pressure.

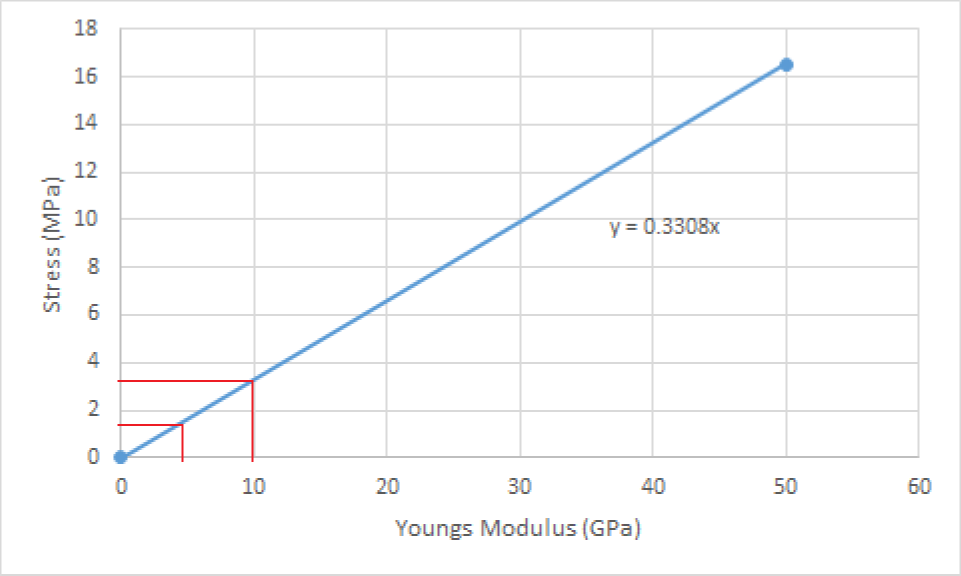

Figure 54: In-situ stress vs. Young's modulus graph for 0.25 mm closure at Stellarton developed for the 26-inch drag cut.

The second linear elastic numerical model, shown in Figure 55, was used to determine the unperturbed in-situ stress by correcting the values obtained from the flatjack test for the effect of the open pit. In this way, the undisturbed in-situ stress for the location could be evaluated. The mining in the open pit proceeded in strips, mining down dip with up to two of these 80 m wide strips being excavated concurrently. This mining sequence was replicated using Plaxis3D, as shown in Figure 55. The model dimensions were 2600 m by 2000 m by 400 m deep and contained no stratigraphic layers or historic mining since the addition of these made the model too computationally demanding. This limitation was deemed acceptable as it was mainly the effects of pit geometry being examined and the test location was fully contained within one stratigraphic layer away from historic mining. Gravity loading and the additional in-situ stress component perpendicular to the slot were modeled separately due to software limitations that caused uniform stress on the loaded boundary despite gravity loading. The results of these models were then elastically superimposed to determine the total stress as shown in Equation [17]. Gravity loading used a density of 2.7 t/m^3 and had a water table at -100 m while the additional loading used a massless rock and an applied uniform load on the x maximum boundary of 1 MPa. The node used to measure stresses was representative of the location of pit 3. It was found that at the location of testing the stress was 0.178 MPa due to gravity loading and 1.262 greater than any additional in-situ stresses. The stress at this point due to gravity prior to the perturbation was 0.723 MPa. Using Equations 18 through 20, the final unperturbed in-situ stress component perpendicular to the slot was found to be between 1.82 MPa and 3.23 MPa and is shown in Figure 56.

[17] $$\boldsymbol{\sigma_{\mathrm{H}\ total(perturbed)} = \sigma_{H\ gravity(perturbed)} + \sigma_{H\ additional}}$$

[18] $$\boldsymbol{\sigma_{\mathrm{H\ total}(unperterbed)} = \sigma_{\mathrm{H}\ gravity\ (unpreturbed)} + \frac{\sigma_{H\ additional}}{1.262}}$$

Substituting Equation [17] into Equation [18]

[19] $$\boldsymbol{\sigma_{H\ unperterbed} = \sigma_{H\ gravity\ (unpreturbed)} + \frac{\sigma_{H\ total} - \sigma_{H\ gravity(perturbed)}}{1.262}}$$

Inputting the numbers from the numerical model the Equation [19] simplifies to Equation [20]

[20] $$\boldsymbol{\sigma_{H\ unperterbed} = 0.723 + \frac{0.3308 \times \mathrm{E} - 0.178}{1.262} = 0.582 + .2621 \times E}$$

Where:

$\sigma_{\mathrm{H\ total\ (perturbed)}}$ = The total stress perpendicular to the slot measured at the bottom of the pit after correcting for slot geometry (i.e. Result from the first numerical model)

$\sigma_{\mathrm{H\ gravity(perturbed)}}$ = The stress perpendicular to the slot due to gravity at the bottom of the pit during mining.

$\sigma_{\mathrm{H\ additional}}$ = The stress perpendicular to the slot measured at the bottom of the p due to additional causes other than gravity (ex. tectonic, residual, etc.)

$\sigma_{H\ total\ (unperturbed)}$ = The total stress perpendicular to the slot measured at the bottom of the pit prior to mining taking place

$\sigma_{H\ gravity(perturbed)}$ = The stress perpendicular to the slot due to gravity at the bottom of the pit prior to mining taking place

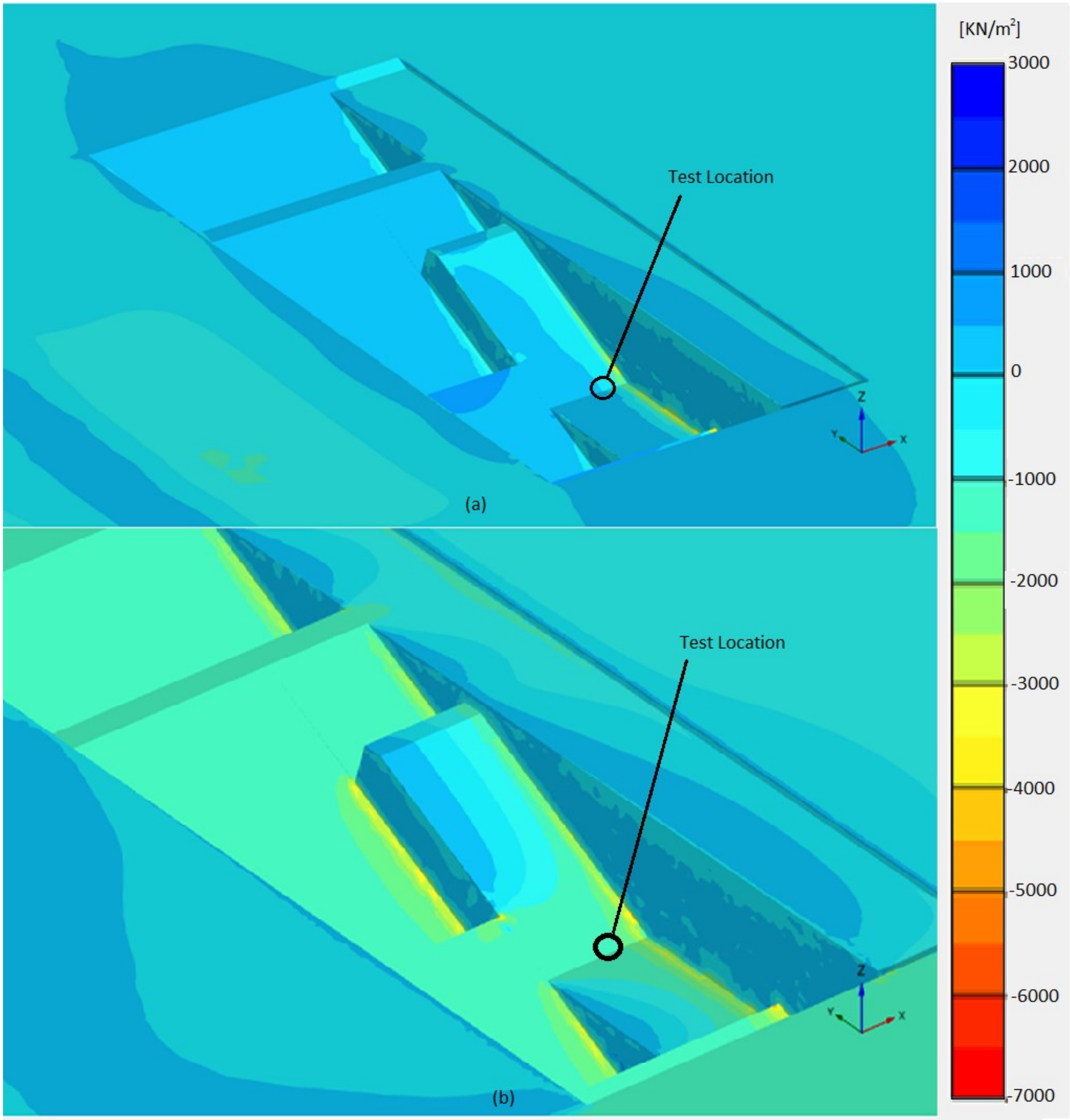

Figure 55: Numerical model of the Stellarton open pit developed using the pit schedule, geology and field observations. The image (a) is the stress in the x direction induced by gravitational loading (ρ=2.7 t/m^3) and (b) is the additional stress in the x direction due to other factors simulated by applying a 1 MPa load on the x maximum boundary.

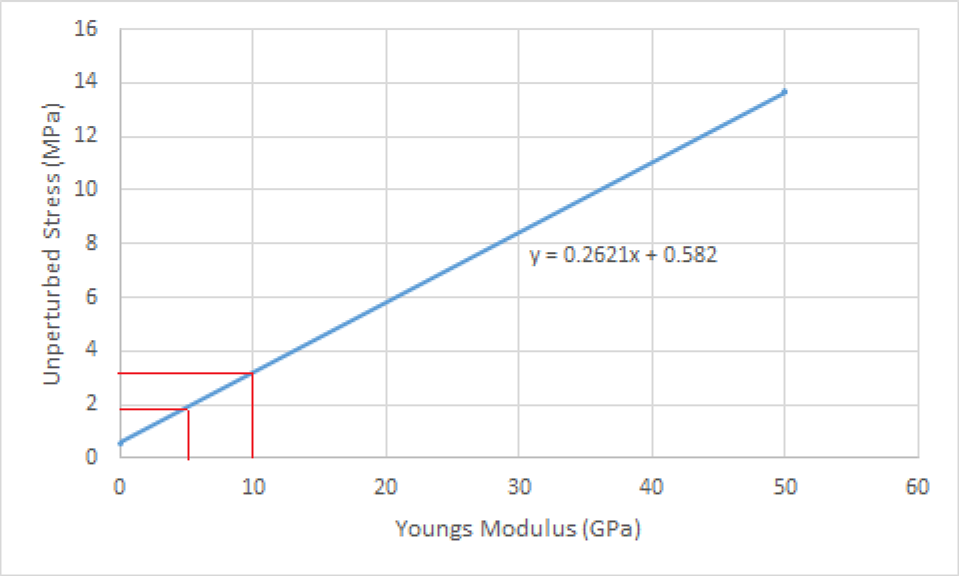

Figure 56: The pre-mining unperturbed stress with as a function of the rock's Young's modulus.

4.8 Summary of Results and Discussion

The results of the field tests certainly have their limitations, uncertainty in the Young's modulus and having only one test result being principle among them. The uncertainty in the Young's modulus gives an equally large uncertainty in the stress when using the linear elastic model. Since the material in which measurement was conducted is very friable, a sufficiently large sample could not be obtained to determine the modulus and other methods such as Leeb's hardness would produce unreliable results. Another source of error was the numerical model of the pit that did not account for the effects of previous mining and had no stratigraphy. Although these were originally included in the model it proved to large be calculated using the available hardware and had to be discarded for a simpler model.

Although the field test did not yield a full stress tensor for the Stellarton pit due to the inaccessibility of the sandstone layer, it did demonstrate that the modifications to the ASTM could be scaled to a larger flatjack and that the flatjack could be recoverable. The numerical modeling techniques demonstrated can be useful for negating the effects the open pit on the stress field. The test also emphasised the versatility of using non-specialised equipment that is easily used in any rock type and can be used to widen slots such as a hand-held rock saw. The lack of flatjack measurements led to the realisation that the use of the slot closure from a particular geometry can be used to estimate the in-situ stress. This could prove to be a useful method of determining in-situ stress without the need for specialised jacking equipment since all that is needed is a saw, measurement pins and a suitably accurate measurement device.

5.0 CONCLUSIONS AND RECOMMENDATIONS

In-situ stresses are highly variable and are affected by multiple different loading mechanisms on heterogenic and often perturbed material. This makes single measurements less representative of the overall stress tensor when compared to many measurements because of the variability of the stress within the rock mass. The use of field observations such as the topography can help to understand the stresses in an area and can be used to optimise positioning of stress tests. The flatjack test is one of the lowest cost stress tests since it requires minimal equipment and does not require mobilisation of a drill rig. This situation makes the flatjack test ideal for collecting large data sets and for more cost sensitive projects. In addition, since the Young's modulus is not needed for the test there is one less variable to contribute to error in the results.

The goal of this research was to reduce the time and cost of performing an in-situ stress test. By using the correction factor (*J*) and a saw cut slot, the time required to cut the slot is reduced and wait time for grout to set can be eliminated. In addition, slot closure for a specific slot geometry has demonstrated the ability to determine in-situ stress without the use of specialised flatjack equipment if the modulus of the rock mass is known.

The lab tests established correction factors (J) for slot geometries that varied from the flatjacks geometry. The maximum error between the lab results and the numerical modeling cancelation pressure results was 23.5% in test R-P-14. This uncertainty in the results is somewhat large; it is comparable to other in-situ measurement techniques(Heidbach et al., 2008). The numerical modeling indicated a strong correlation (R^2=0.989) between the relative jack/slot area and the cancelation pressure however variability in the lab results indicated that this trend was not a strong correlation (R^2=0.156). The geometry of the flatjack itself did not affect the accuracy of the results when compared to numerical modeling predictions.

The lab tests also established correction factors ($G_{C\text{-}D}$) to correlate slot closure to the modulus and applied stress. Analysis of slot area relative to the slot closure both the modeling and the lab results indicated a relationship with R^2=0.618 and R^2=0.799 respectively. Although there is a relationship between slot area and closure between pins C-D, it is clear by tests ASTM-OB and C-P-12, which have similar slot areas, that slot geometry also plays an important role in closure measurements. The closure results for the plunge cuts with a rectangular jack are inconsistent between the numerical model and the lab tests with an error of up to 34.9%. No issue was found with the model and another lab test is recommended to try and isolate the cause of the error.

It is recommended that the techniques in this paper can be used to determine correction factors, J and $G_{C\text{-}D}$ for more slot geometries. Finally, the flatjacks used were ungrouted and provided results consistent with theoretical results and ASTM specification tests. This result means it is possible to conduct many tests with the same jack; however, the amount of times a jack can be used is still unknown but presumably they can be used until damaged.

Results from the field test showed that non-square slots and an ungrouted jack used in the lab could be applied to a larger flatjack in the field and the jack could be recovered and reused. While the flatjack test in the field did not successfully measure in-situ stress, the limited data collected directly resulted in analysing the slot closure for a relationship to the stress. The slot closure measured at Pioneer Coal was 241 μm and after correcting for slot and pit effects the pre-mining stress was found to be between 1.82 MPa and 3.23 MPa for the pre-mining stress and 1.56 MPa and 3.31 MPa post mining. Both values are for the stress acting along the strike of the seam.

The impact of these conclusions is to reduce the cost and time to perform a flatjack test by providing correction factors for quickly-made slots, demonstrate recovery of the jacks and produce reasonably reliable results using ungrouted jacks and pins. In addition, a novel method of determining the in-situ stress was developed that can be done with minimal specialised equipment.

After completing the tests, several recommendations about the test setup are made. Firstly, a template is necessary for the proper placement of the measurement pins as the drill can easily deviate while drilling. In addition, a portable saw is recommended over a mounted saw as it allows for slot widening, can be used in friable rock and is readily available on many project sites.

Much was learned about measurement of the pins as well. LVDT's could not be used as they would interfere with the saw when cutting the slot. It is for this reason that for the measurements before and after the saw cut should be done with a calibrated micrometer and pins with a 45^{o} countersink. This provided an edge to surface contact between the device and the pins that was insensitive to misalignment and damage to the pin. It would be possible to set up LVDT's after cutting the slot to get better result and this is recommended if the modulus is required as the displacements are so small that the measurements between pins on the same side of the slot from that the dial gauge micrometer has a very large relative error. If only the stress is required only pins C and D are needed and the test can be reduced to one loading cycle as additional tests are to establish if hysteresis is present and if it is present only the first cycle can be used to determine in-situ stress.

Finally, larger cuts such as the drag cut produce larger closures and require higher jack pressure to achieve cancelation. This makes the measurements larger relative to the instrument error and therefore provided more accurate results.

REFERENCES

Aiyeru, S. G. (2014). In-situ stress measurement from LOT data using inversion method. Stavanger Norway: University of Stavanger.

Al-maamori, H. M. S., Hesham, M., Naggar, E., & Micic, S. (2014). A Compilation of the Geo-Mechanical Properties of Rocks in Southern Ontario and the Neighbouring Regions, *2014*(May), 210–227.

Amadei, B., & Stephansson, O. (1997). *Rock Stress and its Measurement*. Springer Science and Business Media.

ASTM International. (2003). Standard Test Method for In Situ Compressive Stress Within Solid Unit Masonry. *Annual Book of ASTM Standards*, (C1196 − 09), 1–5. http://doi.org/10.1520/C1196-09.2

ASTM International. (2005). Standard Test Method for Determination of In Situ Stress in Rock Mass by Overcoring Method — USBM Borehole Deformation Gage 1. *Annual Book of ASTM Standards*, (D4623 − 08), 1–14. http://doi.org/10.1520/D4623-08.2

ASTM International. (2008). Standard Test Method for In Situ Stress and Modulus of Deformation Using Flatjack Method. *Annual Book of ASTM Standards*, (D4729), 1–7. http://doi.org/10.1520/D4729-08.

ASTM International. (2009). Standard Test Method for Determination of In-Situ Stress in Rock Using Hydraulic. *Annual Book of ASTM Standards*, (D4645-8), 1–7. http://doi.org/10.1520/D4645-08.2

Atkinson, J. N. R., & Schuller, M. (1990). *Masonry Evaluation using the Flatjack Method* (Vol.

1). Boulder CO.

Brinkgreve, R. B. J., Kumarswamy, S., & Swolfs, W. M. (2015). Plaxis 2015. In *User Manual*. Delft.

Brown, E. T., & Hoek, E. (1978). Technical Note: Trends in Relationships between Measured In-Situ Stresses and Depth. *International Journal of Rock Mechanics and Mining Sciences*, *15*, 211–215.

Carpinteri, A., Invernizzi, S., & Lacidogna, G. (2005). In Situ Damage Assessment and Nonlinear Modelling of a Historical Masonry Tower. *Engineering Structures*, *27*(3), 387–395. http://doi.org/10.1016/j.engstruct.2004.11.001

Christiansson, R., & Janson, T. (2003). A test of different stress measurement methods in two orthogonal bore holes in Äspö Hard Rock Laboratory (HRL), Sweden. *International Journal of Rock Mechanics and Mining Sciences*, *40*(7–8), 1161–1172. http://doi.org/10.1016/j.ijrmms.2003.07.006

Corthésy, R., He, G., Gill, D. E., & Leite, M. H. (1999). A stress calculation model for the 3D borehole slotter. *International Journal of Rock Mechanics and Mining Sciences*, *36*(4), 493–508. http://doi.org/10.1016/S0148-9062(99)00023-6

Dongshen, S., Qunce, C., Zhongxiu, W., Zhao;, W., & Li, A. (2015). In situ stress measurement method and its application in unconventional oil and gas exploration and development. *Acta Seismologica Sinica*, *89*(2), 685–686.

Eberhardt, E., & Stead, D. (2011). Geotechnical Instrumentation. In P. Darling (Ed.), *SME Mining Engineering Handbook* (Third Edit, pp. 551–571). Society For Mining, Metallurgy and

Exploration Inc.

Ellerbrok, G. W. (1998). The Louis Frost Notes 1685 to 1962. Retrieved November 24, 2017, from http://www.mininghistory.ns.ca

Engelder, T., & Sbar, M. L. (1984). Near-Surface in Situ Stress: Introduction. *Journal of Geophysical Research*, *89*(B11), 9321–9322.

Figueiredo, B., Lamas, L., & Muralha, J. (2010). Determination of in Situ Stresses Using Large Flat Jack Tests. *ISRM International Symposium*, (October 2015), 23–27. http://doi.org/10.13140/2.1.3118.9762

Froidevaux, C., Paquin, C., & Souriau, M. (1980). Tectonic Stresses in France: In Situ Measurements With a Flat Jack. *Journal of Geophysical Research*, *85*(B11), 6342–6346. Retrieved from http://www.agu.org/pubs/crossref/1980/JB085iB11p06342.shtml

George Wimpy Canada LTD. (1977). *Method Statement For Stellarton Pictou County, Nova Scotia Opencast Coal Project November 1977*. Toronto.

Gillis, K. S., & Dewolfe, J. D. (1992). *Open File Report 92-001: Nova Scotia Department of Natural Resources Report on th Location of Abandoned Mine Workings in the Pictou Coalfield*.

Gillis, K. S., Naylor, R. D., & Waldron, J. W. F. (1996). *Minerals and Energy Branch Open File Report 96-005: Geology of the Foord Seam and Associated Strat in the Area of the Stellarton Pit Mine, Pictou Coalfield, Stellarton Basin, Nova Scotia*.

Google Maps. (2018). Google Maps. Retrieved from https://www.google.ca/maps/@45.5029696,-62.6308115,7.96z

Gregorczyk, P., & Lourenço, P. B. (2000). A Review on Flat-Jack Testing. *A Revista de Engenharia Civil*, (9), 39–50.

Harper, T. R., & Szymanski, J. S. (1991). The nature and determination of stress in the accessible lithosphere. *Philosophical Transactions of the Royal Society A: Mathematical, Physical and Engineering Sciences*, *A*(337), 5–24. http://doi.org/10.1098/rsta.1991.0102

Heidbach, O., Tingay, M., Barth, A., Reinecker, J., Kurfeß, D., & Müller, B. (2008). The World Stress Map database release 2008. http://doi.org/10.1594/GFZ.WSM.Rel2008

Hoek, E. (2008). Practical Rock Engineering. *Environmental and Engineering Geoscience*, *14*(1), 57. http://doi.org/10.2113/gseegeosci.14.1.55

Holcomb, D. J. (1993). General Theory of the Kaiser Effect. *International Journal of Rock Mechanics and Mining Sciences*, *30:929-35*.

Hoskins, E. R. (1966). An Investigation of the Flatjack Method of Measuring Rock Stress. *International Journal of Rock Mechanics and Mining Sciences*, *3*, 249–264.

Jaeger, J. C., Cook, N. G. W., & Zimmerman, R. (2009). *Fundamentals of Rock Mechanics* (4th Editio). Wiley-Blackwell.

Kim, K., & Franklin, J. (1987). Suggested methods for rock stress determination. *Int J Rock Mech Min Sci Geomech Abstr*, *24*(I), 1987.

Ljunggren, C., Chang, Y., Janson, T., & Christiansson, R. (2003). An overview of rock stress measurement methods. *International Journal of Rock Mechanics and Mining Sciences*, *40*(7–8), 975–989. http://doi.org/10.1016/j.ijrmms.2003.07.003

Martel, S. J. (2016). Effects of small-amplitude periodic topography on combined stresses due to gravity and tectonics. *International Journal of Rock Mechanics and Mining Sciences*, *89*, 1–13. http://doi.org/10.1016/j.ijrmms.2016.07.026

Matthes, F. E. (2006). Early History of The Yosemite Valley. Retrieved November 25, 2017, from https://www.nps.gov/parkhistory/online_books/geology/publications/pp/160/sec2a.htm

Mayer, A., Habib, P., & Marchand, R. (1951). Underground Rock Pressure Testing. *International Conference about Rock Pressure and Support in the Working Liege*, 217–221.

Men in the Mines: A History of Mining Activity in Nova Scotia, 1720-1992. (2017). Retrieved November 24, 2017, from https://novascotia.ca/archives/meninmines/timeline.asp?Language=English#1600

Ming, Z., Yi, W., & Tiedemann, J. (2005). Analysis of Mechanical Properties of Sedimentary Rocks of Coal Measures and Their Influencing Factors. In *ARMA/USRMS 05-687*.

Morris, W. A. (2002). Paleomagnetism of Carboniferous strata from the Stellarton Gap, *1540*, 1527–1540. http://doi.org/10.1139/E02-055

Mortazavi, A., & Saati, V. (2016). Numerical investigation of Extra Large Flat Jack Testing of Bakhtiyari Dam Project.

Nelson, S. (2011). Weathering, Soils and Sedimentary Rocks. Retrieved November 25, 2017, from http://www.tulane.edu/~sanelson/eens1110/weathering_sedrx.htm

Nezhadshahmohamad, F., & Moosazadeh, S. (2015). Devlopment of New Equations to Determine In Situ Stresses from Borehole Slotter Test Results. *International Journal of Research Science and Management*, *2*(2), 1–9.

Palmström, A., & Singh, R. (2001). The deformation modulus of rock masses - Comparisons between in situ tests and indirect estimates. *Tunnelling and Underground Space Technology*, *16*(3), 115–131. http://doi.org/10.1016/S0886-7798(01)00038-4

Panek, L. A. (1966). Calculation of the Average Ground Stress Componants from Measurments of the Diametral Deformation of a Drillhole. *American Society of Testing Materials*, (ASTM STP402), 106.

Pariseau, W. G. (1971). Influence of Topography on the Pre-Mining State of Stress. *Proceedings from the 7th Canadian Symposium on Rock Mechanics*, (7), 191–200.

R. Holzhausenab, G., & M. Johnson, A. (1978). The concept of residual stress in rock. *Tectonophysics*, *58*(3–4), 237–267.

Rummel, F., Klee, G., & Weber, U. (2002). Rock stress measurement by means of hydraulic fracturing in borehole KOV01. Oskarshamn, Sweden. http://doi.org/SKB IPR-02-01

Serata, S., Sakuma, S., Kikushi, S., & Misuta, Y. (1992). Double Fracture Method of In Situ Stress Measurement in Brittle Rock. *Rock Mechanics and Rock Engineering*, (25), 89–108.

Simkin, T., Unger, J. D., Tilling, R. I., Vogt, P. R., & Spall, H. (1994). This Dynamic Planet. Retrieved November 25, 2017, from http://topex.ucsd.edu/erth01/DynamicPlanet.pdf

Tincelin, O. (1951). Research on the Iron Mines of Lorraine (France). *Proceedings of the International Conference on Rock Pressure and Support in Workings, Liege*.

Ulusay, R. (2015). *The ISRM Suggested Methods for Rock Characterization, Testing and Monitoring: 2007-2014*. Cham: Springer International Publishign.

Vreed, F. A. (1981). Critical Study of the Method of Calculation Virgin Rock Stresses from Measurement of Results of the CSIR Triaxial Strain Cell. Pretoria, South Africa: National

Mechanical Engineering Research Institute.

Waldron, J. W. F. (2004). Anatomy and evolution of a pull-apart basin , Stellarton , Nova Scotia, (1), 109–127. http://doi.org/10.1130/B25312.1

White, O. L., & Russell, D. (1982). High Horizontal Stresses in Southern Ontario - Their Orientation and Their Origin. In *IV Congress Intaernational Association of Engineering Geology* (Vol. 5). New Delhi.

Yamamoto, K. (2009). A Theory of Rock Core-Based Methods for Iin-situ Stress Measurement. *Earth Planets Space*, *61*, 1143–1161. Retrieved from http://kynmt.in.coocan.jp/REFERENCE/ 15_61101143.pdf

Yokoyama, T., Sano, O., Hirata, A., Ogawa, K., Nakayama, Y., Ishida, T., & Mizuta, Y. (2014). Development of borehole-jack fracturing technique for in situ stress measurement. *International Journal of Rock Mechanics and Mining Sciences*, *67*, 9–19. http://doi.org/10.1016/j.ijrmms.2013.12.008

Zoback, M. D., Barton, C. A., Brudy, M., Castillo, D. A., & Finkbeiner, T. (2003). Determination of stress orientation and magnitude in deep wells, *40*, 1049–1076. http://doi.org/10.1016/j.ijrmms.2003.07.001

Zoback, M. Lou, & Magee, M. (1991). Stress magnitudes in the crust; constraints from stress orientation and relative magnitude data. *Philosophical Transactions of the Royal Society of London, Series A: Mathematical and Physical Sciences*, *337*(1645), 181–194.

APPENDIX A: LAB FLATJACK DATA

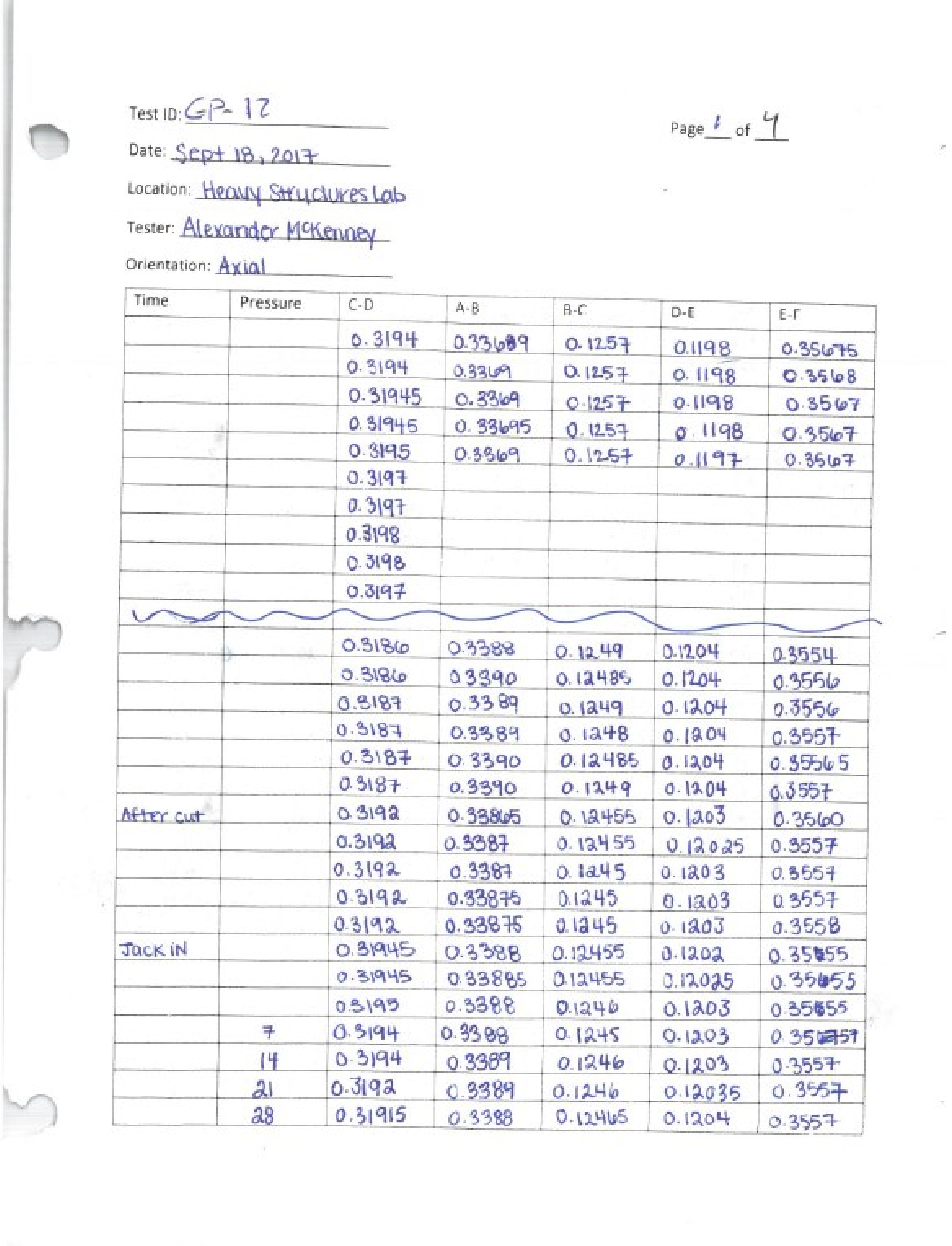

Test ID: GP- 12

Page 1 of 4

Date: Sept 18, 2017

Location: Heavy Structures Lab

Tester: Alexander McKenney

Orientation: Axial

Time	Pressure	C-D	A-B	B-C	D-E	E-F
		0.3194	0.33689	0.1257	0.1198	0.35675
		0.3194	0.3369	0.1257	0.1198	0.3568
		0.31945	0.3369	0.1257	0.1198	0.3567
		0.31945	0.33695	0.1257	0.1198	0.3567
		0.3195	0.3369	0.1257	0.1197	0.3567
		0.3197				
		0.3197				
		0.3198				
		0.3198				
		0.3197				
		0.3186	0.3388	0.1249	0.1204	0.3554
		0.3186	0.3390	0.12485	0.1204	0.3556
		0.3187	0.3389	0.1249	0.1204	0.3556
		0.3187	0.3389	0.1248	0.1204	0.3557
		0.3187	0.3390	0.12485	0.1204	0.35565
		0.3187	0.3390	0.1249	0.1204	0.3557
After cut		0.3192	0.33865	0.12455	0.1203	0.3560
		0.3192	0.3387	0.12455	0.12025	0.3557
		0.3192	0.3387	0.1245	0.1203	0.3557
		0.3192	0.33875	0.1245	0.1203	0.3557
		0.3192	0.33875	0.1245	0.1203	0.3558
Jack in		0.31945	0.3388	0.12455	0.1202	0.35655
		0.31945	0.33885	0.12455	0.12025	0.35655
		0.3195	0.3388	0.1246	0.1203	0.35655
	7	0.3194	0.3388	0.1245	0.1203	0.35657
	14	0.3194	0.3389	0.1246	0.1203	0.3557
	21	0.3192	0.3389	0.1246	0.12035	0.3557
	28	0.31915	0.3388	0.12465	0.1204	0.3557

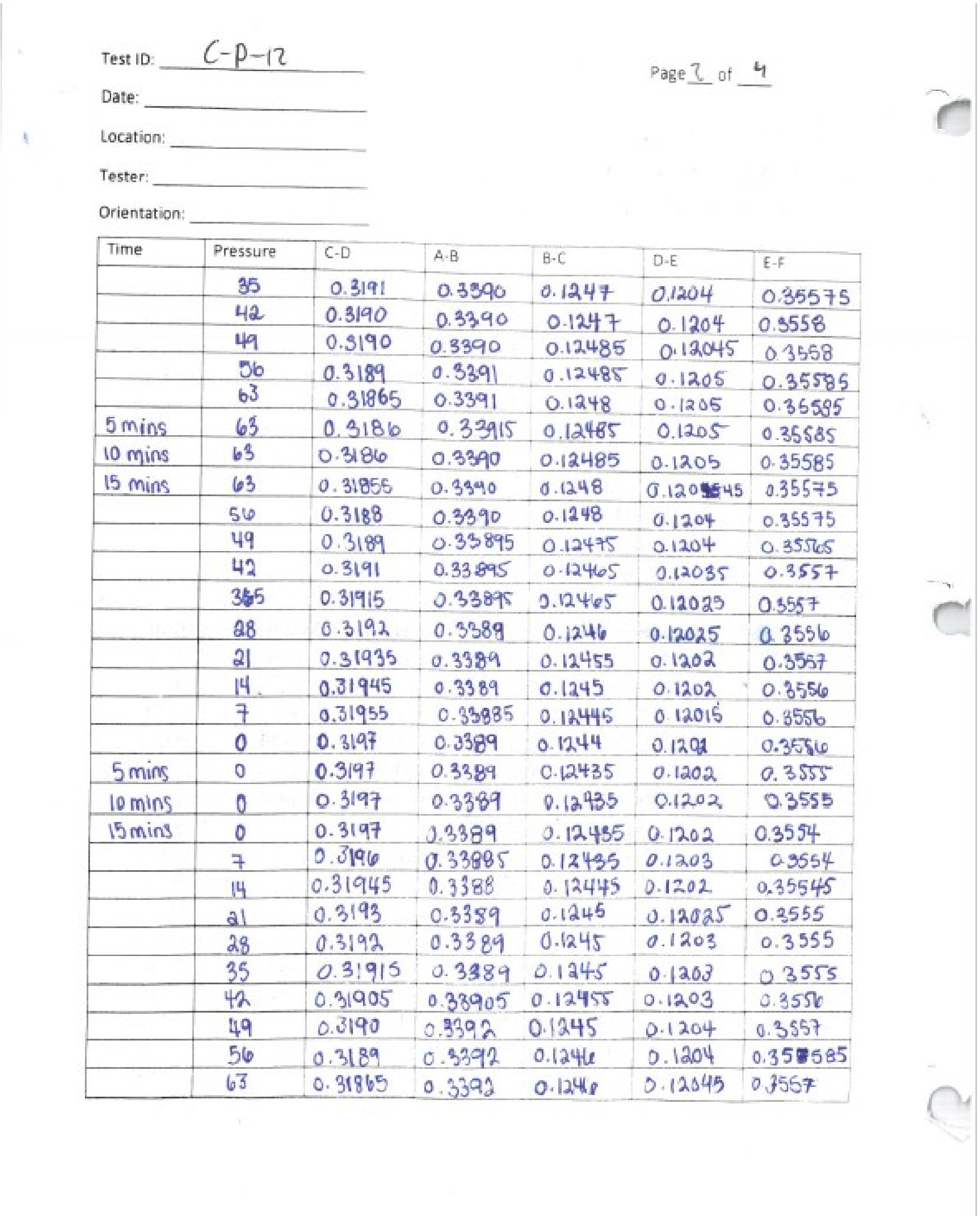

Test ID: C-P-12

Page 2 of 4

Date:

Location:

Tester:

Orientation:

Time	Pressure	C-D	A-B	B-C	D-E	E-F
	35	0.3191	0.3390	0.1247	0.1204	0.35575
	42	0.3190	0.3390	0.1247	0.1204	0.3558
	49	0.3190	0.3390	0.12485	0.12045	0.3558
	56	0.3189	0.3391	0.12485	0.1205	0.35585
	63	0.31865	0.3391	0.1248	0.1205	0.35595
5 mins	63	0.3186	0.33915	0.12485	0.1205	0.35585
10 mins	63	0.3186	0.3390	0.12485	0.1205	0.35585
15 mins	63	0.31855	0.3390	0.1248	0.120[illegible]45	0.35575
	56	0.3188	0.3390	0.1248	0.1204	0.35575
	49	0.3189	0.33895	0.12475	0.1204	0.35565
	42	0.3191	0.33895	0.12465	0.12035	0.3557
	35	0.31915	0.33895	0.12465	0.12025	0.3557
	28	0.3192	0.3389	0.1246	0.12025	0.3556
	21	0.31935	0.3389	0.12455	0.1202	0.3557
	14	0.31945	0.3389	0.1245	0.1202	0.3556
	7	0.31955	0.33885	0.12445	0.12015	0.3556
	0	0.3197	0.3389	0.1244	0.1201	0.3556
5 mins	0	0.3197	0.3389	0.12435	0.1202	0.3555
10 mins	0	0.3197	0.3389	0.12435	0.1202	0.3555
15 mins	0	0.3197	0.3389	0.12435	0.1202	0.3554
	7	0.3196	0.33885	0.12435	0.1203	0.3554
	14	0.31945	0.3388	0.12445	0.1202	0.35545
	21	0.3193	0.3389	0.1245	0.12025	0.3555
	28	0.3192	0.3389	0.1245	0.1203	0.3555
	35	0.31915	0.3389	0.1245	0.1203	0.3555
	42	0.31905	0.33905	0.12455	0.1203	0.3556
	49	0.3190	0.3392	0.1245	0.1204	0.3557
	56	0.3189	0.3392	0.1246	0.1204	0.35[illegible]585
	63	0.31865	0.3392	0.1246	0.12045	0.3557

Test ID: CP-12

Page 3 of 4

Date:

Location:

Tester:

Orientation:

Time	Pressure	C-D	A-B	B-C	D-E	E-F
5 min	63	0.31865	0.3390	0.1246	0.1205	0.3556
10 min	63	0.31865	0.33915	0.1246	0.1204	0.3555
15 min	63	0.31865	0.3392	0.1246	0.1204	0.3556
	56	88	91	45	035	55
	49	89	91	455	0.1203	0.3555
	42	0.31890	0.3390	0.12445	0.1203	0.3555
	35	0.318915	0.3390	0.1244	0.1203	0.3555
	28	0.31893	0.3390	0.1244	0.12025	0.3555
	21	0.31894	0.33895	0.12435	0.12025	0.35545
	14	0.31896	0.3389	0.12435	0.12025	0.35545
	7	0.31897	0.33885	0.1243	0.1202	0.3554
	0	0.31897	0.3388	0.1243	0.1202	0.35545
5min	0	0.31897	0.3388	0.12425	0.1202	0.3554
10min	0	0.31897	0.3388	0.1242	0.1202	0.35585
15min	0	0.31897	0.3387	0.12435	0.1202	0.3554
	7	0.31955	0.33885	0.1243	0.12025	0.35545
	14	0.3195	0.3389	0.12435	0.12025	0.35545
	21	0.3194	0.3389	0.1244	0.1203	0.3555
	28	0.3193	0.3389	0.1244	0.1203	0.3555
	35	0.3192	0.33895	0.1245	0.12035	0.3555
	42	0.3191	0.33895	0.1245	0.12035	0.3556
	49	0.3189	0.33895	0.1245	0.12035	0.3555
	56	0.3188	0.33891	0.12455	0.1204	0.3556
	63	0.31865	0.33915	0.1246	0.12045	0.3556
5min	63	0.31865	0.33892	46	04	57
10min	63	0.31865	0.33905	455	04	56
15min	63	3165	405	46	04	56
	56	88	90	455	04	56
	49	89	89	45	035	55

Test ID: C-P-12

Page 4 of 4

Date:

Location:

Tester:

Orientation:

Time	Pressure	C-D	A-B	B-C	D-E	E-F
	42	91	89	445	035	55
	35	925	88	45	03	54
	28	94	88	44	03	54
	21	95	875	44	025	54
	14	96	87	435	02	54
	7	97	87	425	02	54
5min	0	975	875	425	015	53
10min	0	98	86	42	02	53
15min	0	98	87	425	02	53
	0	975	86	43	02	53

Test ID: GP-14

Page 1 of 4

Date: Sept 23

Location:

Tester:

Orientation:

Time	Pressure	C-D	A-B	B-C	D-E	E-F
		3179	33845	1279	1200	3546
		79	84	395	1200	46
		80	84	39	1200	47
		79	84	39	1200	46
		785	84	39	1200	46
load (15kn)		31845	88	1242	03	55
		845	885	415	02	54
		85	88	415	025	54
		85	88	42	03	54
		85	88	415	02	535
Cut		96	84	38	01	51
		96	84	39	005	51
		96	83	39	005	515
5Min		965	83	38	01	515
10Min		96	835	375	005	525
15Min		955	83	375	005	50
Jackin	0	945	83	38	005	50
	7	94	825	385	01	50
	14	93	84	40	02	51
	21	925	84	40	02	51
	28	91	85	405	02	51
	35	90	84	415	03	52
	42	89	85	43	03	52
	49	87	865	415	035	52
	56	86	855	425	03	53
	63	85	87	42	035	53
5Min	63	86	865	43	035	52
10 Min	63	85	865	43	04	525
15 Min	63	855	86	43	03	525

Test ID: C-P-14

Page 2 of 4

Date:

Location:

Tester:

Orientation:

Time	Pressure	C-D	A-B	B-C	D-E	E-F
	56	.3186	.2386	.1242	.1203	.3552
	49	885	88	415	02	51
	42	895	855	405	015	515
	35	91	86	40	02	506
	28	93	84	395	015	505
	21	94	835	40	01	495
	14	935	835	39	01	52 ?
	7	96	835	39	005	52
	0	96	83	385	005	51
5 Min	0	96	825	385	005	52
10 Min	0	96	825	38	00	50
15 Min	0	965	83	38	00	50
	7	95	835	39	005	505
	14	93	835	395	01	51
	21	925	845	395	01	505
	28	915	84	41	01	51
	35	905	85	405	02	515
	42	89	865	415	015	52
	49	88	86	42	015	53
	56	87	87	42	02	53
	63	865	865	43	02	53
*	63	855	88	45	05	555
5Min	63	865	88	45	05	56
10Min	63	865	89	445	045	55
15Min	63	87	87	45	04	54
	56	865	89	45	035	545
	49	895	85	44	03	54
	42	905	84	435	035	54
	35	915	84	435	025	595

zero check

*

ORS bag

recheck?

Test ID: C-P-14

Page 3 of 4

Date:

Location:

Tester:

Orientation:

zero check ✓ good

Time	Pressure	C-D	A-B	B-C	D-E	E-F
	28	.3192	3383	.12425	.12025	.35525
	21	3194	835	415	02	52
	14	945	84	40	015	52
	7	97	825	39	01	515
	0	98	83	39	01	515
5 Min	0	97	825	395	01	505
10 Min	0	97	835	40	01	52
15 Min	0	96	825	40	01	51
	7	955	83	405	02	53
	14	95	825	405	015	525
	21	935	83	415	02	54
	28	915	84	42	025	54
	35	91	84	425	03	55
	42	905	84	425	03	55
	49	895	84	43	04	55
	56	88	85	43	04	55
	63	86	85	44	04	555
	70	85	86	45	045	55
5 Min	70	845	85	455	045	55
10 Min	70	845	855	455	045	545
15 Min	70	85	855	45	05	545
	63	865	85	45	04	55
	56	89	85	44	04	545
	49	895	84	435	04	545
	42	91	84	435	03	535
	35	92	84	435	025	54
	28	93	835	425	025	54
	21	945	835	42	02	53
	14	96	83	41	03	52

zero check ✓

Test ID: C-P-14

Page 4 of 4

Date:

Location:

Tester:

Orientation:

zero check ✓

Time	Pressure	C-D	A-B	B-C	D-E	E-F
	7	97	84	41	025	54
	0	965	82	41	04[illegible]	54
5Min	0	98	84	40	02	54
10Min	0	98	83	395	02	53
15Min	0	97	83	395	02	535

Test ID: CP 16

Page 1 of 4

Date: Sept 28

Location: ____________

Tester: ____________

Orientation: ____________

ccw clock

Time	Pressure	C-D	A-B	B-C	D-E	E-F
		37795	3480	13345	1298	3647
		3780	80	355	1300	47
		3781	80	362	1301	47
		3781	80	36	1301	47
		3781	80	355	[illegible]	465
load		885	86	37	03	545
		88	86	375	025	54
		88	85	375	03	54
		88	855	375	025	535
		88	86	38	025	545
Cut		985	84	37	02	525
		975	84	765	015	52
		98	825	37	02	52
5 Min		975	83	365	015	52
10 Min		975	83	365	01	52
15 Min		980	83	37	015	525
Jack in	0	96	825	38	015	52
	7	965	83	365	02	52
	14	97	825	365	02	53
	21	95	835	375	025	53
	28	94	835	375	03	53
	35	93	85	38	03	53
	42	925	85	38	03	53
	49	92	855	38	035	54
	56	90	85	38	03	55
	63	89	86	39	03	55
	70	885	86	39	035	555
	79	88	87	395	04	56
5Min	77	875	86	595	63	565

ccw clock

Test ID: C-P-16

Page 2 of 4

Date:

Location:

Tester:

Orientation:

zero check

Time	Pressure	C-D	A-B	B-C	D-E	E-F
10 Min	77	870	86	395	03	55
15 Min	77	870	86	405	03	56
	70	88	855	39	05	56
	63	895	865	39	02	555
	56	91	855	39	02	555
	49	92	86	38	025	56
	42	94	86	37	025	56
	35	96	87	375	03	55
	28	98	87	375	025	55
	21	985	87	375	025	555
	14	3800	87	37	015	555
	7	01	87	37	01	55
	0	02	865	365	01	55
5 Min	0	01	86	365	01	545
10 Min	0	005	85	365	01	54
15 Min	0	00	85	365	01	54
	7	99	85	36	015	53
	14	98	855	37	015	54
	21	97	855	375	02	54
	28	96	86	375	02	545
	35	95	86	38	025	555
	42	94	87	38	03	55
	49	93	87	38	03	55
	56	92	87	385	035	55
	63	905	87	38	035	56
	70	895	875	395	035	56
	77	885	88	40	04	56
5	77	88	87	40	04	55
10	77	87	875	40	04	56

zero check

zero check

Test ID: CP-16

Page 2 of 4

Date:

Location:

Tester:

Orientation:

Time	Pressure	C-D	A-B	B-C	D-E	E-F
15 Min	77	865	86	40	04	545
	70	88	865	40	035	54
	63	89	865	40	035	54
	56	91	86	395	03	54
	49	92	865	39	025	54
	42	93	86	385	03	555
	35	945	86	38	025	54
	28	96	86	375	02	54
	21	97	855	37	02	53
	14	985	85	365	01	53
	7	00	85	365	01	535
	0	01	85	365	005	53
5 Min	0	00	85	36	00	535
10 Min	0	995	85	36	00	525
15 Min	0	99	84	355	005	52
	7	98	84	365	01	53
	14	97	845	36	01	52
	21	96	85	36	01	525
	28	96	86	37	02	53
	35	95	87	375	025	545
	42	94	87	38	025	545
	49	935	875	39	03	55
	56	925	88	39	035	55
	63	91	88	39	035	535
	70	90	88	395	035	555
	77	885	885	40	04	56
5 Min	77	88	88	41	04	555
10 Min	77	88	885	40	04	56
15 Min	77	875	88	40	04	55

zero check ✓

zero check ✓

Test ID: C-P-16

Page 4 of 4

Date:

Location:

Tester:

Orientation:

Time	Pressure	C-D	A-B	B-C	D-E	E-F
	70	89	89	395	03	545
	63	895	87	39	03	55
	56	915	87	385	03	54
	49	925	87	38	02	535
	42	94	875	38	025	53
	35	95	87	37	025	53
	28	965	865	37	015	54
	21	98	87	37	015	535
	14	99	87	36	005	54
	7	00	87	355	01	54
	0	01	86	35	00	54
5Min	0	00	85	355	005	53
10Min	0	00	85	345	01	54
15Min	0	00	85	345	00	525

Zero check

The saw contacted pin D and created a bur that was filed off. unknown if this contact moved the position of pin D

Test ID: D-R-12

Date: Sept 19 2017

Location: Heavy Structures

Tester: Alexander McKeaney

Orientation: Axial

Page 1 of 5

pre loading

Time	Pressure	C-D	A-B	B-C	D-E	E-F
	0	.2393	.3166	1892	23 42	.2677
	0	2393	66	92	42	77
	0	93	67	92.5	42	78
r x		98	68	93.5	45	84
		2398	3171	93	45	84
		98	72	94	45	85
		98	71	94	45.5	84
		98	72	94	45	85
		13	67.5	89	43	82.5
		13	67	89.5	43	82.5
		13	67.5	89.5	43.5	82.5
15 Min wait		12.5	68	89	42	82
		12.5	68	89.5	42	82
		13	68	89.5	42	82
Flat jack in	0	13	68	89.5	42	83
	0	13	67.5	89.5	42	83
	0	13	68	89.5	42	83
	7	12	69	90	42.5	82
	7	12	70	90	42.5	82.5
	7	12	69	90	42.5	82.5
	14	11	70	90	43	83
	14	10	69	90	43	83
	14	11	69	91	43	83
	21	09	70	91	43.5	84
	21	09	70.5	91	43.5	83.5
	21	09	70.5	91	43.5	83.5
	28	08	71	89	43.5	88
	28	08	72	90	43	83
	23	08	71	89	43	83

Test ID: DR - 12

Page 2 of 5

Date:

Location:

Tester:

Orientation:

Time	Pressure	C-D	A-B	B-C	D-E	E-F
	35	06	72	91	44.5	84
	35	06	71	91	44	84
	35	06	72	91	44	84
	42	05	71	92	44.5	84
	42	05	71	92	44.5	84.5
	42	05	72	92	44.	84
	49	02.5	73	92.5	44.5	85.5
	49	02	72.5	92.5	45	85
	49	02	72.5	92.5	45	85
	56	00	74	93	45	85
	56	00.5	73	93	45.5	85.5
	56	00	73	93	45.5	85.5
	63	98	74	93	45.5	86
	63	98	73	93	45.5	85.5
	63	98	73	93	46	85.5
5 Min	63	97	72	935	455	85
	63	97	72	935	455	85
	63	97	73	93	455	85
10 Min	63	97	73	93	46	845
	63	97	73	93	46	855
	63	97	72.5	93	46	85
15 Min	63	975	725	94	46	86
	63	97	73	93	46	85
	63	97	73	93.5	46	85
	56	99	73	935	45	85
	56	99	73	935	455	855
	56	985	72.5	93	455	85
	49	01	73	925	45	84
	49	01	73	925	45	85
	4.9	01	72	925	45	85

Test ID: R-D-12

Page 3 of 5

Date:

Location:

Tester:

Orientation:

Time	Pressure	C-D	A-B	B-C	D-E	E-F
	42	035	72	92	445	84
	42	03	72	92	45	85
	42	03	72	92	44	85
	~~142~~					
	35	055	72	92	44	84
	35	05	71	92	44.5	85
	35	05	72	92	44	85
	28	07	71	91	44	84
	28	07	71	915	44	84
	28	07	70	91	44	84
	21	10	70	91.	44	84
	21	09	70.5	91	44	84
	21	09	71	91	44	84.5
	14	11	72	90.5	44	83
	14	11	71.5	90.5	43.5	83
	14	11	71	90.5	44	84
	7	13	72	90	44	83.5
	7	13	71	90	44	84
	7	13	71	90	44	84
	0	15	69	895	43	83
	0	145	695	895	435	83
	0	145	695	90	435	83
5Min	0	15	695	895	435	83
	0	15	69	90	435	835
	0	145	695	90	435	83
10 Min	0	15	69	90	43	84
	0	15	69	90	43	835
	0	15	69	90	435	83
15 Min	0	15	69	90	44	84
	0	15	69	90	43	83
	0	15	69	90	435	835

Zero check ✓

Test ID: RD 12

Page 4 of 5

Date:

Location:

Tester: Alexander McKenney

Orientation:

Time	Pressure	C-D	A-B	B-C	D-E	E-F
	7	13	69.5	90	435	83.5
	14	12	72	91	44	84.5
	21	09	71	91	45	83.5
	28	07	72	91.5	44.5	84.5
	35	05	71	91.5	45	85
	42	04	72	92.5	45.5	85.5
	44	02	74	93	45.5	85.5
	56	00	74	93	46	85.0
	63	099	74	93	46.5	87
Forgot hold	70	975	75.0	890	47	87
	63	98.5	74	94	46.5	87
	56	00	73	94	46	86.5
	49	01.5	72	93	46	86
	42	04	71	91	45.5	86
	35	06	71	91.5	44.5	85.5
	28	08	072	92	45	85.5
	21	10	72	90.5	44	85
	14	12.5	72	88	44	85
	7	14	71.5	90.5	43	84
	0	16	70	90	42.5	84.5
5 Min	0	15	70	90	435	84
10 Min	0	15	70	895	425	835
15 Min	0	15	69	895	435	835
	7	13	70	90	435	845
	14	11	70	905	44	845
	21	08	70	90	445	85
	28	07	71	92	45	85
	35	05	71	91	45	855
	42	03	71	925	46	85

Test ID: D-R-12

Page 5 of 5

Date:

Location:

Tester: Alexander McKenney

Orientation:

Time	Pressure	C-D	A-B	B-C	D-E	E-F
	49	01.5	71	93	46	85
	56	99	73	93	46.5	86.5
	63	98	75	94	47	86.5
5 Min	63	97.5	73.5	94	47	86.5
10 Min	63	98	73	94	47	87
15 Min	63	97.5	73.5	94.0	46.5	87
	56	99	72.5	93.5	47	86
	99	01.5	73.5	93	46.5	85.5
	42	3	72	92.5	46.5	85.0
	35	05	71.5	92	45.5	85.0
	28	07	71.5	91	45	84
	21	09	70	90.5	44.5	85
	14	11	71	90.5	44.5	85
	7	13	70.5	89.5	44.5	84.5
	0	15.5	71	89	43.5	84
5 Min	0	15	71	89	435	84
10 Min	0	15	73	89	435	84
15 Min	0	15	72	89	435	84
			Zero check ✓			
Jack Removed						
(un pressurized)		2392		14845	17495	2680
			3173 AM			

Test ID: R-D-14

Page 1 of 4

Date: Sept 22 2017

Location:

Tester:

Orientation:

Calabrated

5 2? 5

Time	Pressure	C-D	A-B	B-C	D-E	E-F
Pre load.		2391	2377	1989	2244	26905
		2391	2377	1989	22445	26 91
		23915	2377	19885	22445	26 91
load 15Min		97	23795	915	48	96
		97	79	915	475	955
		965	79	915	475	96
		965	79	91	48	96
		97	795	91	48	96
Cut		2419	23755	86	44	935
		19	755	865	44	935
		195	755	82	44	93
5Min		19	76	87	44	925
10 Min		19	755	87	44	93
15 Min		19	755	87	435	93
Jack in	0	18	765	87	435	93
	7	16	76	88	44	94
	14	15	778	88	44	935
	21	13	78	89	445	95
	28	105	79	885	45	945
	35	09	785	90	455	95
	42	065	79	90	465	96
	49	05	80	91	46	965
	56	025	805	905	46	96
	63	005	81	92	47	97
	70	23985	815	92	47	975
	77	965	82	92	475	98
5 Min	77	96	82	92	48	975
10 Min	77	955	815	92	475	47
15 Min	77	95	81	92	475	97

Test ID: ______________

Page 2 of 4

Date: ______________

Location: ______________

Tester: ______________

Orientation: ______________

Time	Pressure	C-D	A-B	B-C	D-E	E-F
	70	.23975	2381	.14925	2247	2696
	63	94	805	93	463	2696
	56	2400	800	92	460	95
	49	025	80	915	465	96
	42	05	795	91	455	955
	35	07	795	91	45	95
	28	10	79	90	45	95
	21	12	785	89	44	945
	14	145	78	895	44	945
	7	165	775	89	44	94
	0	18	775	89	435	94
5min	0	18	775	885	435	94
10min.	0	18	775	885	435	94
15min	6	18	77	885	43	935
	7	16	77	890	435	933
	14	14	775	845	44	94
	21	12	78	90	44	945
	28	095	785	90	445	95
	35	08	79	905	45	955
	42	06	795	905	46	96
	44	04	80	91	46	96
	56	02	80	91	465	97
	63	00	81	915	465	975
	70	985	815	915	47	98
	77	96	815	92	475	985
5min	77	96	81	92	475	975
10min	77	96	815	925	48	975
15min	77	955	81	925	475	98
	70	975	81	92	47	98

Test ID: 8-D-14

Page 3 of 4

Date:

Location:

Tester:

Orientation:

Time	Pressure	C-D	A-B	B-C	D-E	E-F
	63	24 00	805	915	47	98
	56	01	805	91	465	965
	49	03	81	91	46	96
	42	055	80	90	46	965
	35	075	795	90	45	955
	28	10	79	90	45	96
	21	115	775	90	445	95
	14	14	79	90	445	95
	7	17	78	89	44	945
	0	19	79	89	44	94
5 Min	0	19	79	88	43	94
10 Min	0	185	775	88	44	935
15 Min	0	19	775	88	43	935
	7	16	78	885	44	94
	14	14	78	895	445	945
	21	12	785	895	44	945
	28	10	79	90	445	955
	35	08	795	905	45	96
	42	06	80	91	46	96
	49	04	80	915	46	96
	56	02	81	915	46	97
	63	23 995	81	915	47	965
	70	98	815	92	47	97
	77	96	815	93	48	98
	77	955	82	935	475	97
	77	955	82	93	48	975
	77	96	815	93	48	97
	70	97	81	92	475	97
	63	985	81	925	465	965

Zero check ✓

Test ID: ____________________

Page 4 of 4

Date: ____________________

Location: ____________________

Tester: ____________________

Orientation: ____________________

Time	Pressure	C-D	A-B	B-C	D-E	E-F
	56	24 01	805	91	46	965
	49	04	805	91	455	46
	42	06	795	91	455	96
	35	075	795	90	45	95
	28	10	80	90	45	94
	21	12	79	895	445	94
	14	145	785	89	44	94
	7	16	78	895	44	94
	0	19	775	885	435	935
5 Min	0	19	78	885	43	93
10 Min	0	185	78	88	43	93
15 Min	0	185	775	88	43	93
		Zero	check	passed		

Test ID: R-D-16

Page 1 of 1

Date: Sept 26

Location:

Tester:

Orientation:

zeroed

Time	Pressure	C-D	A-B	B-C	D-E	E-F
		2588	2476	2087	2442	28905
		89	76	88	425	90
		88	76	88	43	90
		885	76	88	425	905
		885	76	88	425	91
load (15Min		25945	795	89	45	955
		95	80	89	445	95
		94	805	895	455	95
		945	795	90	45	955
		945	795	90	45	95
Cut		26185	765	85	41	925
		18	755	855	42	93
		185	75	855	42	93
5 Min		20	76	85	415	94
10 Min		19	745	86	43	925
15 Min		18	75	855	42	92
	0	18	75	85	42	925
	7	16	76	86	425	92
	14	145	755	86	42	935
	21	135	755	87	42	93
	28	115	76	87	425	94
	35	09	76	87	43	94
	42	07	775	87	435	945
	49	06	775	88	435	95
	56	04	79	88	435	955
	63	02	79	88	44	955
	70	00	79	89	445	96
	77	98	795	89	45	96
	84	96	80	89	45	965

zero check ✓

[illegible]

Test ID: RD 16

Page___ of ____

Date: ______________________

Location: ______________________

Tester: ______________________

Orientation: ______________________

Time	Pressure	C-D	A-B	B-C	D-E	E-F
	91	94	775	90	45	97
5 Min	91	93	79	895	45	97
10 Min	91	93	79	90	45	96
15 Min.	91	93	795	90	45	96
	84	95	785	895	44	96
	77	96	78	89	435	95
	70	98	775	885	435	95
	63	00	78	89	43	95
	56	025	77	885	425	95
	49	045	775	88	43	94
	42	065	765	87	43	945
	35	085	765	87	42	945
	28	10	765	865	42	935
	21	125	76	865	41	945
	14	14	755	855	41	945
	7	17	755	85	41	94
	0	18	75	85	41	935
5 Min	0	18	75	85	41	925
10 Min	0	18	75	85	41	925
15 Min	0	17	745	85	41	925
	7	155	755	855	41	93
	14	135	76	86	41	925
	21	12	765	86	415	94
	28	105	76	87	42	94
	35	08	76	865	42	94
	42	07	77	8[illegible]7	425	95
	49	095	78	875	425	95
	54	025	775	88	43	955
	63	01	78	89	435	95

zero check ✓

Test ID: R O 16

Page 7 of 9

Date:

Location:

Tester:

Orientation:

Time	Pressure	C-D	A-B	B-C	D-E	E-F
	70	99	79	89	43	95
	77	965	785	89	44	955
	84	95	795	89	44	95
	91	97	79	89	445	965
5Min	91	97	79	895	445	96
10Min	91	93	785	890	44	96
15Min	91	93	78	895	445	955
	84	945	775	89	44	955
	77	965	78	885	44	95
	70	985	775	875	435	95
	63	00	775	875	435	945
	56	02	77	875	43	945
	49	04	775	87	425	94
	42	06	77	87	42	94
	35	085	77	87	415	94
	28	11	76	86	415	935
	21	12	76	86	415	93
	14	14	765	86	41	93^5
	7	165	755	86	405	93
	0	18	75	85	40	92
5Min	0	18	755	855	40	925
10Min	0	17	745	845	40	92
15Min	0	17	745	845	40	92
	7	15	74	86	405	92
	14	14	74	855	41	935
	21	115	75	865	41	93
	28	10	75	86	415	935
	35	08	765	86	42	945
	42	06	765	86	42	95

Test ID: R-D-16

Page 4 of 4

Date:

Location:

Tester:

Orientation:

2nd check

Time	Pressure	C-D	A-B	B-C	D-E	E-F
	49	05	77	86	42	96
	56	03	765	865	42	96
	63	005	77	87	425	96
	70	99	77	88	43	965
	77	97	78	87	435	965
	84	95	78	88	44	97
	91.	93	78	885	435	96
5Min	91.	94	78	90	445	98
10Min	91.	935	79	90	445	~~98~~ 99
15Min	91.	941	79	89	45	98
	84.	965	785	895	45	98
	77	995	79	90	45	98
	70	02	79	89	445	98
	63	04	786	885	445	98
	56	055	783	885	44	975
	49	07	78	885	435	975
	42	095	775	88	43	97
	35	115	77	875	425	97
	28	13	77	87	425	965
	21	15	765	865	42	96
	14	16	75	87	42	955
	7	145	76	86	41	95
	0	19	75	86	405	95
5Min	0	19	755	86	405	945
10Min	0	19	755	86	41	94
15Min	0	19	75	86	405	945

Test ID: R-D-16

Page 4 of 4

Date:

Location:

Tester:

Orientation:

2nd check

Time	Pressure	C-D	A-B	B-C	D-E	E-F
	49	05	77	86	42	96
	56	03	765	865	42	96
	63	005	77	87	425	96
	70	99	77	88	43	965
	77	97	78	87	935	965
	84	95	78	88	44	97
	91.	93	78	885	435	96
5 Min	91.	94	78	90	445	95
6 min	91.	935	79	90	445	99
15 Min	91.	941	79	89	45	98
	84.	965	785	895	45	98
	77	99	79	90	45	98
	70	02	79	89	445	98
	63	04	786	885	449	98
	56	055	78	885	44	975
	49	07	78	885	435	975
	42	095	775	88	43	97
	35.	115	77	875	425	97
	28	13	77	87	425	965
	21	15	765	865	42	96
	14	16	75	87	42	955
	7	145	76	86	41	95
	0	14	75	86	405	95
5 Min	0	14	755	86	405	945
10 Min	0	14	755	86	41	94
15 Min	0	14	75	86	405	945

Test ID: R-P - 14

Date: Sept 29

Location:

Tester:

Orientation:

Page 1 of ____

Contact with pin made
but very gentle and controlled
jack still sits 0.75 cm out of hole

zero check

Time	Pressure	C-D	A-B	B-C	D-E	E-F
		2488	2478	2087	2342	2792
		2498	24775	2088	42	92
		24885	78	88	415	915
		2488	78	88	415	92
		88	78	88	42	9.5
load		94	805	90	445	97
		94	805	90	44	97
		94	805	98	445	98
		945	81	895	44	98
		44	805	905	44	975
Cut		2511	775	86	40	95
		11	77	88	41	95
		11	77	865	41	955
5 Min		115	78	86	41	955
10 Min		115	78	86	41	95
15 Min		115	77	86	40	95
Jack in	0	105	77	87	42	94
	7	08	77	88	43	945
	14	66	765	88	42	95
	21	035	77	885	43	96
	28	015	77	895	435	96
	35	995	785	88	45	96
	42	47	79	89	44	965
	44	95	79	.90	455	97
	56	935	77	91	46	97
5 min	66	94	79	91	46	97
10	56	925	79	91	46	965
15	56	93	79	90	465	97
	49	95	785	905	46	97

zero check

zero check

Test ID: R-P-14

Page 2 of 4

Date:

Location:

Tester:

Orientation:

Zero check ✓

Time	Pressure	C-D	A-B	B-C	D-E	E-F
	42	47	785	895	45	97
	95	99	78	89	455	96
	28	01	77	89	45	96
	21	035	77	88	44	955
	14	06	775	88	43	95
	7	08	765	88	42	95
	0	105	76	87	43	95
5 Min	0	11	76	875	43	955
10 Min	0	105	76	87	425	95
15 Min	0	11	755	87	43	95
	7	08	76	87	43	955
	14	07	775	88	435	96
	21	04	77	885	44	965
	28	025	77	89	44	96
	35	00	78	90	44	97
	42	97	78	90	44	97
	49	95	79	91	45	975
	56	93	79	91	46	98
5 Min	56	44	79	91	46	98
10 Min	56	93	79	91	465	98
15 Min	56	93	785	91	46	99
	49	95	78	895	445	98
	42	98	785	90	455	98
	35	00	78	90	445	97
	28	02	78	89	44	97
	21	04	78	88	43	965
	14	07	775	88	44	965
	7	09	77	88	425	965
	0	11	77	87	43	955

Test ID: R-P-14

Page 3 of 4

Date:

Location:

Tester:

Orientation:

Time	Pressure	C-D	A-B	B-C	D-E	E-F
5 Min	0	11	76	87	42	955
10 Min	0	115	76	87	425	95
15 Min	0	11	765	87	425	955
	7	09	765	875	425	96
	14	06	775	885	435	96
	21	04	78	88	43	96
	28	02	785	895	435	965
	35	00	78	895	44	475
	42	985	79	890	445	97
	49	965	79	91	46	985
	56	945	795	91	47	985
5 Min	56	93	80	91	465	485
10 Min	56	94	79	91	465	98
15 Min	56	93	79	91	47	98
	49	945	785	905	465	97
	42	97	79	905	46	97
	35	00	785	895	455	96
	28	02	785	89	45	965
	21	04	78	89	445	46
	14	66	77	88	445	96
	7	09	77	88	44	455
	0	11	77	87	42	445
5 Min	0	105	755	87	43	95
10 Min	0	10	75	87	425	94
15 Min	0	105	755	87	413	95

zero check

zero check ✓

Test ID: R-R14

Page 4 of 4

Date:

Location:

Tester:

Orientation:

Time	Pressure	C-D	A-B	B-C	D-E	E-F

Test ID: R - P - 16

Page 1 of 4

Date: Oct 2

Location:

Tester:

Orientation:

all 79

zero check

Time	Pressure	C-D	A-B	B-C	D-E	E-F
		2489	2577	2089	2343	2793
		24885	77	885	44	935
		2488	77	89	44	935
		2489	77	885	435	935
		2488	77	89	44	935
load		95	79	891	47	975
		955	79	905	465	98
		955	79	91	47	985
		96	78	91	47	98
		955	78	91	465	98
Cat		13	74	87	44	95
		13	75	88	43	945
		14	745	89	435	95
5 Min		145	765	88	44	935
10 Min		14	745	87	44	95
15 Min		145	75	87	44	955
Jack in	0	14	76	875	44	95
	7	13	76	89	44	96
	14	115	765	875	44	96
	21	10	77	885	44	975
	28	08	77	89	45	48
	35	065	785	895	45	48
	42	04	79	895	46	98
	49	035	79	90	465	98
	56	01	795	90	47	985
	63	99	795	90	465	99
	70	98	80	905	47	995
	77	96	805	91	475	01
5 Min	77	958	80	91	47	99

zero check

Test ID: R-P-16

Page 2 of 4

Date:

Location:

Tester:

Orientation:

zero check

Time	Pressure	C-D	A-B	B-C	D-E	E-F
10Min	77	95	80	91	47	99
15Min	77	95	80	91	47	99
	70	97	80	91	46	985
	63	985	80	90	46	985
	56	00	785	90	46	98
	49	02	785	91	455	98
	42	035	785	89	45	97
	35	05	78	885	44	97
	28	07	78	88	44	98
	21	09	78	89	44	98
	14	11	78	885	44	97
	7	125	775	885	435	965
	0	145	77	88	43	97
5Min	0	14	765	875	435	965
10Min	0	14	765	875	44	96
15Min	0	135	765	88	44	955
	7	12	76	88	44	965
	14	10	77	885	445	965
	21	09	77	885	445	965
	28	08	775	90	45	98
	35	055	785	895	455	97
	42	04	785	90	45	98
	49	015	78	90	45	98
	56	995	78	91	45	98
	63	98	79	915	46	98
	70	97	795	915	46	98
	77	95	795	92	46	99
5Min	77	945	795	915	465	99
10Min	77	95	80	915	465	98

zero check

zero check ✓

Test ID: R-P-16

Page 3 of 4

Date:

Location:

Tester:

Orientation:

Zero check

Time	Pressure	C-D	A-B	B-C	D-E	E-F
15 Min	77	95	80	91	465	98
	70	965	79	91	46	98
	63	975	79	91	46	975
	56	99	785	90	455	97
	49	01	78	90	46	97
	42	03	78	90	455	96
	35	055	775	895	45	965
	28	075	78	885	445	96
	21	085	78	885	45	96
	14	105	775	89	45	965
	7	12	775	89	44	96
	0	14	77	885	44	955
5 Min	0	14	765	89	435	96
10 Min	0	14	765	88	435	955
15 Min	0	135	76	875	436	95
	7	11	76	89	435	95
	14	10	76	885	44	955
	21	08	765	895	445	96
	28	07	77	89	445	955
	35	05	78	90	445	96
	42	04	78	905	45	96
	44	015	78	91	45	97
	56	00	79	90	45	975
	63	98	79	91	455	99
	70	965	785	92	46	99
	77	95	80	92	46	99
5 Min	77	95	79	92	465	985
10 Min	77	945	79	915	47	98
15 Min	77	945	79	92	47	98

Test ID: R-P-16

Page 4 of 4

Date:

Location:

Tester:

Orientation:

Zero check ✓

Time	Pressure	C-D	A-B	B-C	D-E	E-F
	70	96	78	92	465	98
	63	975	785	91	46	98
	56	00	785	92	46	98
	49	01	785	91	46	98
	42	035	785	91	46	975
	35	05	78	90	455	97
	28	075	78	91	45	97
	21	09	785	89	45	97
	14	105	78	89	445	965
	7	125	775	88	445	965
	0	14	77	88	445	965
5 Min	0	14	77	88	44	95
10 Min	0	135	765	88	44	95
15 Min	0	14	765	88	435	95

Test ID: ASTM -OB

Page 1 of 4

Date: Friday Oct 6

Location:

Tester:

Orientation:

Zero check

Time	Pressure	C-D	A-B	B-C	D-E	E-F
		2488	24765	20875	2341	28 915
		88	76	88	415	93
		88	76	87	415	925
		88	76	875	41	92
		88	76	88	42	93
load		945	80	905	46	98
		94	80	905	46	98
		945	79	905	46	985
		94	795	90	46	98
		945	79	905	46	98
Cut		23095	755	89	42	96
		10	76	88	43	96
		10	76	875	415	97
~~5 Min~~		095	76	88	415	465
~~10 Min~~		095	76	875	43	96
~~15 Min~~		095	755	875	42	96
Jack in	0	09	75	88	42	985
	7	07	765	89	425	95
	14	045	76	89	43	95
	21	03	765	89	425	95
	28	015	77	895	435	965
	35	00	79	90	435	97
	42	24985	785	90	44	97
	49	97	79	90	45	975
	56	95	80	91	465	99
	63	93	80	915	47	99
5 Min	67	93	80	92	475	98
10 Min	63	935	80	915	465	985
15 Min	67	925	80	91	465	985

Zero check

Took 1 hr

~~zero check~~

zero check

2 hr cure time

6.9MPa

Test ID: ASTM 0B

Page 2 of 4

Date:

Location:

Tester:

Orientation:

Time	Pressure	C-D	A-B	B-C	D-E	E-F
56		945	80	91	465	98
49		965	80	90	46	98
42		98	80	905	45	97
35		00	785	90	45	975
28		025	79	905	445	975
21		045	785	90	45	97
14		065	78	89	44	97
7		085	785	895	44	97
0		105	78	89	44	965
0	5 min	11	775	89	44	965
0	10 min	105	78	89	44	96
0	15 min	105	77	89	44	965
7		085	775	89	445	965
14		07	78	90	44	965
21		055	785	90	445	97
28		03	79	905	455	98
35		015	79	90	46	98
42		99	795	91	45	98
49		985	80	91	465	985
56		965	805	92	47	985
63		94	81	92	475	00
63	5	935	805	93	475	995
63	10	93	81	92	475	995
63	15	935	805	92	48	995
56		95	805	92	47	99
44		97	80	91	465	99
42		99	80	905	465	99
35		02	745	90	46	98
28		03	795	91	45	975

Zero check

Test ID: ASTh - 0B

Page 3 of 4

Date:

Location:

Tester:

Orientation:

Time	Pressure	C-D	A-B	B-C	D-E	E-F
	21	05	79	90	455	975
	14	075	79	90	445	97
	7	095	79	89	44	97
	0	11	785	885	44	975
5 Min	0	11	78	89	44	97
10 Min	0	105	78	89	44	97
15 Min	0	105	78	895	44	965
	7	095	78	895	44	97
	14	075	79	895	445	98
	21	05	79	905	45	98
	28	04	795	91	455	98
	35	015	795	905	455	98
	42	00	80	915	46	99
	49	98	81	915	46	995
	56	96	81	92	465	995
	63	94	815	92	465	995
5 Min	63	935	81	925	47	995
10 Min	63	935	81	92	475	99
15 Min	63	435	81	925	475	99
	56	96	80	915	465	99
	49	98	80	915	46	99
	42	995	80	91	46	98
	35	015	79	905	455	99
	28	04	795	90	455	98
	21	06	79	895	445	985
	14	075	785	90	45	98
	7	09	785	895	44	98
	0	115	78	89	44	975
5 Min	0	11	78	89	445	97

Zero check

Test ID: ASTM 013

Page 4 of 4

Date:

Location:

Tester:

Orientation:

zero check

Time	Pressure	C-D	A-B	B-C	D-E	E-F
10 Min	0	105	77	885	445	97
15 Min	0	105	77	885	44	965

APPENDIX B: VOIDED LAB DATA

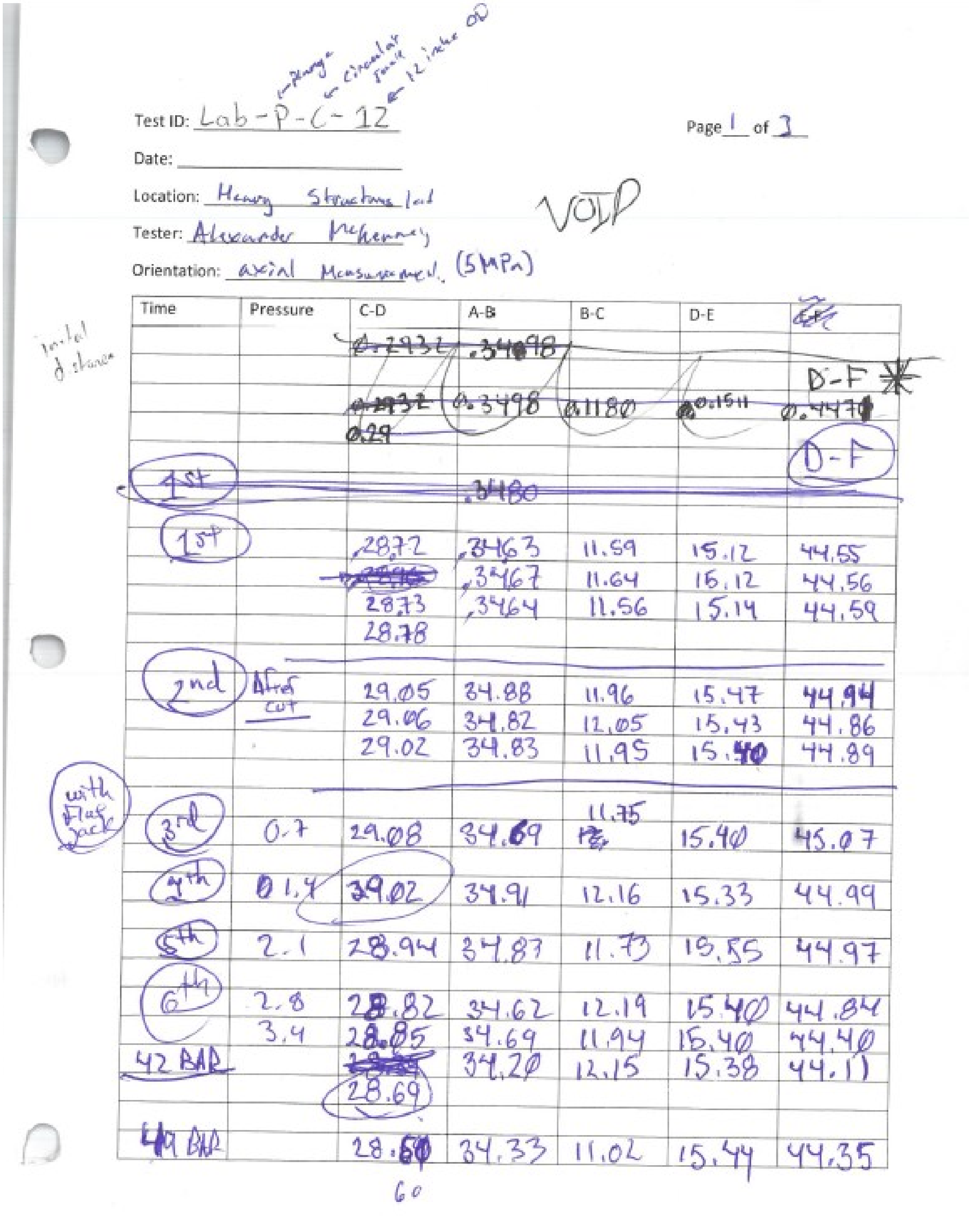

← flange ← circular fault ← 12 inch OD

Test ID: Lab-P-C-12

Page 1 of 3

Date:

Location: Heavy Structures lab

Tester: Alexander McKenney

Orientation: axial Measurement (5MPa)

VOID

initial distance

with flat jack

Time	Pressure	C-D	A-B	B-C	D-E	~~E-F~~
		~~0.2932~~	~~.3498~~			
						D-F ✱
		~~0.2932~~	~~0.3498~~	~~0.1180~~	~~0.1511~~	~~0.4470~~
		~~0.29~~				
						D-F
~~1st~~			~~.3480~~			
1st		.28.72	.3463	11.59	15.12	44.55
		~~[illegible]~~	.3467	11.64	16.12	44.56
		28.73	.3464	11.56	15.14	44.59
		28.78				
2nd	After cut	29.05	34.88	11.96	15.47	44.94
		29.06	34.82	12.05	15.43	44.86
		29.02	34.83	11.95	15.40	44.89
				11.75		
3rd	0.7	29.08	34.69	~~12~~	15.40	45.07
4th	1.4	29.02	34.91	12.16	15.33	44.99
5th	2.1	28.94	34.87	11.73	15.55	44.97
6th	2.8	28.82	34.62	12.19	15.40	44.84
	3.4	28.85	34.69	11.94	15.40	44.40
42 BAR		~~[illegible]~~	34.20	12.15	15.38	44.11
		28.69				
49 BAR		28.60	34.33	11.02	15.44	44.35

60

Test ID: Lab-P-C-12

Page 2 of 3

Date:

Location:

VOID

Tester:

Orientation: all 28

	Time	Pressure	C-D	A-B	B-C	~~A-C~~	D-E	~~E-F~~	D-F	
42BAR	5 mins		28.42	~~[illegible]~~ 34.06	11.90		15.39		44.61	10:04
	10 mins		28.33	34.21	12.16		15.57		44.52	10:11
	15 mins		28.33	34.11	12.10		15.53		44.42	10:1[illegible]
35BAR			28.30	34.06	11.88		15.13		44.15	
	28 BAR		28.31	34.24	11.98		15.42		44.15	
	21 BAR		28.48	34.10	12.14		15.45		44.31	
	14		28.38	34.24	12.04		15.50		44.26	
	7		28.48	34.41	11.98		15.45		44.48	
							~~15.48~~		~~44.50~~	
5M	0		28.32	34.12	12.06		15.48		44.50	11:01
10Min	0		28.30	34.18	12.09		15.44		44.52	11:06
15Min	0		28 ~~[illegible]~~ 39	34.27	12.08		15.44		44.51	11 "
	7		28.38	34.98	12.09		1544		44.53	
	14		28.41	34.25	12.07		15.52		44.85	
	~~[illegible]~~								~~44.55~~	
	21	28.0	~~28.32~~	34.46	12.02		15.48		44.60	
	28		28.35	34.17	12.12		15.50		44.64	
	35	28.43	~~28.28~~	34.33	12.17		15.49		44.70	
	42		28.38	34.74	12.16		1552		44.70	11:47
	42		28.48	34.22	12.07		1549		4464	11 57
	42		28.4	3435	12.01		1544		44.65	
	35		28.42	34.26	12.17		15.48		44.50	
	28		28.48	34.57	1200		15.32		44.58	
	21		28.59	34.24	1206		15.40		44.61	
	14		28.49	34.28	12.04		15.41		44.61	
	7		28.49	34.26	12.01		15.46		4458	

Test ID: P-C-12

Page 3 of 3

Date:

Location:

Tester:

Orientation:

VOID

Bad alignment

Time	Pressure	C-D	A-B	B-C	D-E	~~E-F~~ D-F	
	0	28.49	34.24	12.00	15.40	44.07	12:12
	0	28.54	34.20	12.05	15.41	44 02	12:17
	0	28 58	34 23	12.05	15 43	44 58	12:22
	7	28.55	34.21	12.02	15.48	4455	
	14	28.64	34 25	12.06	15.48		
	21	28.47	34 25	12.05	15.46		
	28	28 39	34 28	12 07	15 44		
	35	28 36	34 37	12 07	15.37		1238
	42	28 35	34 45	12 05	15 35		1242
	42	28 35 ~~35~~	34 30	12 02	15 35		1247
	36 ~~42~~	28.35	34 27	12 09	15 46		
	28	28 40	34 25	12 15	15 53		
	21	28 33	34 32	12 08	15 45		
	14	28 45	34 30	12.00	16 40		
	7	28 55	34 32	12.01	15 45		
	0	60	37	12.07	15 42		1.00
	0	72	50	12.11	15 40		105
	0	68	46	06	16 38		110
	0	74	51	11	15 34		115

lake off.

Notes

- Use template → Make Measurements easier + quicker
- grind surface to let bolts sit flat.
- Make Measurement prior to inserting jack
- Jack was a tight fit so we reamed the slot. + tapped jack in with a wood block
- Pin F is out of position

Test ID: lab-D-R-12-Void

Page 1 of 1

Date: Aug 31 2017 2:44 PM

Location: Heavy Structures lab

Tester: Alexander Mckanney + Mehdi Ghazimi

Orientation: Axial loading 5MPa

E damaged slightly

Time	Pressure	C-D	A-B	B-C	~~A-C~~	D-E	E-F	~~D-F~~
		.2601	.2928	.2642		.2206	.2840	
		.2607	.2916	.2649		.2215	.2737	
2805	2s	2598						
		2613						
10min		2612	2925	2641	9	2213	2895	
930		.2608	2920	2643		2212	2822	
After Tested Horizontal		2609	2928	2639		2208	2732	
	7	2607	2933	2629		2205	2838	
	14	2605	2929	2630		2206	2820	
	21	2604	2925	2623		2210	2821	
	28	2602	2922	2635		2216	2821	
	35	2602	2934	2638		2215	2820	
	42	2599	2937	2630		2205	2822	
	42	2601	2993	2619		2200	2750	
Different method	42	2599	2939	2592		2197	2818	
	42	2600	2895	2616		2209	2829	
	42	2601	2925	2615		2197	2812	
Mehdi test	42	2601	2998	2612		2195	2828	
	35	2602	2920	2618		2192	2813	
	28	2604	2918	2618		2196	2803	
	21	2609	2914	2617		2196	2815	
	14	2609	2948	2638		2196	2833	
	7	2609	2908	2595		2196	2856	
	0	2607	2966	2600		2189	2852	
	0	2509	2486	2549		2196	2869	
	0	2610	2452	2619		2212	2860	

APPENDIX C: GRAPHS AND TABLES OF LAB DATA

C.1 Test 1: Lab-C-P-12

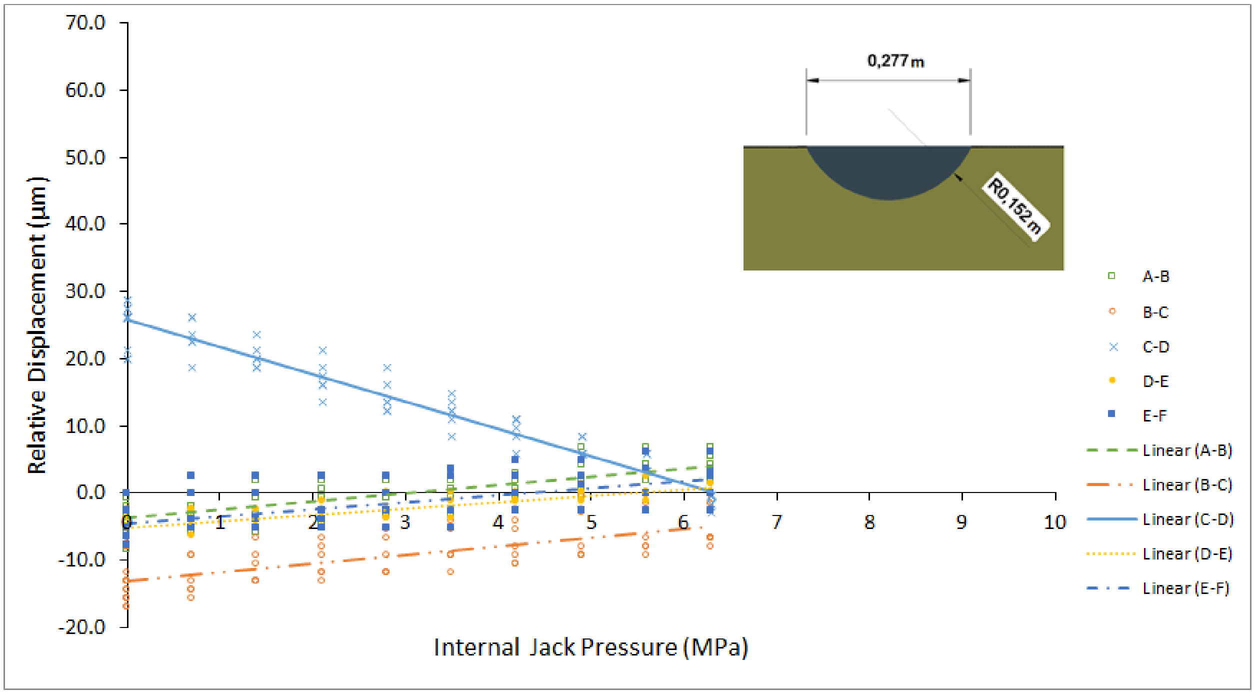

Figure C1: The relative displacement (µm) of pins C-D as a function of measured pressure in the flatjack (MPa) using the circular segment flatjack in a plunge cut with a 305 mm diameter blade. The trend lines are the mean of each data set.

Table C1: Summary of important values in the trend line for each pin span in test C-P-12. Corrected pressure is the output pressure of the jack whereas the internal pressure is the fluid pressure and was the measured pressure during the test.

Span	Closure (µm)	Slope	Flatjack Pressure (MPa)	
			Internal	Corrected (K=0.81)
A-B	-4	1.254	3.00	2.34
B-D	-13	1.309	10.04	7.83
C-D	26	-4.067	6.37	4.97
D-E	-5	0.950	5.41	4.22
E-F	-4	1.046	4.30	3.35

C.2 Test 2: Lab-C-P-14

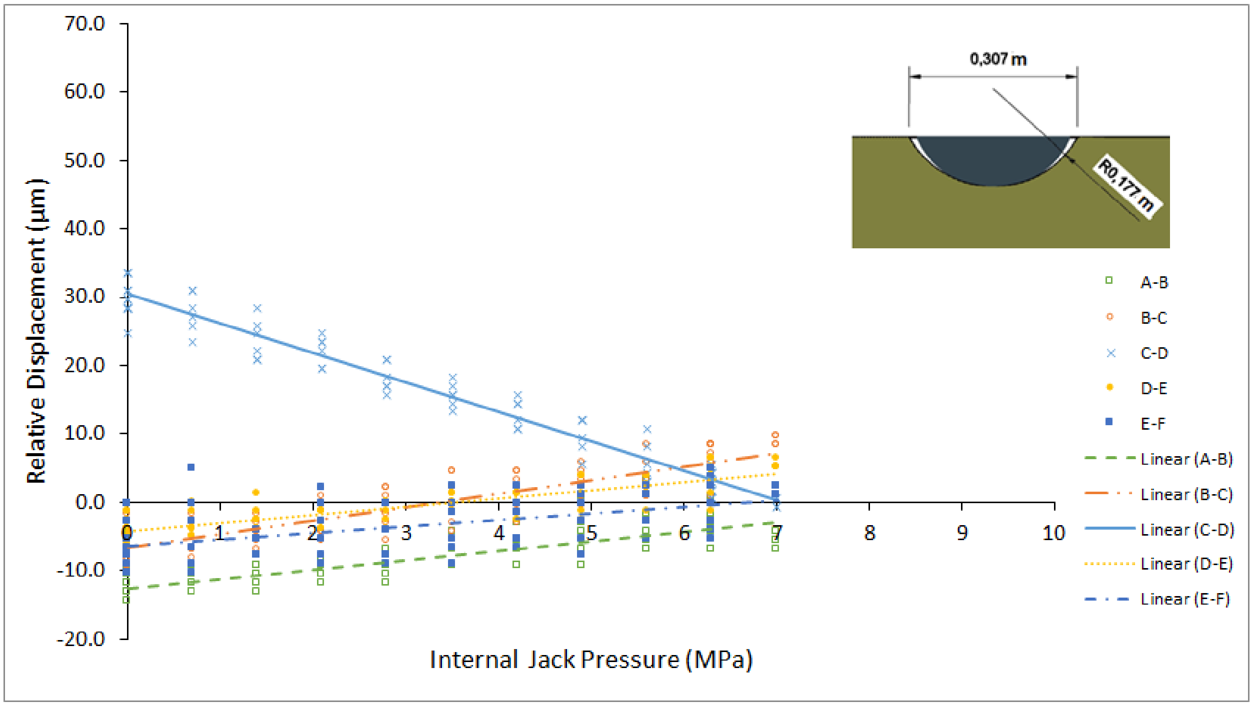

Figure C2: The relative displacement (µm) of pins C-D as a function of measured pressure in the flatjack (MPa) using the circular segment flatjack in a plunge cut with a 356 mm diameter blade. The trend lines are the mean of each data set.

Table C2: Summary of important values in the trend line for each pin span in test C-P-14. Corrected pressure is the output pressure of the jack whereas the internal pressure is the fluid pressure and was the measured pressure during the test.

Span	Closure (µm)	Slope	Flatjack Pressure (MPa)	
			Internal	Corrected (K=0.81)
A-B	-13	1.399	9.04	7.05
B-D	-7	1.973	3.39	2.64
C-D	30	4.3095	-7.06	-5.51
D-E	-4	1.186	3.55	2.77
E-F	6	0.957	-6.69	-5.22

C.3 Test 3: Lab-C-P-16

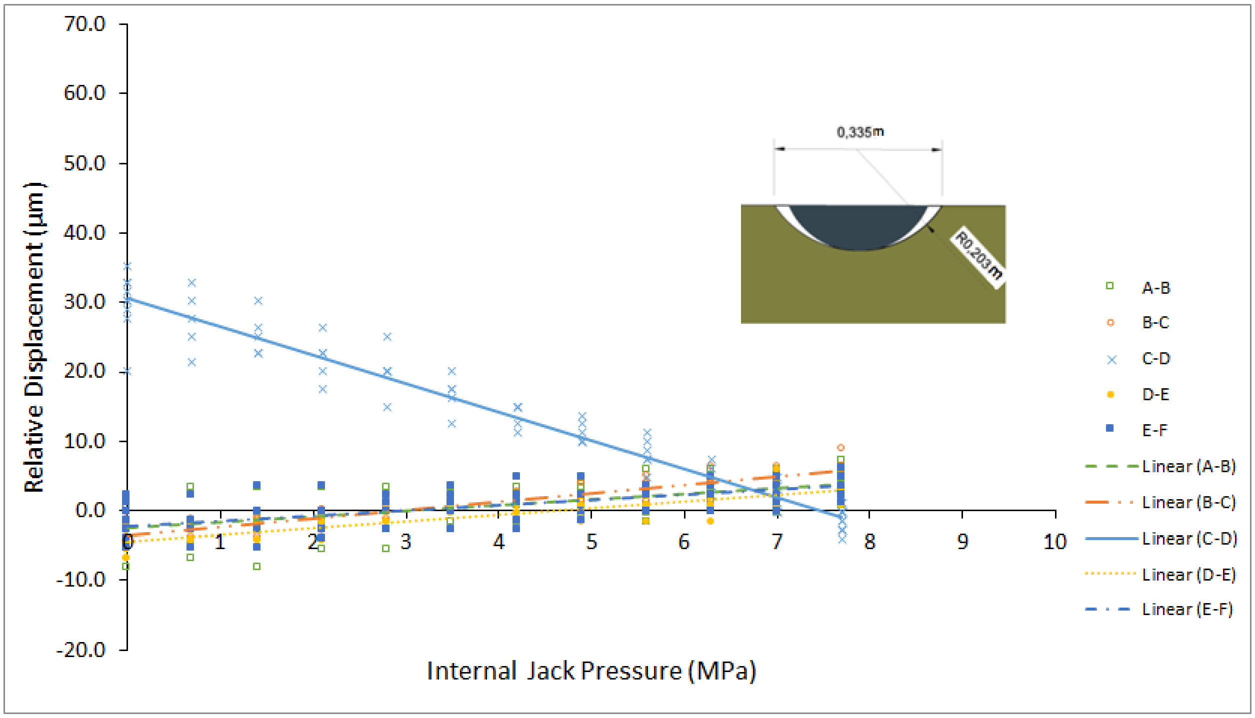

Figure C3: The relative displacement (µm) of pins C-D as a function of measured pressure in the flatjack (MPa) using the circular segment flatjack in a plunge cut with a 406 mm diameter blade. The trend lines are the mean of each data set.

Table C3: Summary of important values in the trend line for each pin span in test C-P-16. Corrected pressure is the output pressure of the jack whereas the internal pressure is the fluid pressure and was the measured pressure during the test.

Span	Closure (µm)	Slope	Flatjack Pressure (MPa)	
			Internal	Corrected (K=0.81)
A-B	-2	0.805	2.94	2.29
B-D	-3	1.203	2.89	2.25
C-D	31	-4.089	7.49	5.84
D-E	-4	0.952	4.56	3.56
E-F	-2	0.769	3.06	2.38

C.4 Test 4: Lab-R-D-12

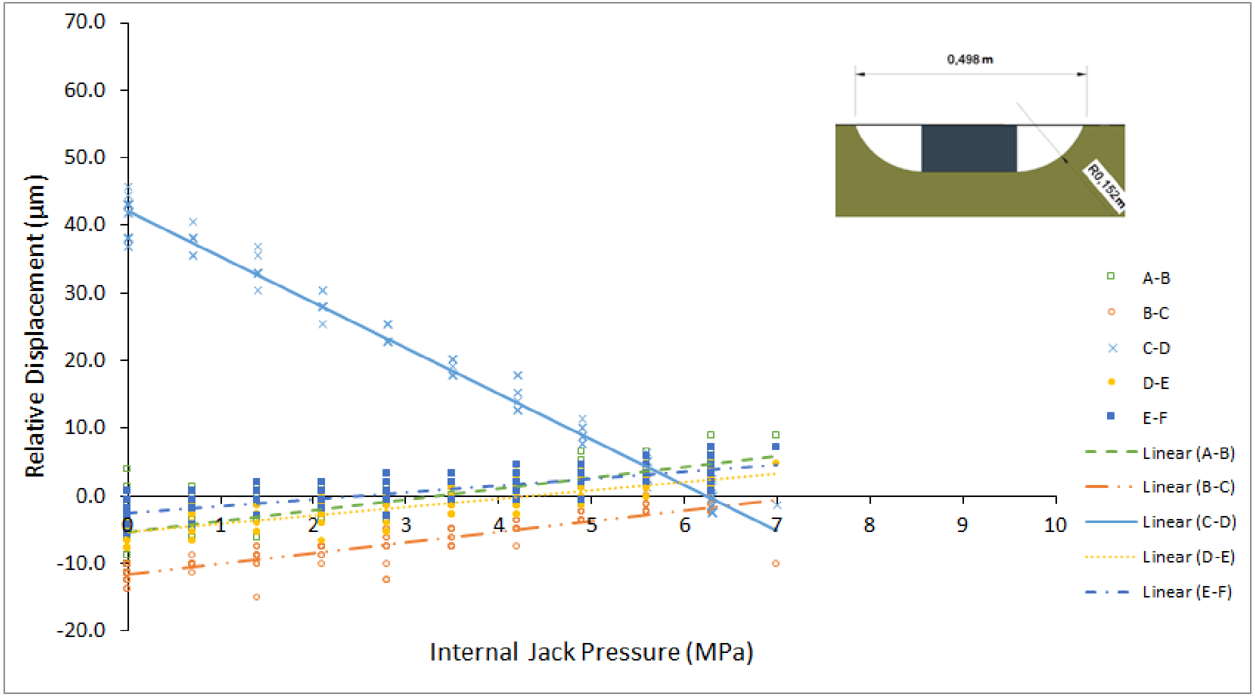

Figure C4: The relative displacement (µm) of pins C-D as a function of measured pressure in the flatjack (MPa) using the rectangular flatjack in a drag cut with a 305 mm diameter blade. The trend lines are the mean of each data set.

Table C4: Summary of important values in the trend line for each pin span in test R-D-12. Corrected pressure is the output pressure of the jack whereas the internal pressure is the fluid pressure and was the measured pressure during the test.

Span	Closure (µm)	Slope	Flatjack Pressure (MPa)	
			Internal	Corrected (K=0.81)
A-B	-5	1.602	3.39	2.74
B-D	-12	1.561	7.38	5.98
C-D	42	-6.736	6.25	5.06
D-E	-4	1.237	3.59	2.90
E-F	-3	1.025	2.59	2.10

C.5 Test 5: Lab-R-D-14

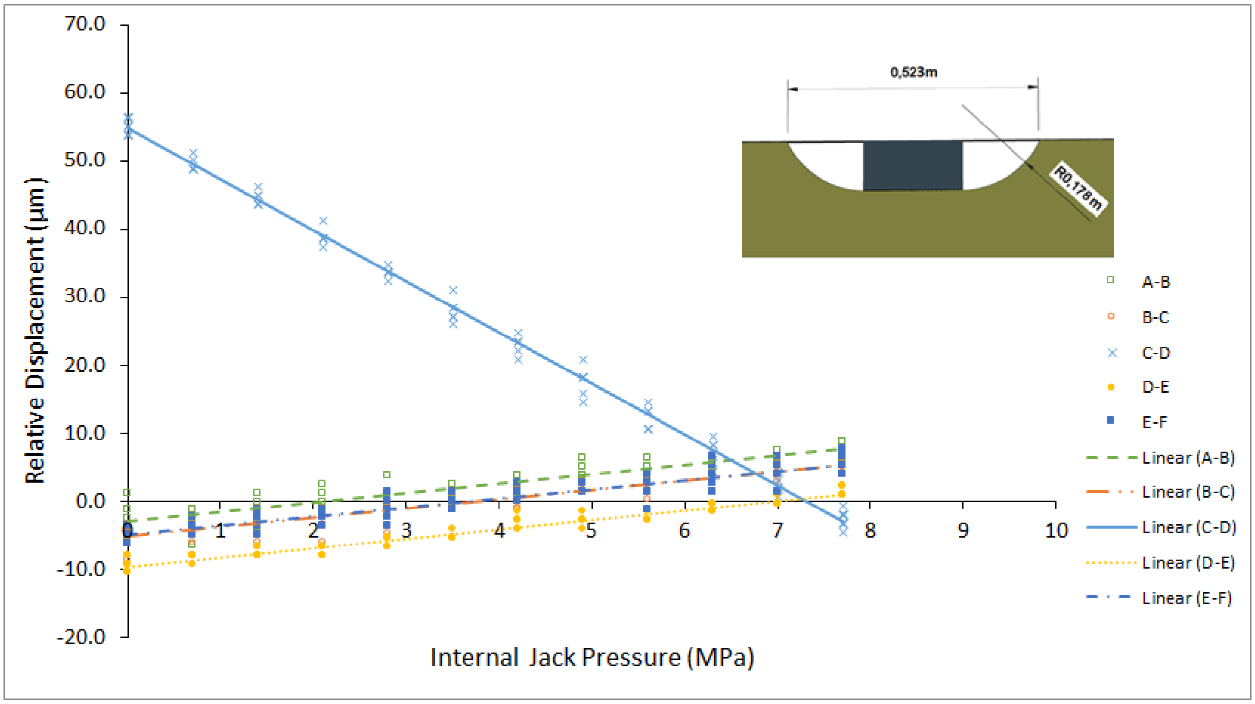

Figure C5: The relative displacement (µm) of pins C-D as a function of measured pressure in the flatjack (MPa) using the rectangular flatjack in a drag cut with a 356 mm diameter blade. The trend lines are the mean of each data set.

Table C5: Summary of important values in the trend line for each pin span in test R-D-14. Corrected pressure is the output pressure of the jack whereas the internal pressure is the fluid pressure and was the measured pressure during the test.

Span	Closure (µm)	Slope	Flatjack Pressure (MPa)	
			Internal	Corrected (K=0.81)
A-B	-3	1.275	2.34	1.89
B-D	-5	1.27	4.15	3.36
C-D	55	-7.508	7.29	5.91
D-E	-10	1.395	6.98	5.65
E-F	-5	1.334	3.74	3.03

C.6 Test 6: Lab-R-D-16

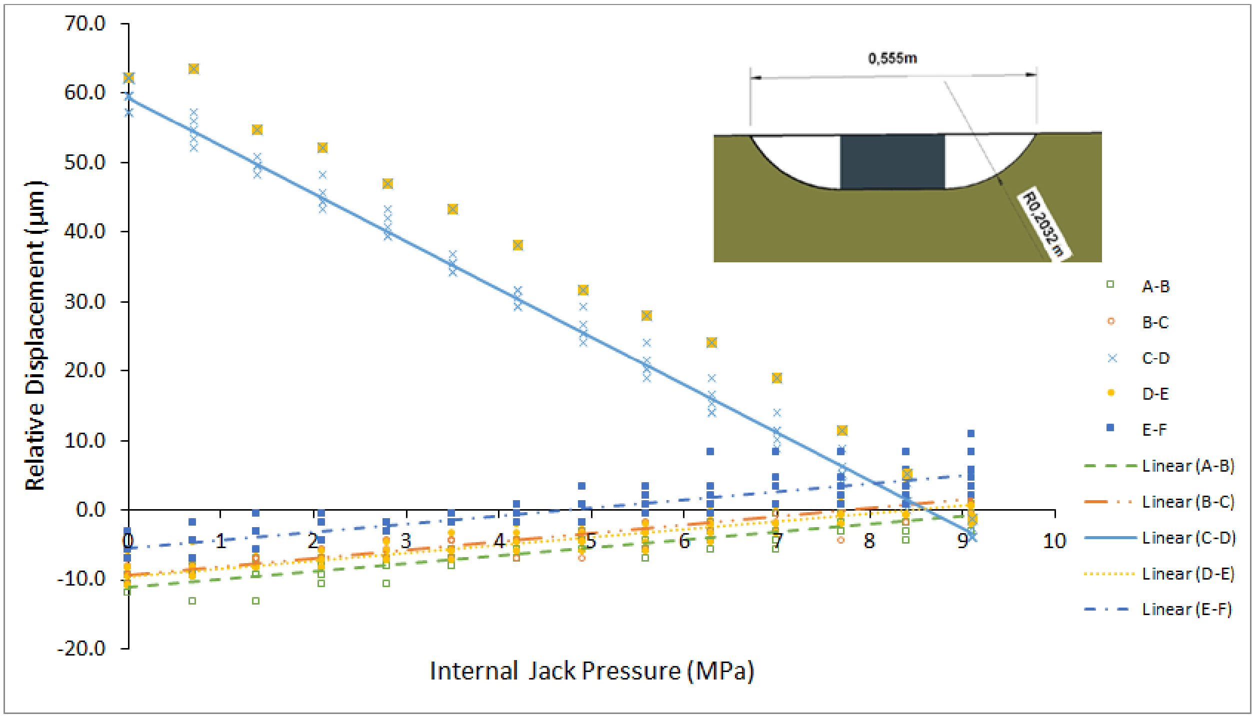

Figure C6: The relative displacement (µm) of pins C-D as a function of measured pressure in the flatjack (MPa) using the rectangular flatjack in a drag cut with a 406 mm diameter blade. The trend lines are the mean of each data set. The data points disregarded due to hysteresis are the crosses with the shaded background.

Table C6: Summary of important values in the trend line for each pin span in test R-D-16. Corrected pressure is the output pressure of the jack whereas the internal pressure is the fluid pressure and was the measured pressure during the test.

Span	Closure (µm)	Slope	Flatjack Pressure (MPa)	
			Internal	Corrected (K=0.81)
A-B	-11	1.1236	9.80	7.93
B-D	-9	1.2078	7.67	6.21
C-D	60	-6.876	8.68	7.03
D-E	-9	1.127	8.39	6.80

E-F	-6	1.18	4.72	3.82

C.7 Test 7: Lab-R-P-14

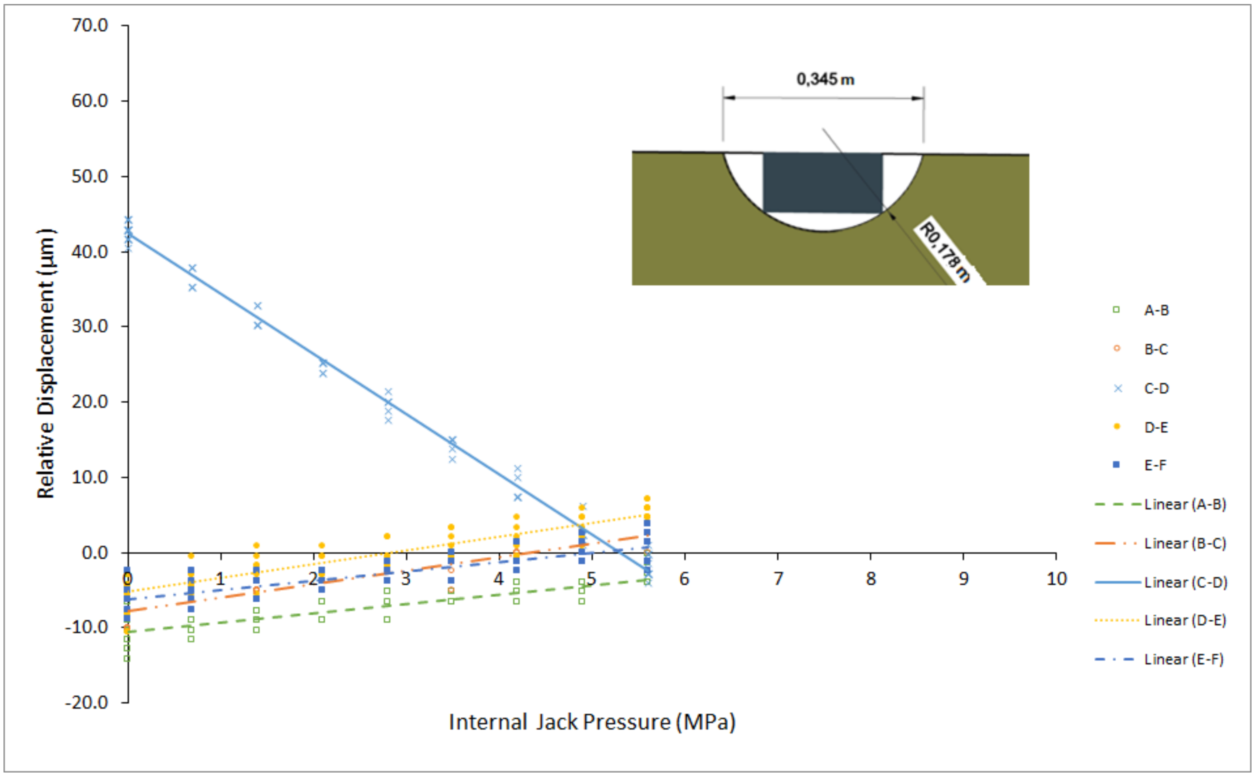

Figure C7: The relative displacement (µm) of pins C-D as a function of measured pressure in the flatjack (MPa) using the rectangular flatjack in a plunge cut with a 356 mm diameter blade. The trend lines are the mean of each data set.

Table C7: Summary of important values in the trend line for each pin span in test R-P-14. Corrected pressure is the output pressure of the jack whereas the internal pressure is the fluid pressure and was the measured pressure during the test.

Span	Closure (µm)	Slope	Flatjack Pressure (MPa)	
			Internal	Corrected (K=0.81)
A-B	-10	1.236	8.49	6.88
B-D	-8	1.817	4.32	3.50
C-D	42	-8.003	5.30	4.29
D-E	-5	1.848	2.84	2.30
E-F	-6	1.217	5.06	4.10

C.8 Test 8: Lab-R-P-16

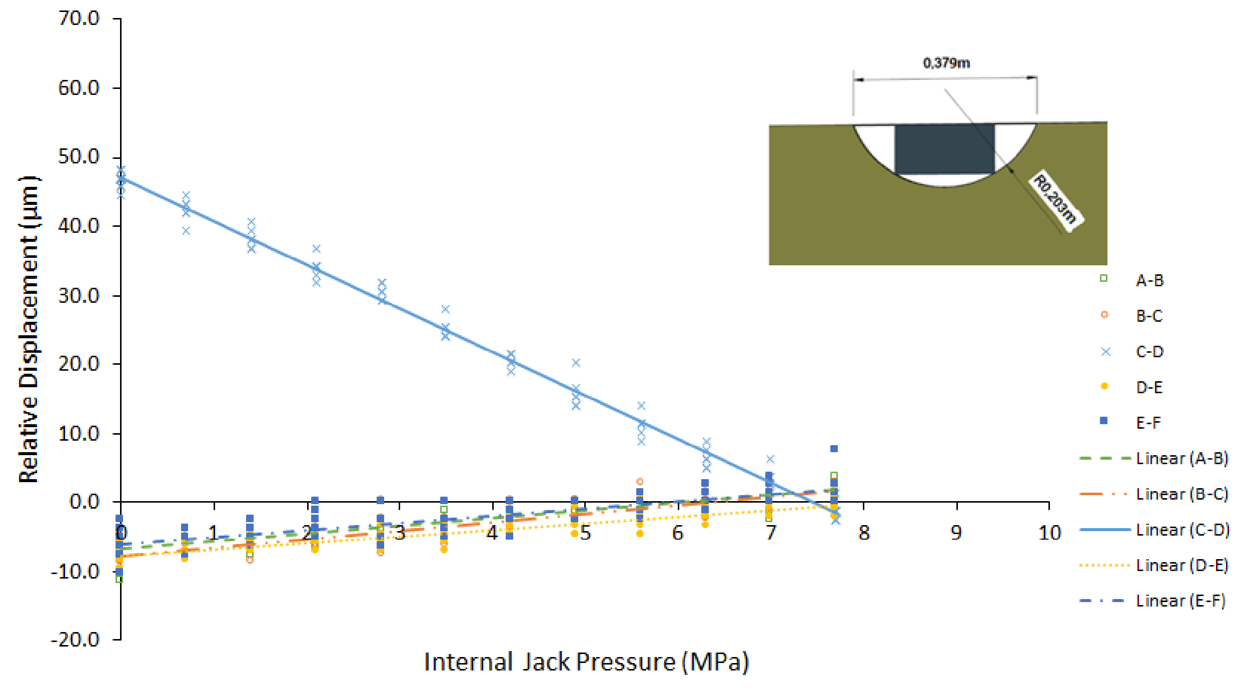

Figure C8: The relative displacement (µm) of pins C-D as a function of measured pressure in the flatjack (MPa) using the rectangular flatjack in a plunge cut with a 356 mm diameter blade. The trend lines are the mean of each data set.

Table C8: Summary of important values in the trend line for each pin span in test R-P-16. Corrected pressure is the output pressure of the jack whereas the internal pressure is the fluid pressure and was the measured pressure during the test.

Span	Closure (µm)	Slope	Flatjack Pressure (MPa)	
			Internal	Corrected (K=0.81)
A-B	-7	1.107	6.08	4.92
B-D	-8	1.221	6.33	5.13
C-D	47	-6.298	7.47	6.05
D-E	-8	0.953	8.17	6.62
E-F	-6	1.04	5.79	4.69

C.9 Test 9: Lab-R-ASTM-OB

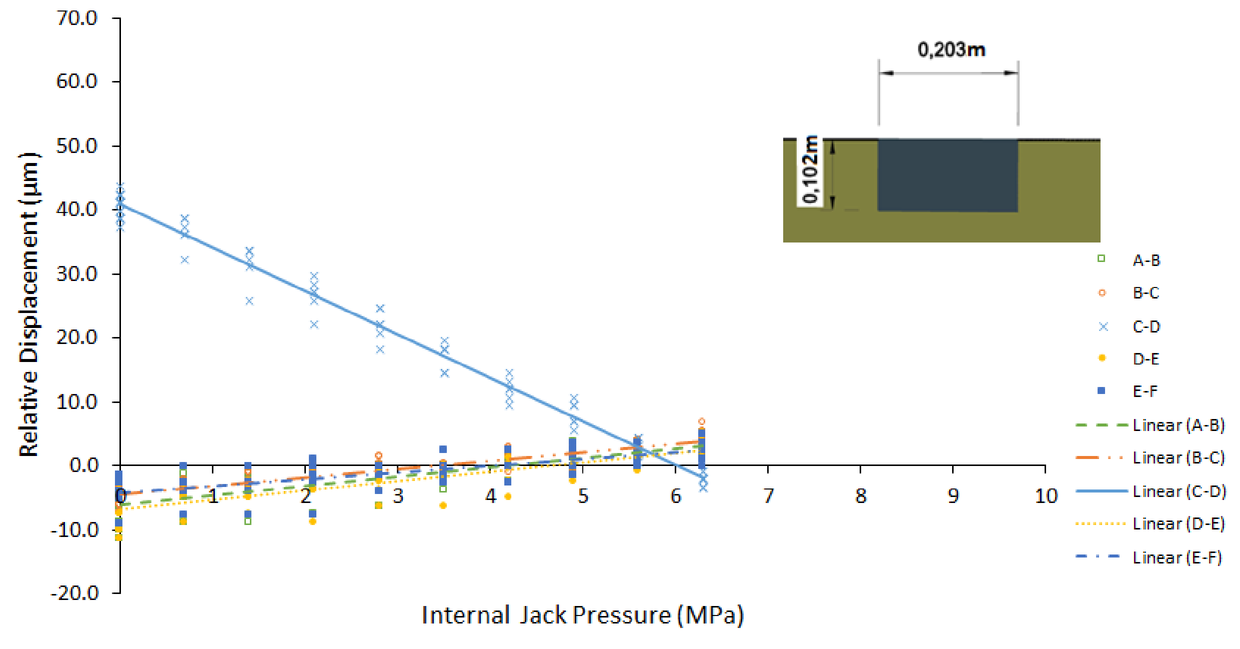

Figure C9: The relative displacement (µm) of pins C-D as a function of measured pressure in the flatjack (MPa) using the rectangular flatjack in a grouted slot made from overlapping boreholes. The trend lines are the mean of each data set.

Table C9: Summary of important values in the trend line for each pin span in test ASTM-OB. Corrected pressure is the output pressure of the jack whereas the internal pressure is the fluid pressure and was the measured pressure during the test.

Span	Closure (µm)	Slope	Flatjack Pressure (MPa)	
			Internal	Corrected (K=0.81)
A-B	-6	1.434	4.14	3.35
B-D	-4	1.311	3.35	2.71
C-D	41	-6.807	6.01	4.87
D-E	-7	1.472	4.61	3.74
E-F	-4	1.051	4.01	3.25

APPENDIX D: FIELD DATA

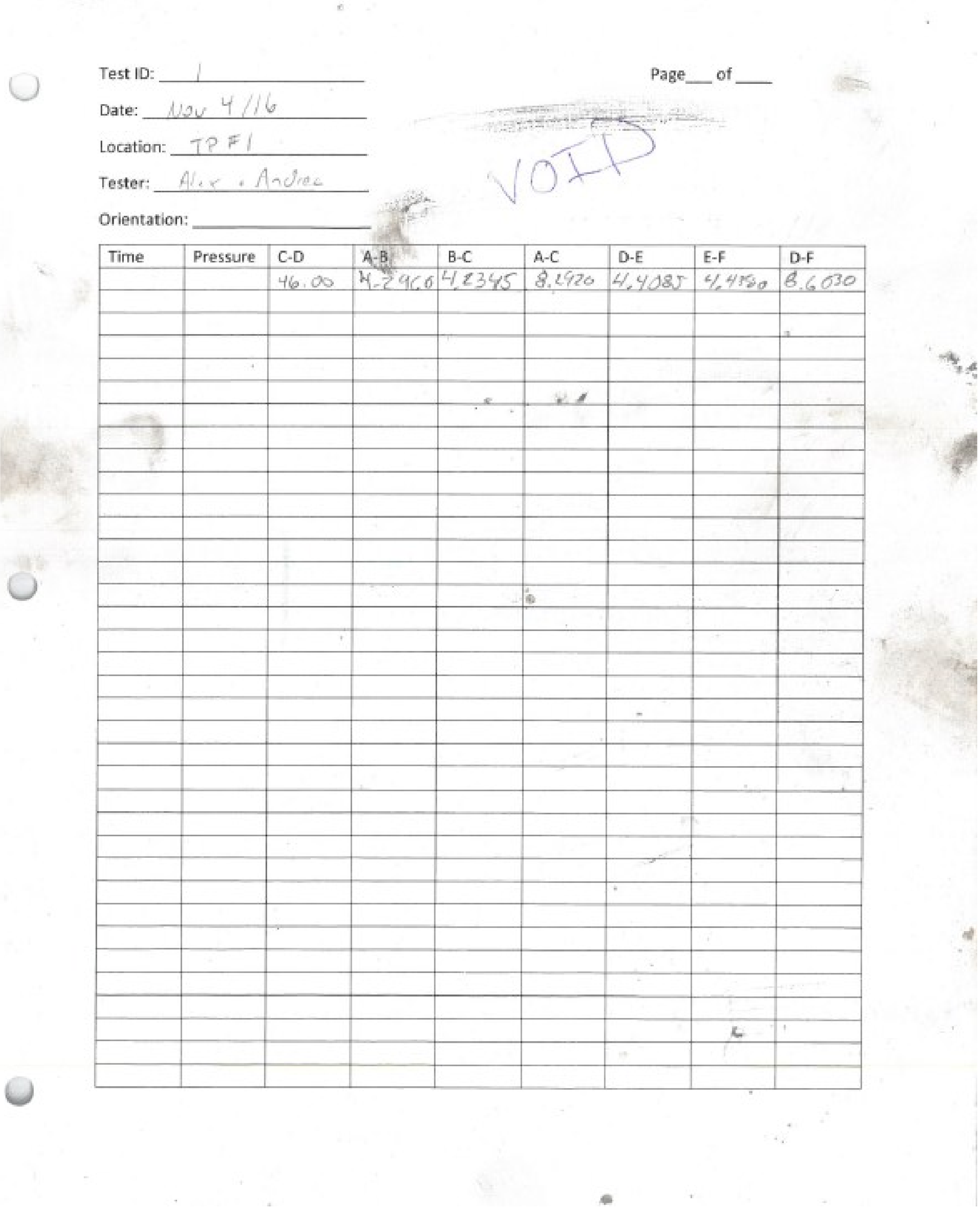

Test ID: 1

Page___ of ____

Date: Nov 4/16

Location: TP F1

Tester: Alex + Andrea

Orientation: ____________________

VOID

Time	Pressure	C-D	A-B	B-C	A-C	D-E	E-F	D-F
		46.00	4.2960	4,2345	8.2920	4,4085	4,4580	8.6030

Test ID: S-wall

Page__ of ____

Date: Nov 4 2016

Location: Pioneer coal Stellarton

Tester: Alex + Andrea

Orientation: along dip

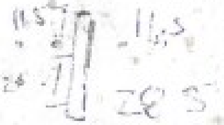

= jack is off center

Time	Pressure	C-D	A-B	B-C	A-C	D-E	E-F	D-F
	[illegible]	29.00	8.7610	4.6400	12.3610	4.5470	8.5400	12.6073
	[illegible]	28.9[illegible]	~~8.6900~~	4.0410	18.152[illegible]	4.2470	7.9805	12.0155
	jack in	28.89	8.6682	AH				
	2 bar	28.88						
	4 bar	28.84						
	6 bar	28.82						
	8 bar	28.81						
	10 bar	28.79						
	15 bar	28.70						
	20 bar	28.56						
holding	3 bar	28.90						
	5 bar	28.90						
	10 bar	28.74						
	15 bar	28.68						
	20 bar	28.63						
	25 bar	28.48						
	30	28.21						
	35	27.95						
	40	27.73						
[illegible] holding	45	27.37						
2869	50	27.02						

37811 - exendo - Dave

Test ID: Hole 3

Page___ of ____

Date: Nov 4 2016

Location: Pioneer Coal stellarton

Tester: Alex + Andrea

Orientation: parallel strike (shale)

Time	Pressure	C-D	A-B	B-C	A-C	D-E	E-F	D-F
	Pre -a	7.7770	8.1040	3.8780	11.7400	4.6325	7.8405	12.2400
		7.7675	8.0935	3.8985	11.7665	46125	7.8400	12.2435

Leeb @ test location

- 489 HL
- 372
- 477
- 482
- 501
- 457
- 524
- 559
- 479
- 613 (dry)
- 472
- 512

Shell LH

- too low to measure
- 198
- too low
- 257
- 217
- 257
- 173
- 223
- 187
- 218
- 214
- 192

D525665
5045701
±1327m

① Shale, black, heavily bedded (bedding spacing ~1mm, undulating bedding), JRC ~ 2-6, GSI ~40, bedding ① 342/29, RQD ~ 0

② Clay/mudstone ("sandstone"), some oxidization present, RQD ~10 ~~%~~, friable, GSI ~65, blocks ~ spaced ~30cm

① 260/65, 2m length, undulating, [illegible], ~1-2cm aberrant rock, JRC 2-4, 3.5m spacing, ~~[illegible]~~

② ~~335/20~~ 315/70, 5m length, JRC 2-4 (at surface), slightly undulating, 2-5 cm broken rock, 2m spacing

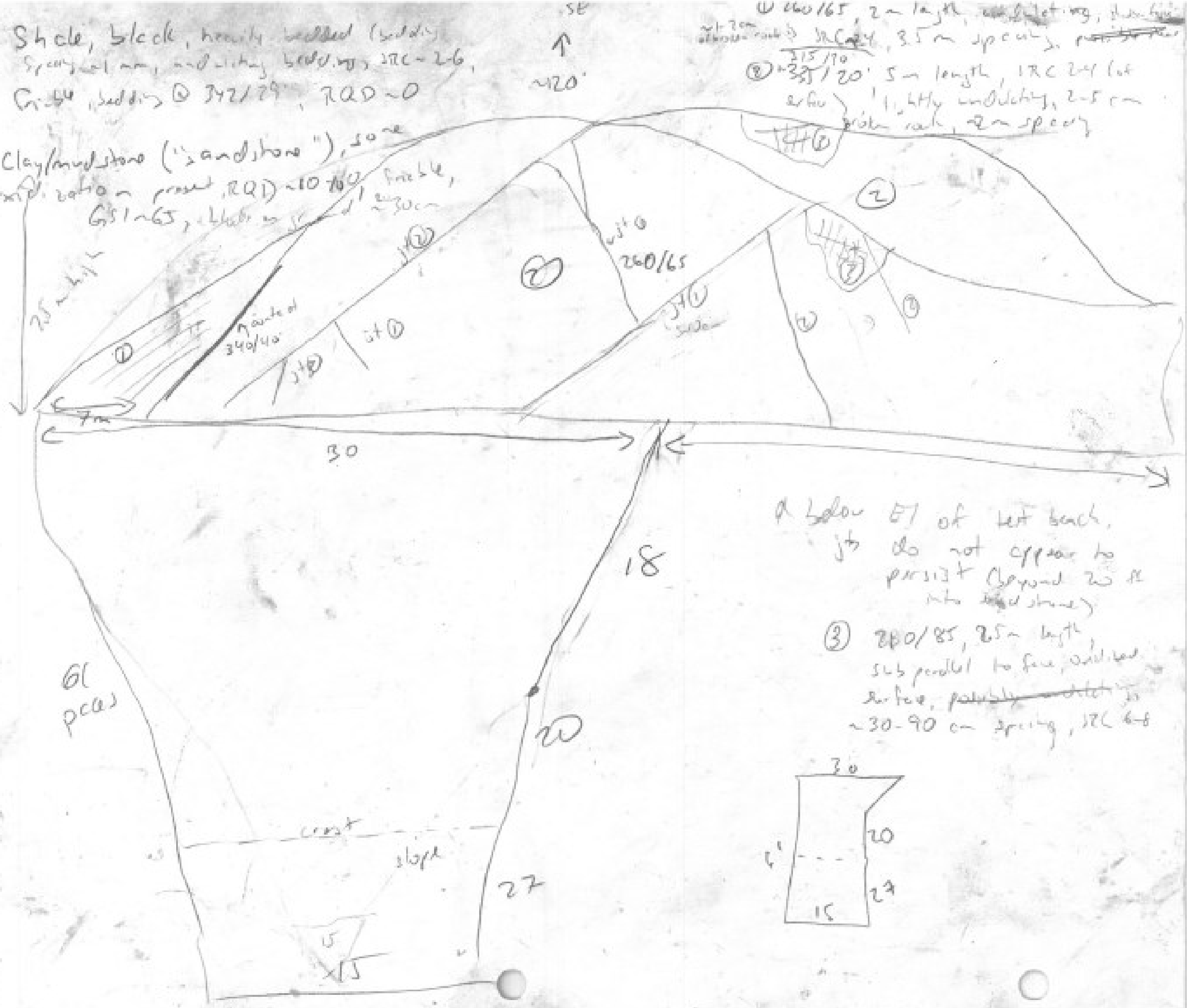

A below E1 of left bench, jts do not appear to persist (beyond 20 ft into sandstone)

③ 280/85, 25m length, sub parallel to face, oxidized surface, ~~probably undulating~~ is ~30-90 cm spacing, JRC 6-8

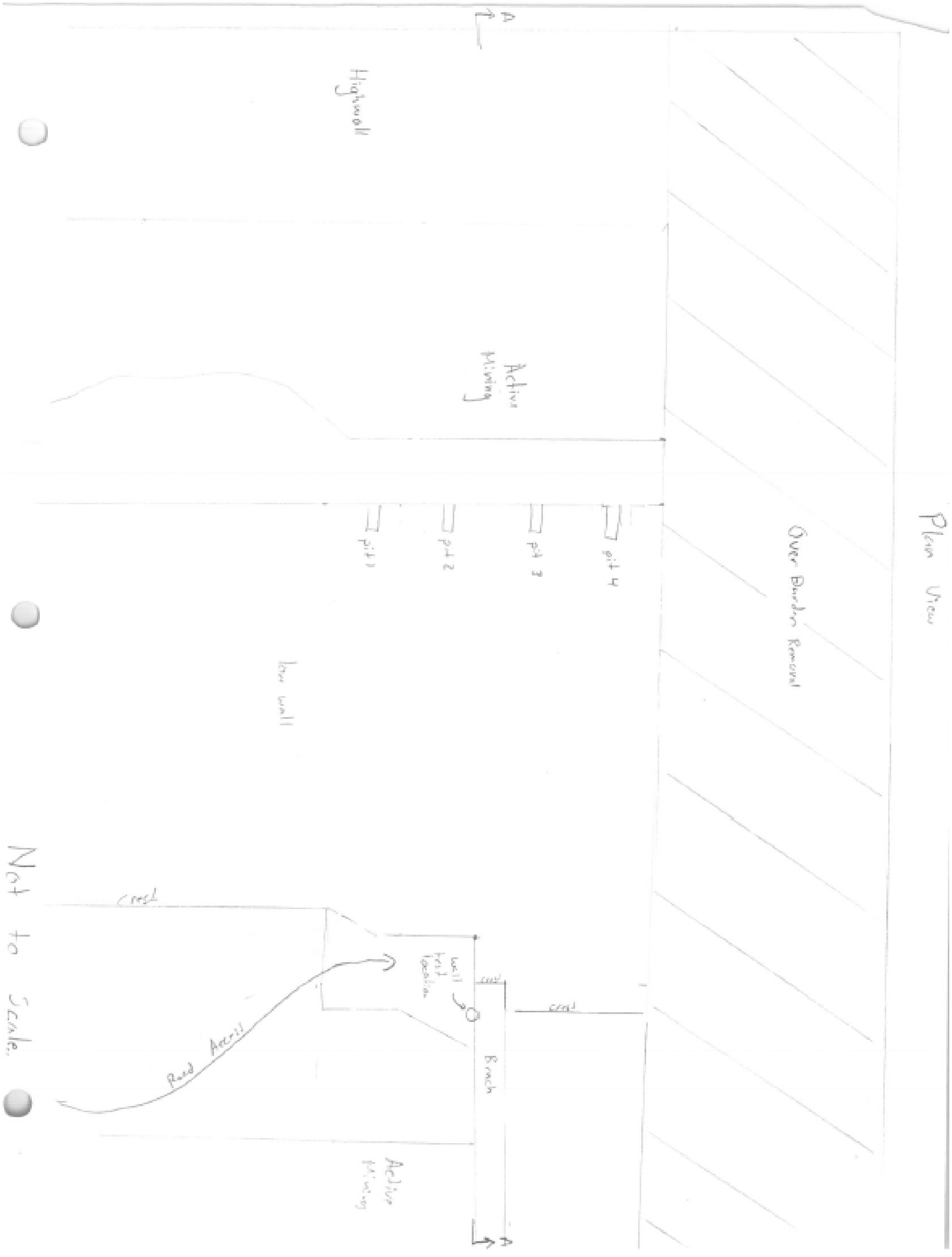
Plan View
Over Burden Removal
Highwall
Active Mining
pit 4
pit 3
pit 2
pit 1
low wall
crest
wall test location
crest
crest
Bench
Road Access
Active Mining
A
A
Not to Scale.

Section View A-A

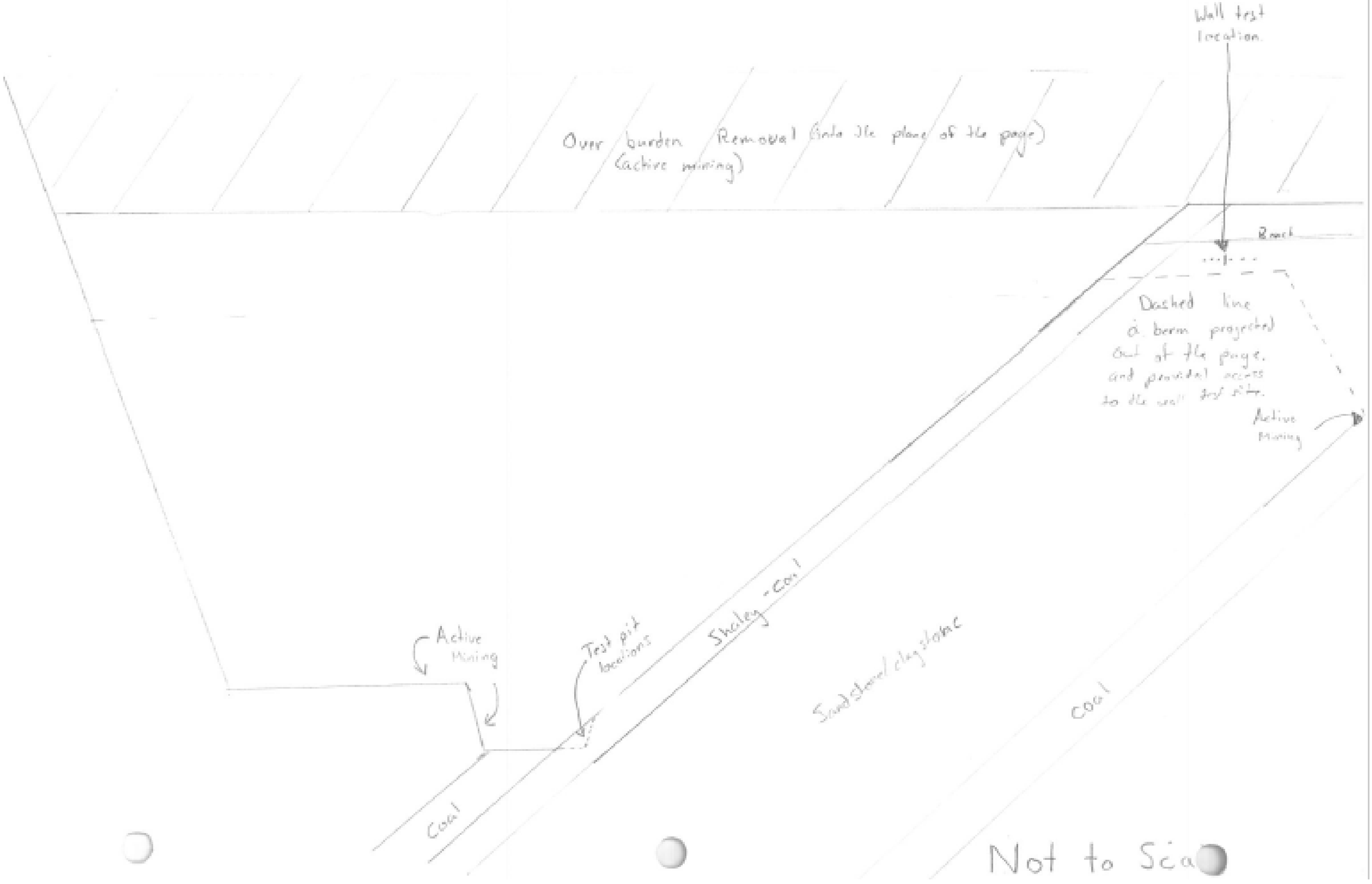

APPENDIX E: MODULUS DATA

	Based on EB1		EB2		EB3		EB4		EB5	
	Force(N)	Pressure(I	Axial	Radial	Axial	Radial	Axial	Radial	Axial	Radial
1	85000	4.660088	0.000125	1.64474E-05	0.000118	8.22368E-06	0.000123	1.64474E-05	0.00012	1.91886E-05
2	170000	9.320175	0.000265	4.11184E-05	0.000255	8.22368E-06	0.00028	4.11184E-05	0.000263	4.38596E-05
3	255000	13.98026	0.0004175	6.57895E-05	0.000398	3.28947E-05	0.00043	7.12719E-05	0.000428	6.85307E-05
4	340000	18.64035	0.00058	9.04605E-05	0.000548	6.0307E-05	0.000583	9.86842E-05	0.00058	9.5943E-05
5	425000	23.30044	0.000735	0.000120614	0.000698	8.77193E-05	0.000735	0.000126096	0.00075	0.000109649
6	510000	27.96053	0.0008975	0.000153509	0.00085	0.000117873	0.000888	0.00015625	0.000908	0.000158991
7	595000	32.62061	0.0010675	0.000186404	0.001008	0.000148026	0.001043	0.000183662	0.001078	0.000191886
8	680000	37.2807	0.0012375	0.000224781	0.001173	0.000186404	0.00119	0.000211075	0.001235	0.000235746
9	765000	41.94079	0.0014225	0.000265899	0.001343	0.000222039	0.001345	0.000241228	0.001423	0.000274123
10	850000	46.60088	0.00162	0.000317982	0.001513	0.000260417	0.001505	0.000274123	0.001608	0.000326206
UCS	1252544	68.67018	1237727	67.85783991	1283204	70.35109649	1276941	70.00773026	1252332	68.65855263
Modulus (Gpa)			28.2		30		30.4		28.2	

APPENDIX F: MODIFICATIONS TO TESTING PROCEEDURE

The first test was performed to help commission the actuator and identify sources of errors in the testing procedure. The location of the holes for the measurement pins were marked on the sample but when the first hole (pin F) was drilled, the bit deviated and the hole was inaccurately drilled. This error was corrected by creating a metal drill jig and securing it to the sample using tape. The remainder of the holes were accurately drilled and the jig was removed for future use. The distance between pin E and F could not be measured using the available dial gauge device because it limited to measure in increments of 51 mm (2”) (+- .25in). This was compensated for by measuring the distance between pin D and F. During testing, a small crack formed and it was observed that arching was occurring in the testing apparatus with the sample being lifted off the ground. This was caused by stretching in the 3-inch diameter bolts in the end blocks when the 2 MN load was applied and rotation along the swivel in the actuator. Subsequently, the actuator was anchored directly to the floor using angle iron and 1-inch bolts to prevent movement in the vertical direction. This restraint method limited rotation of the actuator swivel and reduced the arching effect. The bracket was designed to be the weakest component of the load frame so in the event of overloading it will fail to avoid damaging the actuator.

The installation of the flatjack went well however it was a tight fit. The flatjack had to be inserted by tapping lightly with a mallet. Removal of the flatjack proceeded smoothly however prying tools were required to be used on the underside of the jack to remove it. This tight fit has two impacts on results; firstly, it ensured good contact with the side walls of the slot and secondly it applied a pressure to side walls of the block. Measurements were taken before and after inserting the jack into the hole to evaluate this effect and no displacement due to this pressure was observed.

During the second commissioning test, the actuator had significantly less arch. When the holes for the pins where about to be drilled it was observed that a significant crack had again formed in the specimen and that previous efforts did not fix the root cause of the problem. After unloading the specimen due to safety concerns, a closer look at the specimen and block revealed a small 1 mm bow existed in the end block that occurred during pouring. Despite having tar paper between the specimen and the end block it was this bow had caused the crack in the first two tests. This issue was successfully rectified by using a 6mm (¼") thick sheet of butyl rubber material on the distribution plate side and 13 mm (½") thick sheet on the side with the bow. This setup was first tested on the first specimen with the smaller crack. The crack did not appear to enlarge so testing proceeded to one of the undamaged specimens and the data from the first two tests were considered invalid as they were used to identify errors in the set up and to commission the actuator.

In the commissioning tests, it was found that the pins produced an unacceptably large error. It was determined that this was because the interior bore angle in the pin was the same as the measurement devices angle at 60° as shown in Figure F. This arrangement required the pins to be aligned perfectly perpendicular to the measurement device for proper measurement. This issue was corrected by modifying the interior bore angle of the pin from 60° to 45° to allow the measurement device to seat properly on the interior ridge of the pin even if there was imperfect alignment. In addition, a micrometer was tested by installing a post on the pins for measurements as shown in Figure F. The new pins were tested in a discarded specimen to determine if they produced repeatable results. One set was installed straight and one set was installed crooked and in both cases the 45º pins were found to produce the most repeatable results even when damaged or installed at an angle shown in Table F.

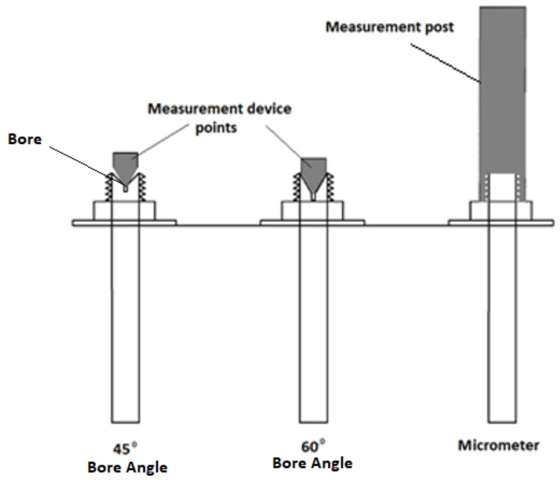

Figure F: Measurement pins and their fit with corresponding measurement device. The two on the left are used with the dial gauge apparatus and the post used a machinist's micrometer.

Table F: Results from preliminary testing of the measurement pins shown in Figure F to ensure consistent measurements. Numbers are truncated to the last 2 digits for simplicity (ex: 0.1336 is 36). There was no load on the block and no flatjack.

Measurement Number	C-D (straight pin)			D-E (Crooked pin E @ 20°)		
	60 °	45 °	Micrometer	60 °	45 °	Micrometer
1	35	15	97	35	89	49
2	34	15	99	39	89	54
3	35	16	99	39	88	55
4	34	15	98	30	88	54
5	36	15	97	40	88	52
6	37	15	99	34	89	48
7	35	15	99	32	89	52
8	37	15	98	37	89	52
9	36	15	100	40	89	55
10	36	15	99	38	89	52
11	36	16	98	37	89	55
12	37	15	97	40	89	48
13	36	16	100	37	89	50
14	37	16	99	41	89	52
15	36	15	98	38	89	37
16	36	15	99	38	88	42
17	38	16	97	39	89	53
18	37	15	99	38	89	48
19	36	16	97	41	89	49
20	36	16	99	41	90	55
Average	36	15.35	98.4	37.7	88.85	50.6
Standard Deviation	1.03	0.49	1.01	2.98	0.49	4.59